Copyright

by

Fang Ye

2010

The Thesis Committee for Fang Ye
Certifies that this is the approved version of the following thesis:

Sensitivity of Seismic Reflections to Variations in Anisotropy in the Bakken Formation, Williston Basin, North Dakota

APPROVED BY
SUPERVISING COMMITTEE:

Supervisor:

Robert H. Tatham

Mrinal K. Sen

Clark R. Wilson

Sensitivity of Seismic Reflections to Variations in Anisotropy in the Bakken Formation, Williston Basin, North Dakota

by

Fang Ye, B.E.; M.E.

Thesis

Presented to the Faculty of the Graduate School of

The University of Texas at Austin

in Partial Fulfillment

of the Requirements

for the Degree of

Master of Science in Geological Sciences

The University of Texas at Austin

May 2010

Dedication

To my parents and grandparents

Acknowledgements

I would like to express my deepest gratitude to my supervisor, Dr. Robert H. Tatham for his guidance, encouragement, inspiration, and discussions. Dr. Tatham gave me the opportunity to study at the Jackson School of Geosciences and to work on this interesting project. He has always been there to help me. I would like to sincerely thank Dr. Mrinal K. Sen for his significant help in seismic modeling and stimulating suggestions throughout my research. I would also like to thank Dr. Clark R. Wilson for his insightful suggestions to improve this thesis.

I would like to thank Eric von Lunen for helpful directions and suggestions. I thank various geoscientists at Kerogen Resources Inc. My sincere thanks to Samik Sil for his help in seismic modeling and many discussions on anisotropy. I would also thank George Stovall, Bob Candito, John Plappert, Mark Porter, Russell Pruitt, Chuck Mosher, Kyle T. Spikes, Steve Roche, Jason Gumble, Jerry Beaudoin, Dmitry Bazykin, Diego Alexander Valentin Navarrete for their valuable inputs to this project. I sincerely thank Thomas E. Hess and Effie Jarrett for their technical support.

Many thanks to Kerogen Resources Inc. for providing the data. Special thanks to the Jackson School of Geosciences and the EDGER Forum for their financial support.

I would like to acknowledge all of my professors and fellow students at the University of Texas at Austin, and all friends and colleagues at BP America Inc.

Finally, I would like to thank my parents and family for their endless love and support.

May 2010

Abstract

Sensitivity of Seismic Reflections to Variations in Anisotropy in the Bakken Formation, Williston Basin, North Dakota

Fang Ye, M.S.Geo.Sci.

The University of Texas at Austin, 2010

Supervisor: Robert H. Tatham

The Upper Devonian–Lower Mississippian Bakken Formation in the Williston Basin is estimated to have significant amount of technically recoverable oil and gas. The objective of this study is to identify differences in the character of the seismic response to Bakken interval between locations with high and poor production rates. The predicted seismic responses of the Bakken Formation will hopefully help achieve such discrimination from surface seismic recordings.

In this study, borehole data of Bakken wells from both the Cottonwood and the Sanish Field were analyzed, including density information and seismic P and S wave velocities from Sonic Scanner logs. The Bakken Formation is deeper and thicker (and somewhat more productive) in the Sanish Field and is shallower and thinner in the Cottonwood Field. The Upper and Lower Bakken shale units are similar and can be

characterized by low density, low P and S wave velocities and low Vp/Vs ratios. The Sonic Scanner data suggest that the Upper and Lower Bakken shales can be treated as VTI media while the Middle Bakken may be considered as seismically isotropic.

Models of seismic response for both fields were constructed, including isotropic models and models with variations in VTI, HTI, and the combination of VTI and HTI in the Bakken intervals. Full offset elastic synthetic seismograms with a vertical point source were generated to simulate the seismic responses of the various models of Bakken Formation. This sensitivity study shows pronounced differences in the seismic reflection response between isotropic and anisotropic models. P-P, P-SV and SV-SV respond differently to anisotropy. VTI anisotropy and HTI anisotropy of the Bakken have different character. In particular, types of seismic data (P-P, P-SV, and SV-SV) and the range of source-receiver offsets that are most sensitive to variations in anisotropic parameters and fluid saturation were identified. Results suggest that bed thickness, anisotropy of the Upper and Lower Bakken shales, fractures/cracks and fluid fill in the fracture/cracks all influence the seismic responses of the Bakken Formation. The paucity of data available for "poorly" producing wells limited the evaluation of the direct seismic response to productivity, but sensitivity to potentially useful parameters was established.

Table of Contents

List of Tables

List of Figures

Chapter 1 Introduction

1.1 MOTIVATION

The Upper Devonian–Lower Mississippian Bakken Formation in the Williston Basin is estimated by the 2008 USGS assessment (Pollastro et al., 2008) to have 3.65 billion barrels of technically recoverable oil, 1.85 trillion cubic feet of associated/dissolved gas, and 148 million barrels of natural gas liquids. The Bakken formation consists of three members: the Lower, Middle and Upper Bakken. Both the Lower and Upper Bakken are dark marine shales with high organic content. The middle Bakken is mixed clastics and carbonates, which is the current producing interval.

The Bakken oil production has a history of about 60 years (Figure 1.1). It was first started with the Antelope Field discovery in 1953, expanded with drilling in the Bakken Fairway, followed by the development of the Elm Coulee Field in 2000 and the Parshall Field in 2006 (Nordeng, 2010, Durham, 2009). In the past few years, production of the low permeability Bakken has been significantly enhanced by technologies like horizontal drilling and new completion techniques, such as multi-stage hydrofracing.

The Bakken may be characterized as a "resource play" where all the wells produce something, and source, reservoir and seal properties are intermixed. This study is located in the Mountrail County and Burke County, North Dakota, east of the Nesson Anticline. Wells from two oil fields, the Cottonwood Field and the Sanish Field, are studied.

Cumulative production from the Bakken Formation reported by the North Dakota Department of Mineral Resources (DMR) shows the production difference between the Cottonwood Field and the Sanish Field (Table 1.1). For example, note the difference between DEADWOOD CANYON RANCH 43-28H well (Well 3) and ROSENCRANS

44-21H well (Well 5). Completion of these two wells started around the same time; the cumulative oil production of Well 3 is about 2 times of Well 5. Table 1.2 lists the best month producing rate (BMR) of Well 1 to Well 5 used in this study. BMR of Well 3 is 2.3 times that of Well 5, which is consistent with the data shown in Table 1.1. Both Table 1.1 and Table 1.2 indicate that the Sanish Field has been more productive than the Cottonwood Field.

The objective of this study is to identify differences in the character of the Bakken interval between locations with high and poor production rates, and to predict the seismic responses of the Bakken Formation to discriminate the difference in seismic character from surface seismic recordings. The wells available for this study, however, do not include a truly poor producer.

1.2 GEOLOGY OF THE BAKKEN FORMATION

The Williston Basin is an intracrationic basin that occupies a major portion of North Dakota and parts of Montana, South Dakota, Saskatchewan, and Manitoba. (Figure 1.2). The deepest North Dakota portion of the Williston Basin contains more than 4878 m of almost continuous sedimentation from Cambrian through Tertiary (Pitman et al., 2001). Cyclical transgressions and regressions resulted in repeated deposition of carbonates, clastics, and evaporites. The subsiding center remained almost unchanged in northwestern North Dakota.

The Upper Devonian–Lower Mississippian Bakken Formation (Figure 1.3) is conformably overlain by the Mississippian Lodgepole Formation and overlies the Devonian Three Forks conformably in the deep part of the basin and unconformably along the basin flank. The Lodgepole Formation consists of dark argillaceous limestones that are cherty and fossiliferous in the basin center, and interbeded with lighter colored peloidal, fossiliferous, and occasional oolitic limestone beds separated by darker colored

shales and argillaceous limestones toward the margins of the basin (Grover, 1996).The Three Forks Formation consists of interbedded dolomitic and argillaceous shales and siltstones, silty and argillaceous dolomite, mudstones, and anhydrite (Karasinski, 2006). The Bakken Formation consists primarily of three members, the Upper Bakken, Middle Bakken and Lower Bakken. Both the Upper and Middle Bakken are organic-rich marine shales and the Middle Bakken is mixed clastics and carbonates. The Bakken Formation in North Dakota reaches a maximum thickness of 160 ft (49 m) (Figure 1.4) and has a well-defined depocenter just east of the north-south trend Nesson Anticline (LeFever, 2008). The Nesson Anticline is the most prominent structural feature in the North Dakota portion of the Williston Basin (Figure 1.2).

The Lower Bakken shales were deposited in an offshore marine environment during periods of sea-level rise; the Middle Bakken was deposited in a costal environment during a rapid sea-level drop and then followed by another sea-level rise during which the Upper Bakken shales were deposited (Webster, 1984; LeFever et al., 1991; Smith and Bustin, 1995; Smith, 1996; Pitman et al., 2001; Sonnenberg and Pramudito, 2009).

The Upper Bakken consists of dark-gray to brownish-black, fillile, slightly calcareous, organic-rich shale (Webster, 1982; Hayes, 1984, Pitman et al., 2001). The Lower Bakken consists of dark-gray to brownish-black to black, fissile, slightly to highly organic rich shale that is locally calcareous at the base (Pitman et al., 2001). The difference between the Upper and Lower Bakken shales is that the Upper Bakken shale lacks the crystallized limestones and greenish-gray shale beds that is found in the Lower Bakken shale (Pitman et al., 2001; LeFever, 2008). The Middle Bakken varies in lithology, ranging from calcareous siltstones to sandstones dominated by quartz with

minor amounts of feldspar, to dolostones, silty limestones, and occasionally oolitic limestone (Pitman et al., 2001; LeFever, 2008).

The Upper and Lower Bakken shales are both source and seals. Most oil generated was expelled into the Middle Bakken, and did not migrate into the overlying Madison group (Price and LeFever, 1994; Pitman et al., 2001). The thermal maturity of shales varies widely and has an important influence on the reservoir quality of the Middle Bakken (Pitman et al., 2001). Maturity of the Bakken shales has been studied using electric resistivity (Meissner, 1976, 1978) as well as Time-Temperature Index (TTI) method (Nordeng, 2008; Nordeng and LeFever, 2008).

No	Well Name	Field	Completion Date	Cum Oil (Barrel)	Cum Water (Barrel)	Cum Gas (MCF)
1	ANNALA 11-36H	SANISH	1/10/2008	84030	13115	44721
2	DEADWOOD CANYON RANCH 11-5H	SANISH	3/8/2008	67766	26559	25457
3	DEADWOOD CANYON RANCH 43-28H	SANISH	7/4/2008	49662	11934	27720
4	FARHART 11-11H	COTTONWOOD	6/2/2008	25123	20578	7946
5	ROSENCRANS 44-21H	COTTONWOOD	6/23/2008	24991	20103	10385
6	EDWARDS 44-9H	COTTONWOOD	6/21/2008	28878	20142	8930
7	LUCY 11-23H	COTTONWOOD	9/10/2008	14092	21211	3983

Table 1.1: Cumulative production from the Bakken Formation reported by the North Dakota Department of Mineral Resources (DMR).

No	Well Name	Field	BMR (BOPD)
1	ANNALA 11-36H	SANISH	428
2	DEADWOOD CANYON RANCH 11-5H	SANISH	456
3	DEADWOOD CANYON RANCH 43-28H	SANISH	463
4	FARHART 11-11H	COTTONWOOD	218
5	ROSENCRANS 44-21H	COTTONWOOD	201

Table 1.2 : Best month producing rate in the five wells used for this study.

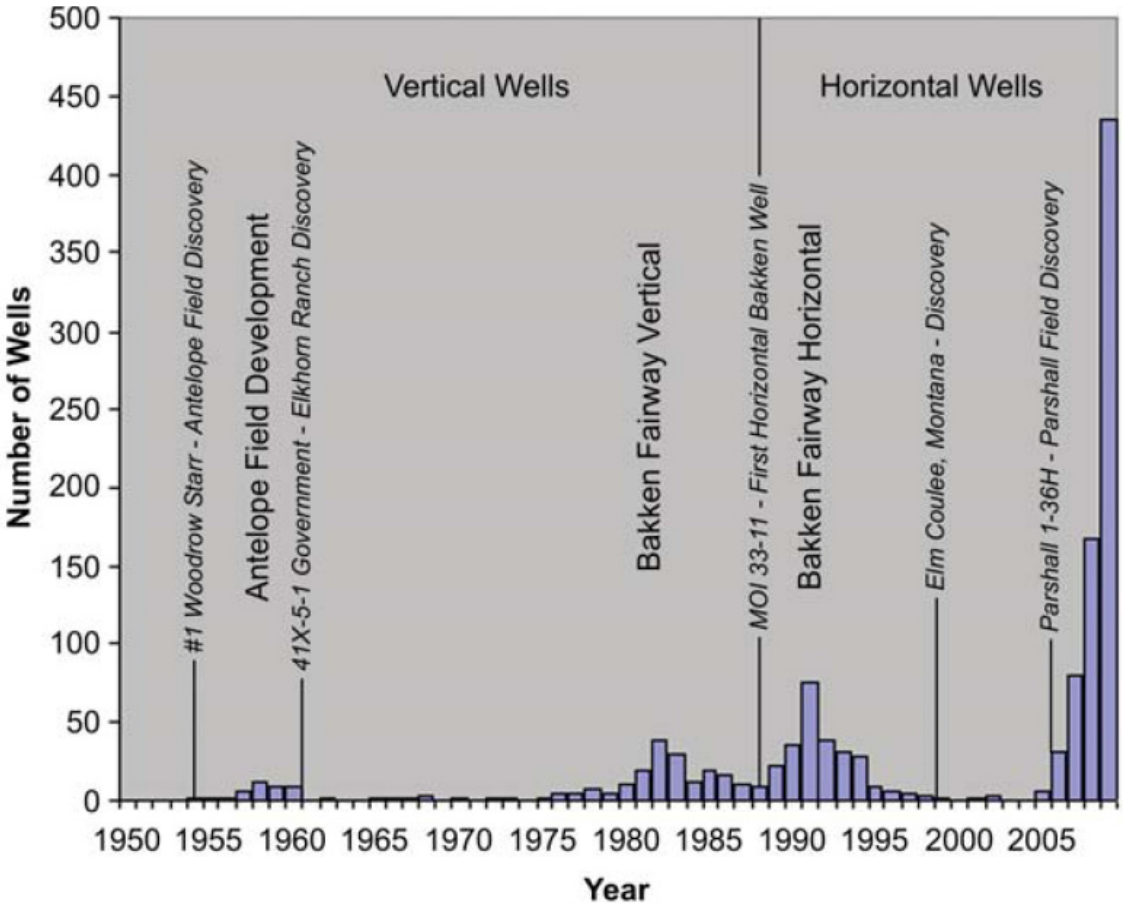

Figure 1.1: Historic distribution of Bakken tests, significant discoveries and technologic advances in the Williston Basin (taken from Nordeng, 2010).

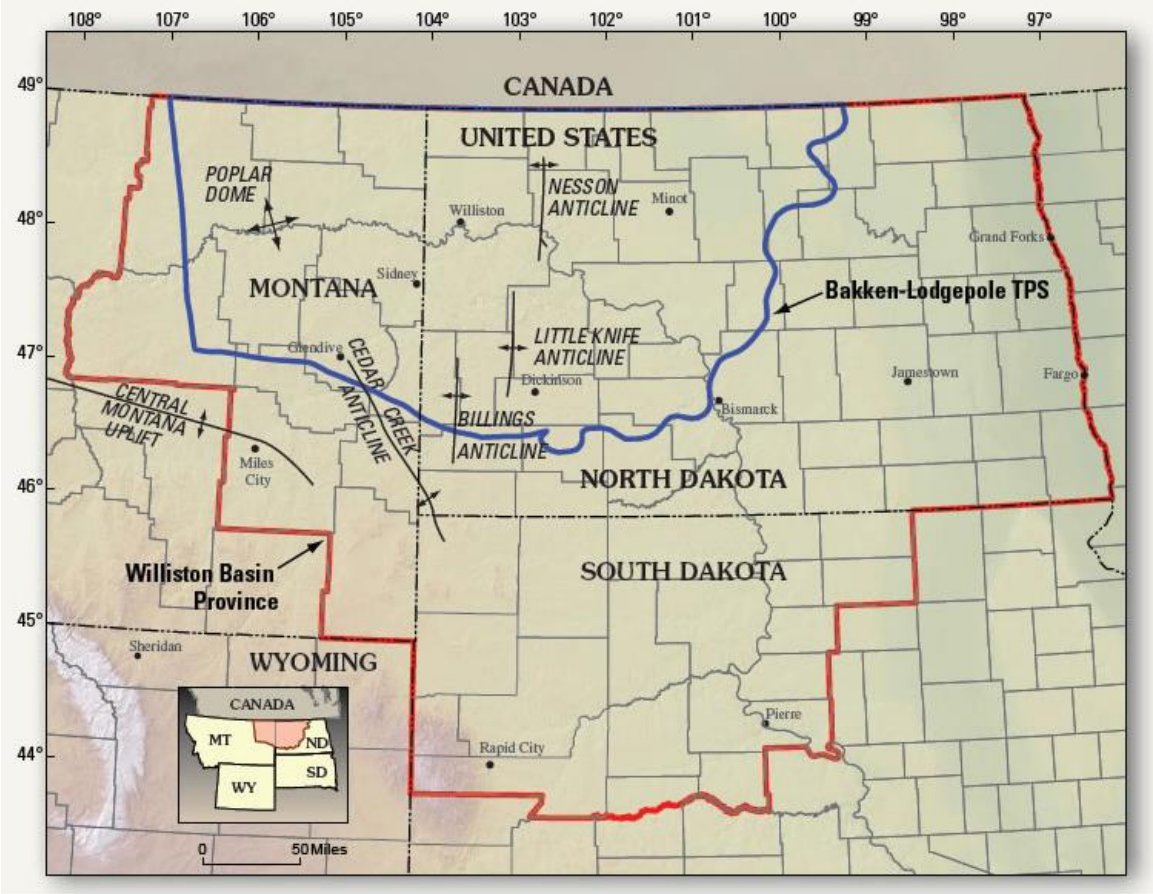

Figure 1.2: Williston Basin Province (in red), Bakken-Lodgepole Total Petroleum System (TPS) (in blue), and major structural features (taken from Pollastro et al., 2008).

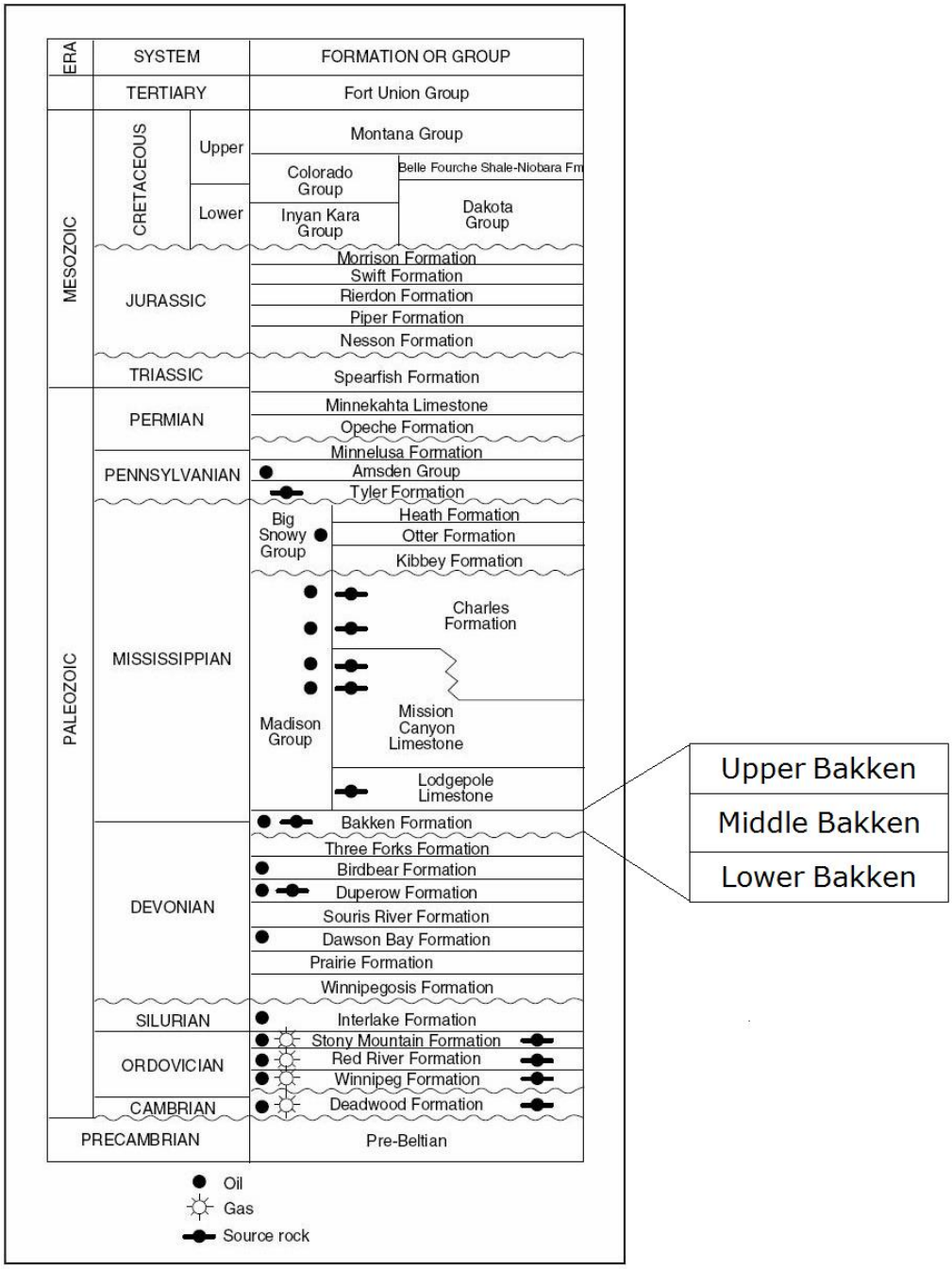

Figure 1.3: Stratigraphic chart of the Williston Basin (modified from Peterson, 1995).

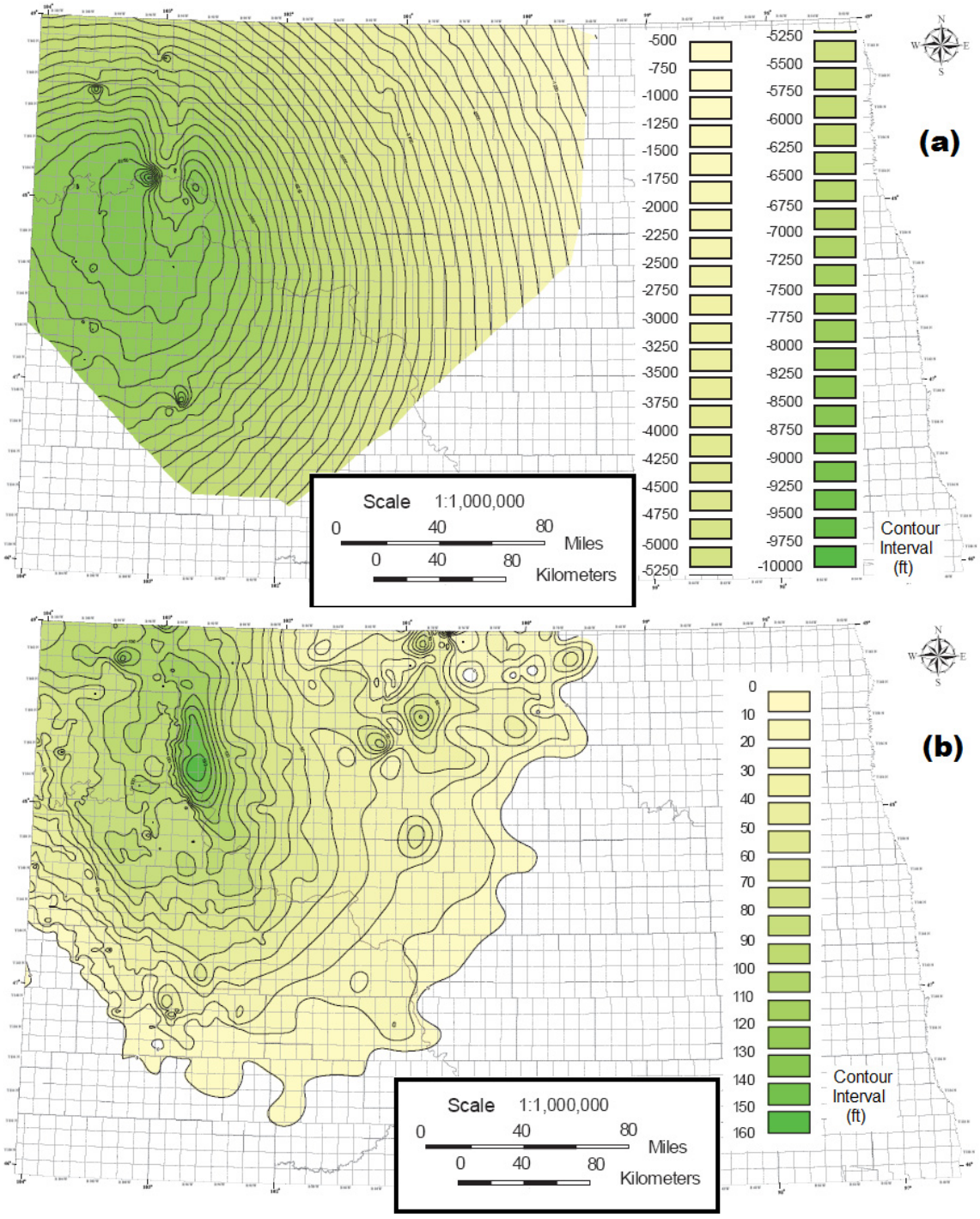

Figure 1.4: Structure on top of the Bakken Formation (a) and isopach (b) (modified from LeFever, 2008). Depth and thickness units are in feet.

Chapter 2 Seismic Anisotropy

2.1 INTRODUCTION

Anisotropy is defined as a variation of a physical property with the direction in which it is measured, either the propagation direction or, for shear wave propagation, the polarization direction (Tatham and McCormack, 1991).

In this Chapter, I will first review the classification and origin of anisotropy and show the differences between the two transversely anisotropic symmetries, VTI and HTI symmetries. Next, I will explain the anisotropy parameters for both VTI and HTI media and their relations to rock materials of interest. After that, I will review the anisotropy caused by fractures and cracks (HTI) and the anisotropy of hydrocarbon source rock (VTI), both of which are relevant to this study.

2.2 ORIGIN AND CLASSIFICATION

There are many causes of anisotropy. MacBeth and Lynn (2000) suggested that clay minerals in shales, layering, cracks and fractures are the four main categories that are important to exploration seismology. Both shales and layering give rise to VTI media and both vertical cracks and fractures may result in HTI media.

Transverse isotropy is a special symmetry within the general category of anisotropy. VTI and HTI, shown in Figure 2.1, are two common types of transverse isotropy, a special case of general anisotropy. Both of them have a single axis of symmetry, and are classified as transverse isotropy. VTI is transverse isotropy with vertical axis of symmetry. HTI is transverse isotropy with horizontal axis of symmetry. Tsvankin (1997) pointed out that the only difference between VTI and HTI is simply a 90° rotation of the symmetry axis.

For transverse isotropy media, both VTI and HTI, there are five independent elastic constants in the stiffness tensor (general anisotropy requires 21 elastic constants). In the simplified Voigt notation, the VTI stiffness tensor is

$$C^{(VTI)} = \begin{pmatrix} c_{11} & c_{11}-2c_{66} & c_{13} & 0 & 0 & 0 \\ c_{11}-2c_{66} & c_{11} & c_{13} & 0 & 0 & 0 \\ c_{13} & c_{13} & c_{33} & 0 & 0 & 0 \\ 0 & 0 & 0 & c_{55} & 0 & 0 \\ 0 & 0 & 0 & 0 & c_{55} & 0 \\ 0 & 0 & 0 & 0 & 0 & c_{66} \end{pmatrix}, \tag{1.1}$$

and the HTI stiffness tensor is

$$C^{(HTI)} = \begin{pmatrix} c_{11} & c_{13} & c_{13} & 0 & 0 & 0 \\ c_{13} & c_{33} & c_{33}-2c_{44} & 0 & 0 & 0 \\ c_{13} & c_{33}-2c_{44} & c_{33} & 0 & 0 & 0 \\ 0 & 0 & 0 & c_{44} & 0 & 0 \\ 0 & 0 & 0 & 0 & c_{55} & 0 \\ 0 & 0 & 0 & 0 & 0 & c_{55} \end{pmatrix}. \tag{1.2}$$

2.3 ANISOTROPY PARAMETERS

Thomsen (1986) introduced a set of parameters in terms of elastic constants for weakly anisotropic media. Thomsen's parameters provide physical meanings of elastic constants. These parameters were first established for VTI media. Ruger (1997) and Tsvankin (1997) later extended the anisotropic parameters to HTI media and suggested Thomsen-style parameters. Both Thomsen's and Thomsen-style parameters are dimensionless.

2.3.1 Thomsen's parameters for VTI media

Thomsen's parameters (1986) for VTI media are:

$$Vp(0) \equiv \sqrt{\frac{c_{33}}{\rho}} \tag{1.3}$$

$$Vs(0) \equiv \sqrt{\frac{c_{55}}{\rho}}, \tag{1.4}$$

$$\varepsilon \equiv \frac{c_{11} - c_{33}}{2c_{33}}, \tag{1.5}$$

$$\delta \equiv \frac{\left(c_{13} + c_{55}\right)^2 - \left(c_{33} - c_{55}\right)^2}{2c_{33}\left(c_{33} - c_{55}\right)}, \tag{1.6}$$

$$\gamma \equiv \frac{c_{66} - c_{55}}{2c_{55}}, \tag{1.7}$$

where $Vp(0)$ and $Vs(0)$ are the vertical velocities of the P and S waves, and ρ is the density. ε is the fractional difference between vertical and horizontal P velocities and γ shows SH anisotropy. δ controls the near vertical anisotropy (Thomsen, 1986), and is the second derivative of the P wave phase velocity (Sil, 2009)

2.3.3 Thomsen-style parameters for HTI media

Thomsen-style parameters for HTI media can be written as (Tsvankin, 1997):

$$Vp(0) \equiv \sqrt{\frac{c_{33}}{\rho}}, \tag{1.8}$$

$$Vs(0) \equiv \sqrt{\frac{c_{55}}{\rho}}, \tag{1.9}$$

$$\varepsilon^{(V)} \equiv \frac{c_{11} - c_{33}}{2c_{33}}, \tag{1.10}$$

$$\delta^{(V)} \equiv \frac{\left(c_{13} + c_{55}\right)^2 - \left(c_{33} - c_{55}\right)^2}{2c_{33}\left(c_{33} - c_{55}\right)}, \tag{1.11}$$

$$\gamma^{(V)} \equiv \frac{c_{66} - c_{44}}{2c_{44}}. \tag{1.12}$$

Tsvankin (1997) denoted these HTI anisotropy parameters with the superscript V. All the other parameters have similar physical meaning as Thomsen's parameters.

2.4 ANISOTROPY OF FRACTURES AND CRACKS

Seismic wavelengths are on a scale that is much larger than the scale of the subsurface heterogeneities (Hudson, 1991). Therefore, we can use an equivalent medium as a replacement of the fractured medium. Parameters of the equivalent medium depend on the orientation and intensity of the fractures, properties of infill materials and the elastic coefficients of the host rock (Bakulin et al., 2000). Two widely accepted equivalent media theories are linear slip theory (Schoenberg, 1980, 1983; Schoenberg and Sayers, 1995) for parallel infinite fractures with linear slip boundary conditions and Hudson's model (1980, 1981) for isolated parallel penny-shaped cracks.

Schoenberg (1980, 1983) suggested that the fractures can be treated as either infinitely thin and highly compliant layers or planes of weakness with linear-slip boundary conditions. The compliance matrix (inverse of stiffness matrix) of the fractured medium, s, can be expressed as

$$s = s_b + s_f, \tag{1.13}$$

where s_b is the compliance of the host rock and s_f is the excess compliance (Schoenberg and Muir, 1989; Schoenberg and Sayers, 1995; Molotkov and Bakulin, 1997).

In case of one set of vertical rotationally invariant fractures embedded in an isotropic host rock, Schoenberg and Sayers (1995) derived the stiffness matrix of the equivalent medium:

$$c = s^{-1} = c_b - \begin{pmatrix} (\lambda+2\mu)\Delta N & \lambda\Delta N & \lambda\Delta N & 0 & 0 & 0 \\ \lambda\Delta N & \frac{\lambda^2}{(\lambda+2\mu)}\Delta N & \frac{\lambda^2}{(\lambda+2\mu)}\Delta N & 0 & 0 & 0 \\ \lambda\Delta N & \frac{\lambda^2}{(\lambda+2\mu)}\Delta N & \frac{\lambda^2}{(\lambda+2\mu)}\Delta N & 0 & 0 & 0 \\ 0 & 0 & 0 & 0 & 0 & 0 \\ 0 & 0 & 0 & 0 & \mu\Delta T & 0 \\ 0 & 0 & 0 & 0 & 0 & \mu\Delta T \end{pmatrix}, \tag{1.14}$$

where c_b is the stiffness matrix of the isotropic host rock and λ and μ are the elastic Lame's constants of the host rock. ΔN is normal weakness and ΔT is tangential weakness, which were introduced by Hsu and Schoenberg (1993). Both ΔN and ΔT are dimensionless quantities that vary from zero to one. The weaknesses is zero if the medium is unfractured, thus isotropic, while the weaknesses goes to unity to show the medium is highly fractured.

Hudson's model (1980, 1981) is based on the assumption of isolated parallel penny-shaped cracks with small aspect ratios and crack density evenly distributed in an isotropic host rock. Aspect ratio α is defined as

$$\alpha \equiv c / a, \tag{1.15}$$

where c and a are the minor and major axes of the penny-shaped pore (Tatham and McCormack, 1991). In Hudson's model, crack density is defined as

$$e \equiv \nu \left\langle a^3 \right\rangle, \tag{1.16}$$

where ν is the number of cracks per unit volume and $\langle\ \rangle$ denotes volume averaging (Hudson, 1980).

If thin, penny-shaped cracks are aligned normal to the x-direction, the stiffness matrix of equivalent medium c can be written as (Hudson, 1980, 1981)

$$c = c_b - \frac{e}{\mu}\begin{pmatrix} (\lambda+2\mu)^2 U_{11} & \lambda(\lambda+2\mu)U_{11} & \lambda(\lambda+2\mu)U_{11} & 0 & 0 & 0 \\ \lambda(\lambda+2\mu)U_{11} & \lambda^2 U_{11} & \lambda^2 U_{11} & 0 & 0 & 0 \\ \lambda(\lambda+2\mu)U_{11} & \lambda^2 U_{11} & \lambda^2 U_{11} & 0 & 0 & 0 \\ 0 & 0 & 0 & 0 & 0 & 0 \\ 0 & 0 & 0 & 0 & \mu^2 U_{33} & 0 \\ 0 & 0 & 0 & 0 & 0 & \mu^2 U_{33} \end{pmatrix} + O(e^2), \tag{1.17}$$

where c_b is the stiffness matrix of the isotropic host rock, λ and μ are the elastic Lame's constants of the host rock, U_{11} and U_{33} are dimensionless quantities that depend on the

boundary conditions of the crack faces, fracture infill, and direction of cracks (Hudson, 1981).

Schoenberg and Douma (1988) showed that penny-shaped cracks (Hudson, 1980, 1981) and infinite parallel fractures with linear slip (Schoenberg, 1980, 1983) have the same stiffness tensor if the following relationships are fulfilled:

$$\Delta N = \frac{(\lambda + 2\mu)}{\mu} U_{11} e, \tag{1.18}$$

$$\Delta T = U_{33} e. \tag{1.19}$$

In other words, equation (1.14) and (1.17) become identical. This indicates that it is impossible to distinguish between fractures (as described by Schoenberg and Sayers, 1995) and cracks (as described by Hudson, 1980) from the seismic data.

When the fractures are filled with weak solid, equation (1.18) and (1.19) can be written as (Schoenberg and Douma, 1988)

$$\Delta N = \frac{4e}{3g(1-g)\left[1 + \frac{1}{\pi g(1-g)}\left(\frac{k' + 4/3\mu'}{\mu}\right)\left(\frac{a}{c}\right)\right]}, \tag{1.20}$$

$$\Delta T = \frac{16e}{3(3-2g)\left[1 + \frac{4}{\pi(3-2g)}\left(\frac{\mu'}{\mu}\right)\left(\frac{a}{c}\right)\right]}, \tag{1.21}$$

where k' and μ' are bulk modulus and shear modulus of the infill material. The parameter g is defined as

$$g \equiv \frac{\mu}{\lambda + 2\mu} = \frac{V_s^2}{V_p^2}, \tag{1.22}$$

where Vp and Vs are the P wave velocity and S wave velocity of the host rock.

For dry cracks, both the bulk modulus k' and shear modulus μ' of the infill material vanish. Thus,

$$\Delta N = \frac{4e}{3g(1-g)}, \tag{1.23}$$

and

$$\Delta T = \frac{16e}{3(3-2g)}. \tag{1.24}$$

If the cracks are wet (oil or water saturated), while the shear modulus μ' goes to zero, the bulk modulus k' of the fluid is comparable to the shear modulus μ of the host rock. For very flat cracks with small aspect ratio c/a, $(\frac{k'+4/3\mu'}{\mu})(\frac{a}{c}) \gg 1$, which yields

$$\Delta N = 0, \tag{1.25}$$

$$\Delta T = \frac{16e}{3(3-2g)}. \tag{1.26}$$

Under the assumption of weak anisotropy, exact expressions for $\varepsilon^{(v)}$, $\delta^{(v)}$ and $\gamma^{(v)}$ in terms of the fracture weaknesses can be linearized with respect to normal weakness ΔN and tangential weakness ΔT:

$$\varepsilon^{(v)} = -2g(1-g)\Delta N, \tag{1.27}$$

$$\delta^{(V)} = -2g[(1-2g)\Delta N + \Delta T], \tag{1.28}$$

$$\gamma^{(V)} = -\frac{\Delta T}{2}. \tag{1.29}$$

In case of thin, isolated, penny-shaped dry cracks, by substituting equation (1.23) and (1.24), Bakulin et al., (2000) rewrote equation (1.27) - (1.29) in terms of the crack density using Hudson's (1981) theory as:

$$\varepsilon^{(v)} = -\frac{8}{3}e, \tag{1.30}$$

$$\delta^{(V)} = -\frac{8}{3}e\left[1 + \frac{g(1-2g)}{(3-2g)(1-g)}\right], \tag{1.31}$$

$$\gamma^{(V)} = -\frac{8e}{3(3-2g)}. \tag{1.32}$$

For fluid-filled cracks, equation (1.25) and (1.26) can be substituted into equation (1.27) - (1.29) to get:

$$\varepsilon^{(v)} = 0, \tag{1.33}$$

$$\delta^{(V)} = -\frac{32ge}{3(3-2g)}, \tag{1.34}$$

$$\gamma^{(V)} = -\frac{8e}{3(3-2g)}. \tag{1.35}$$

2.5 ANISOTROPY OF SHALES

Shales make up 75 percent of the infill in most sedimentary basins and overlie most hydrocarbon bearing reservoirs (Hornby, 1998). Generally speaking, shales are known to be seismically anisotropic (McDonal et al., 1958; Levin, 1979; White et al., 1983; Banik, 1984; Winterstein, 1986; Brocher and Christensen, 1990; Lynn and Thomsen, 1990; Carrion et al., 1992; Johnston and Christensen, 1995; Hornby, 1998)

In addition to the mineralogy, the velocity and anisotropy of shales are related to the organic richness of kerogen content (Meissner, 1984). A series of papers (Vernik and Nur, 1990, 1992; Vernik and Landis, 1996; Vernik and Liu, 1997) was published based on the laboratory experiments on a variety of shales, including the Bakken Formation from the Williston Basin, with different clay and kerogen content, clay mineralogy and porosity at different effective pressure. They found that black, kerogen-rich shales are transversely isotropic, and anisotropy of shales increases substantially with compaction and kerogen content. Vernik and Nur (1992) pointed out that anisotropy of shales is enhanced by bedding-parallel microcracks especially at high pore pressure typical of the Bakken Formation at depths of about 3 km.

Prasad and Mukerji (2003), and Mukerji and Prasad (2004, 2007) analyzed scanning acoustic microscope (SAM) images of the Bakken shale and found that the textural heterogeneity, P wave impedance and velocity, and density increase with increasing maturity (decreasing kerogen content), while textural anisotropy decreases with maturity.

These considerations suggest that observations of variations in VTI anisotropy for the Upper and Lower Bakken may potentially offer an observable proxy for kerogen content (source richness) in the Bakken shales.

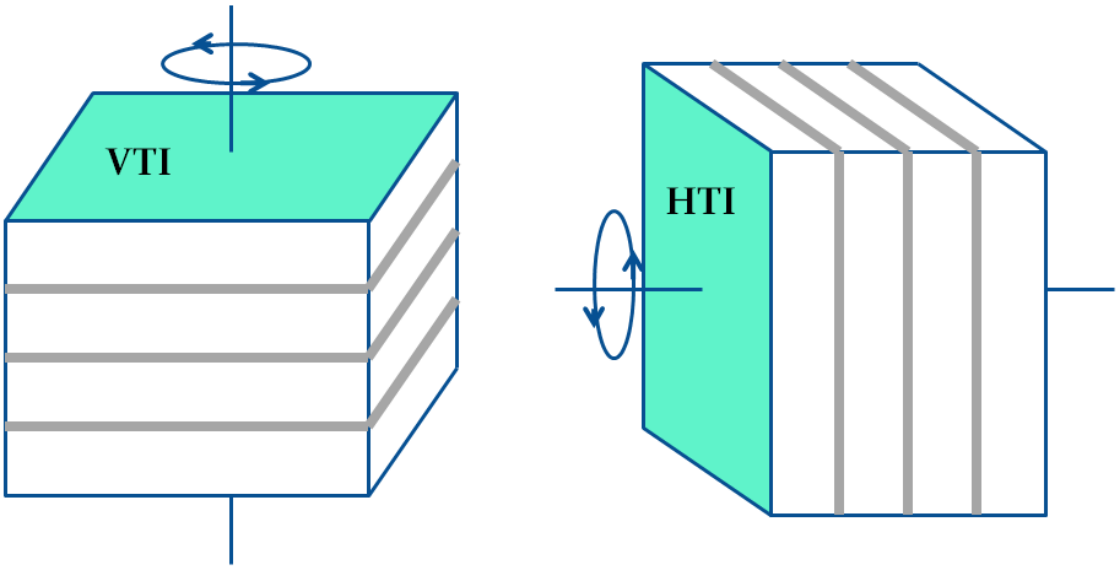

Figure 2.1: VTI and HTI media.

Chapter 3 Well Log Analysis

3.1 INTRODUCTION

The geographic area in this study is located in Mountrail County and Burke County, North Dakota, east of the Nesson Anticline. Figure 3.1 shows the well locations. Well 1 is Annala 11-36H; Well 2 is Deadwood Canyon Ranch 11-5H; Well 3 is Deadwood Canyon Ranch 43-28H; Well 4 is Farhart 11-11H; Well 5 is Rosencrans 44-21H; Well 6 is Edwards 44-9H; Well 7 is Lucy 11-23H. Well 1 to Well 3 are from the Sanish Field while Well 4 to Well 7 are from the Cottonwood Field.

Well log data were acquired by the Sonic Scanner tool developed by Schlumberger. The Sonic Scanner tool has a long receiver array that consists of 13 stations with 8 azimuthal receivers at each station. On both sides of the receiver array, there is a near-monopole transmitter. It also has a third far monopole transmitter and two dipole transmitters. Thus, the Sonic Scanner tool can provide axial, azimuthal and radial measurements, including shear wave propagation.

3.2 LOG DATA ANALYSIS

I analyze the well log data including depth and thickness, density, velocity, Vp/Vs ratio, Young's modulus and Poisson's ratio. The purpose of analyzing the well log data is to characterize the Bakken Formation at the wellbore and to construct models for studying the seismic responses in Chapter 4.

Figure 3.2 shows the well log data for Farhart 11-11H in the Cottonwood Field. The Bakken Formation can be readily identified in the log suite. The Upper and Lower Bakken shales have very high gamma ray responses. Besides the Bakken Formation, the

log data also cover the overlying Lodgepole Formation and part of the underlying Three Forks Formation.

3.2.1Depth and thickness

Figure 3.3 shows a summary of the depth and thickness of the Bakken interval. It can be seen that the Bakken Formation is at a depth of about 10000 ft. It is deeper in the Sanish Field and shallower in the Cottonwood Field. The average depth of the Bakken is 10194 ft in the Sanish Field and is 9505 ft in the Cottonwood Field (Table 3.1). The difference of the average depth between the two fields is 689 ft.

The total thickness of the Bakken is about 100 ft. The Bakken is thicker in the Sanish Field while it is thinner in the Cottonwood Field. The average total thickness of the Bakken is 127.30 ft in the Sanish Field, which is 1.4 times the average thickness in the Cottonwood Field (90.86 ft). Table 3.1 also shows that the thickness of the Upper Bakken shale is quite consistent across all the wells. However, there is dramatic thickness variation of the Middle and Lower Bakken. The increase in the total Bakken thickness in the Sanish Field is mostly caused by the thickening of the Middle Bakken.

3.2.2 Density

Figure 3.4 shows the bulk density of the Lodgepole, the Upper, Middle and Lower Bakken and the Three Forks at Farhart 11-11H. Average values in five intervals are calculated and listed (Figure 3.5). It can be seen that the density decreases dramatically at the Upper and Lower Bakken shales. The Middle Bakken has slightly lower density than the Lodgepole and Three Forks. Data from other wells show similar results. Figure 3.5 plots the average density value of five wells. There is minimal variation in density among these wells. The average density is 2.68 g/cm^3 for the Lodgepole, 2.24 g/cm^3 for both the

Upper and Lower Bakken, 2.62 g/cm^3 for the Middle Bakken and 2.69 g/cm^3 for the Three Forks.

3.2.3 Velocity

Both the P wave and S wave velocities are plotted in Figure 3.6 for Farhart 11-11H. Dots are actual data values. Solid lines are the average values calculated for the selected intervals from the Lodgepole to the Three Forks Formation. It can be seen that the Upper and Lower Bakken have similar velocities, which are quite low compared to all the other intervals. There is a large velocity decrease from the Lodegepole to the Upper Bakken. At this well, P wave velocity drops 48% from 18783 ft/s to 9780 ft/s and S wave velocity drops 43% from 10474 ft/s to 5956 ft/s. There are slight velocity variations within the Middle Bakken because of interval lithology changes. Data from other wells show similar results. Only minimal velocity variation is found among wells. The average P wave velocity is about 9500 ft/s for the Upper and Lower Bakken and about 16000 ft/s for the Middle Bakken. The average S wave velocity is about 5700 ft/s for the Upper and Lower Bakken and around 9400 ft/s for the Middle Bakken.

One of the distinct features of the shear wave propagating through an anisotropic medium is splitting (birefringence) into two different components, which has been observed in both laboratory and in physical models (Cheadle et al., 1991; Tatham et al., 1992), as well as in the field (Lewis et al., 1992; Mueller, 1992; Beckham, 1996; Li and Mueller, 1997). For near-vertical propagation in the medium dominated by vertically aligned fractures (HTI), one component (S1) is polarized parallel to the fracture orientation and the other (S2) is polarized perpendicular to the fracture orientation. The first splitting component mentioned above is referred to as the S1 wave, which propagates faster than the second splitting component, known as the S2 wave. The Sonic Scanner also measures the fast shear (S1) and slow shear (S2) velocities, which are

shown in Figure3.7. The fast shear and slow shear wave velocities are quite similar, which suggests no shear wave splitting. Therefore, no obvious HTI is observed for the Bakken Formation from the well log data.

3.2.4 Vp/Vs ratio

Vp/Vs ratio is the ratio of P wave and S wave velocities. Studies show that there is a correlation between Vp/Vs ratio and lithology (Pickett, 1963; Domenico,1984; Tatham, 1982; Tatham and McCormack, 1991). The typical Vp/Vs value is from 1.84 to 1.99 for limestone, from 1.78 to 1.84 for dolomite, from1.59 to1.76 for sandstone and from 1.70 to 3.00 for shale (Tatham and McCormack, 1991). The Vp/Vs value of shale is in a rather broad range, and it is usually higher than the Vp/Vs value of sandstone, particularly in porous clastic sequences.

Figure 3.8 shows the Vp/Vs ratio of one Bakken wells, Farhart 11-11H. It shows that the Vp/Vs ratio of the Bakken Formation is lower than that of the Lodgepole Formation. The Lodgepole Formation is mainly limestones, therefore, it has a somewhat higher Vp/Vs ratio. The Upper and Lower Bakken shales have slightly lower Vp/Vs ratio than the Middle Bakken, suggesting greater siliceous content, even in the shales, of the upper and lower units. The Vp/Vs ratios of the Bakken Shales are about 1.64, which are quite low for clay-rich shales. Table 3.2 lists the ultrasonic velocities measured on Bakken shale samples reported by Vernik and Liu (1997). Vp/Vs ratios are calculated based on these data. The average Vp/Vs ratio of 13 dry samples is 1.67, which is only slightly higher than the average Vp/Vs ratio I observed in the log data. The oil saturated laboratory sample has the same Vp/Vs value as found in the log data.

3.2.5 Young's modulus and Poisson's ratio

Young's modulus is defined as the stress-strain ratio when a rod is pulled or compressed (Sheriff, 2002). Poisson's ratio is defined as minus the ratio of lateral strain to axial strain in a uniaxial stress state (Mavko et al., 2003).

The definition of anisotropy indicates that a particular physical property varies with direction for anisotropic medium and stays the same in all directions for isotropic medium. The sonic scanner estimates the velocity in both vertical and horizontal directions and/or polarizations, and thus provides the dynamic Young's modus and Poisson's ratio in both vertical and horizontal directions.

Figure 3.9 shows the dynamic horizontal Young's modulus and vertical Young's modulus from the sonic scanner log in the Farhart 11-11H borehole. Average value of each interval is calculated from Lodgepole to Three Forks. It can be seen that the Upper and Lower Bakken shales have lower Young's modulus than the rest intervals. For the Lodgepole, Three Forks and the Middle Bakken, the vertical and horizontal Young's modulus are quiet similar. However, for the Upper and Lower Bakken shales, the vertical Young's modulus is much less than the horizontal Young's modulus. Take the Lower Bakken as an example, the average horizontal value is 4.21 Mpsi, which is 1.55 times the vertical value (2.72Mpsi).

Figure 3.10 shows the dynamic horizontal Poisson's ratio and vertical Poisson's ratio in the Farhart 11-11H well. Average values of each interval is also calculated and listed. The vertical and horizontal Poisson's ratios are quite similar for the Lodgepole, Three Forks and the Middle Bakken. There are distinct differences between the horizontal and vertical Poisson's ratio for the Upper and Lower Bakken shales. The vertical value is much greater than the horizontal value. For example, the average vertical values of both the Upper and Lower Bakken shales are 2.22, which are 1.69 times the

average horizontal values (0.13). It can also be noticed that the variation of the horizontal Poisson's ratio with changing lithology is much greater than the variation of the vertical Poisson's ratio. This is consistent with a strong VTI orientation of the anisotropy in the Upper and Lower Bakken.

Figure 3.11 shows two Young's modulus-Poisson's ratio crossplots. Figure 3.11a shows vertical Young's modulus versus vertical Poisson's ratio. Figure 3.11b shows horizontal Young's modulus versus horizontal Poisson's ratio. All the data here can be divided into three groups. The first group is the Upper and Lower Bakken shales in the red ellipses. From the vertical plot to the horizontal plot, the shales show a decrease in Poisson's ratio and increase in Young's modulus, and thus shift from the more brittle region to the more ductile region which are separated by the red line. The second group is the Lodgepole limestone in dark blue. The third group consists of the Middle Bakken and Three Forks, which shows the similarity between these two intervals. This figure shows that from a mechanical point of view, the Upper and Lower Bakken shales are very different from all the rest of the intervals.

Table 3.3 lists the ratios of horizontal Young's modulus to vertical Young's modulus and the ratios of horizontal Poisson's ratio to vertical Poisson's ratio for different layers at different wells. If the rock is isotropic, either the Young's modulus or the Poisson's ratio should be the same in all directions. Therefore, the ratio of horizontal to vertical properties should be 1. On the contrary, if the rock is anisotropic, then the ratio should deviate from unity. The greater the difference between the ratio and 1, the more anisotropic the rocks is. It can be seen from Table 3.3 that the ratios of both the Upper Bakken and the Lower Bakken are far from 1 while the ratios of the Middle Bakken are close to 1. This suggests that, from the log data, the Upper Bakken and the Lower Bakken

may be considered quite anisotropic (VTI) while the Middle may be considered as essentially isotropic.

3.3 SUMMARY

Well log data acquired by the Sonic Scanner are analyzed for both the Cottonwood and Sanish Fields. Depth and thickness of the Bakken are compared for all the wells. Density, velocity, Vp/Vs ratio, Young's modus and Poisson's ratio are analyzed and averaged for all five intervals, i.e., the Lodgepole, Upper Bakken, Middle Bakken, Lower Bakken and Three Forks. It shows that the Bakken Formation is about 100 ft thick and at a depth of about 10000 ft. The Bakken Formation is deeper and thicker in the Sanish Field and is shallower and thinner in the Cottonwood Field. The Upper and Lower Bakken shales have similar characters, and can be distinguished from other intervals from the log data. The Upper and Lower Bakken shales are characterized by low density and low P and S wave velocities and low Vp/Vs ratios. The Vp/Vs ratio of the Bakken shale is slightly lower than that of the Middle Bakken. Therefore the Vp/Vs ratio may not be an effective lithology indicator to differentiate between the shales and Middle Bakken.

The anisotropy of Bakken intervals can be estimated from borehole data. For the Upper and Lower Bakken shales, the vertical Young's modulus is much less than the horizontal Young's modulus while the vertical Poisson's ratio is much greater than the horizontal Poisson's ratio. However, the ratios of horizontal to vertical Young's modulus and Poisson's ratio of the Middle Bakken are close to one. The difference in mechanical (elastic) properties in different directions together with the observation that S1 and S2 are almost the same suggests that the Upper and Lower Baken shales are anisotropic while the Middle Bakken may be considered isotropic.

Although there is some variation of physical properties among wells, there are no remarkable differences, except in depth and thickness, between the Sanish Field and the Cottonwood Field.

No	Well Name	Field	Depth (ft)	Thickness (ft)			
				Total Bakken	Upper Bakken	Middle Bakken	Lower Bakken
1	ANNALA 11-36H	SANISH	10371	118.70	19.00	55.30	44.40
2	DEADWOOD CANYON RANCH 11-5H		10140	133.90	17.10	67.90	48.90
3	DEADWOOD CANYON RANCH 43-28H		10071	129.30	15.00	68.10	46.20
4	FARHART 11-11H	COTTONWOOD	9629	94.92	14.12	42.80	38.00
5	ROSENCRANS 44-21H		9381	86.80	16.34	34.63	35.83
-	Average of 1-3	SANISH	10194	127.30	17.03	63.77	46.50
-	Average of 4-5	COTTONWOOD	9505	90.86	15.23	38.72	36.92
-	Average of 1-5	-	9918	112.72	16.31	53.75	42.67

Table 3.1: Depth and thickness of the Bakken Formation.

Type	Depth(ft)	Vp(0) (km/s)	Vsv(0) (km/s)	Vp/Vs	Average of Vp/Vs
Dry	7570	3.13	1.88	1.67	1.67
	8634	3.02	1.76	1.72	
	9831	3.41	2.07	1.65	
	10164	3.38	2.12	1.59	
	10487	3.18	1.93	1.65	
	10495	3.62	2.22	1.63	
	10575	3.36	2.06	1.63	
	10733	3.46	2.00	1.73	
	10734	3.51	2.03	1.73	
	10931	3.29	1.86	1.77	
	11230	4.21	2.52	1.67	
	11246	3.72	2.25	1.65	
	11280	3.85	2.40	1.60	
Brine-saturated	10931	3.34	1.86	1.80	1.80
Silicon oil-saturated	11280	3.96	2.42	1.64	1.64

Table 3.2: Ultrasonic velocities and corresponding Vp/Vs ratios of the Bakken shale (Adapted from Vernik and Liu, 1997).

		Young's Modulus Horizontal / Vertical					Poisson's Ratio Horizontal / Vertical				
		Rosencrans 44-21H	Farhart 11-11H	DCR 43-28H	DCR 11-5H	Annala 11-36H	Rosencrans 44-21H	Farhart 11-11H	DCR 43-28H	DCR 11-5H	Annala 11-36H
Upper Bakken Shale		1.62	1.52	1.74	1.47	1.52	0.5	0.59	0.5	0.6	0.58
Middle Bakken	C	1.00	1.04	1.20	1.04	0.98	0.99	0.95	0.79	0.94	1.02
	B	0.93	0.97	1.12	1.05	0.98	1.09	1.04	0.84	0.93	1.03
	A	1.01	1.02	1.08	1.02	1.09	0.94	0.98	0.91	0.97	0.89
Lower Bakken Shale		1.64	1.55	1.67	1.60	1.60	0.52	0.58	0.54	0.55	0.54

Table 3.3: Horizontal to vertical ratios of Young's modulus and Poisson's ratio.

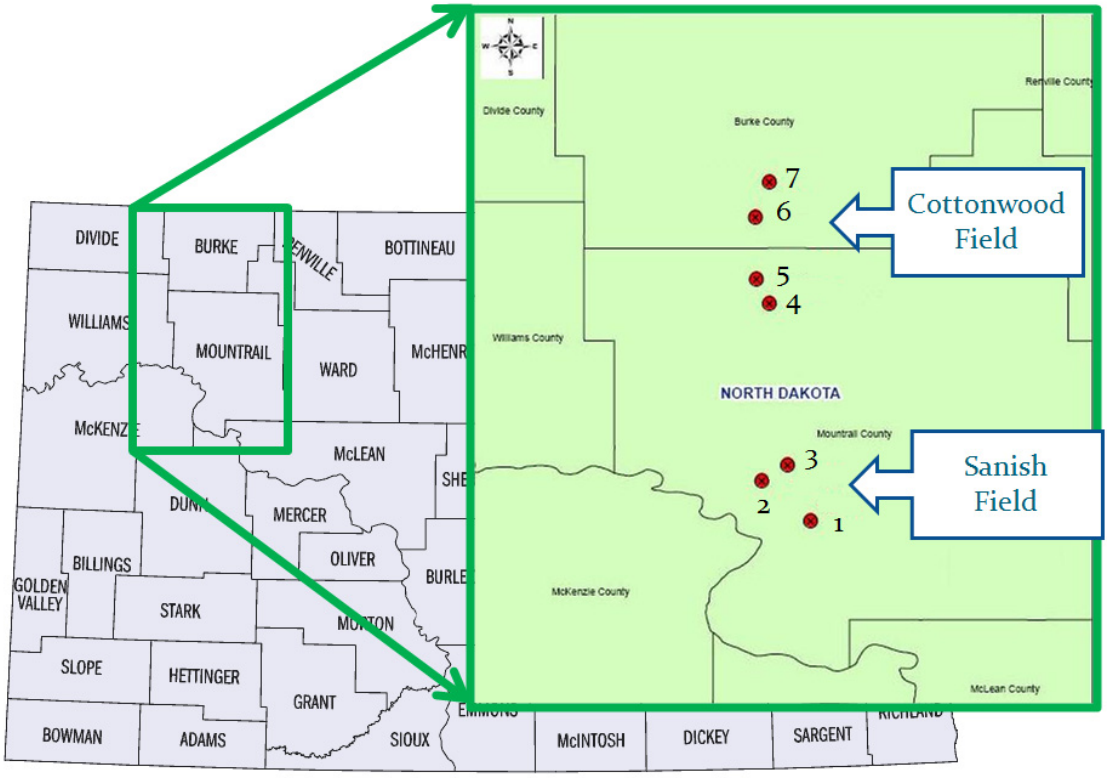

Figure 3.1: Well locations. Well 1 is Annala 11-36H; Well 2 is Deadwood Canyon Ranch 11-5H; Well 3 is Deadwood Canyon Ranch 43-28H; Well 4 is Farhart 11-11H; Well 5 is Rosencrans 44-21H; Well 6 is Edwards 44-9H; Well 7 is Lucy 11-23H. Well 1 to Well 3 are from the Sanish Field while Well 4 to Well 7 are from the Cottonwood Field.

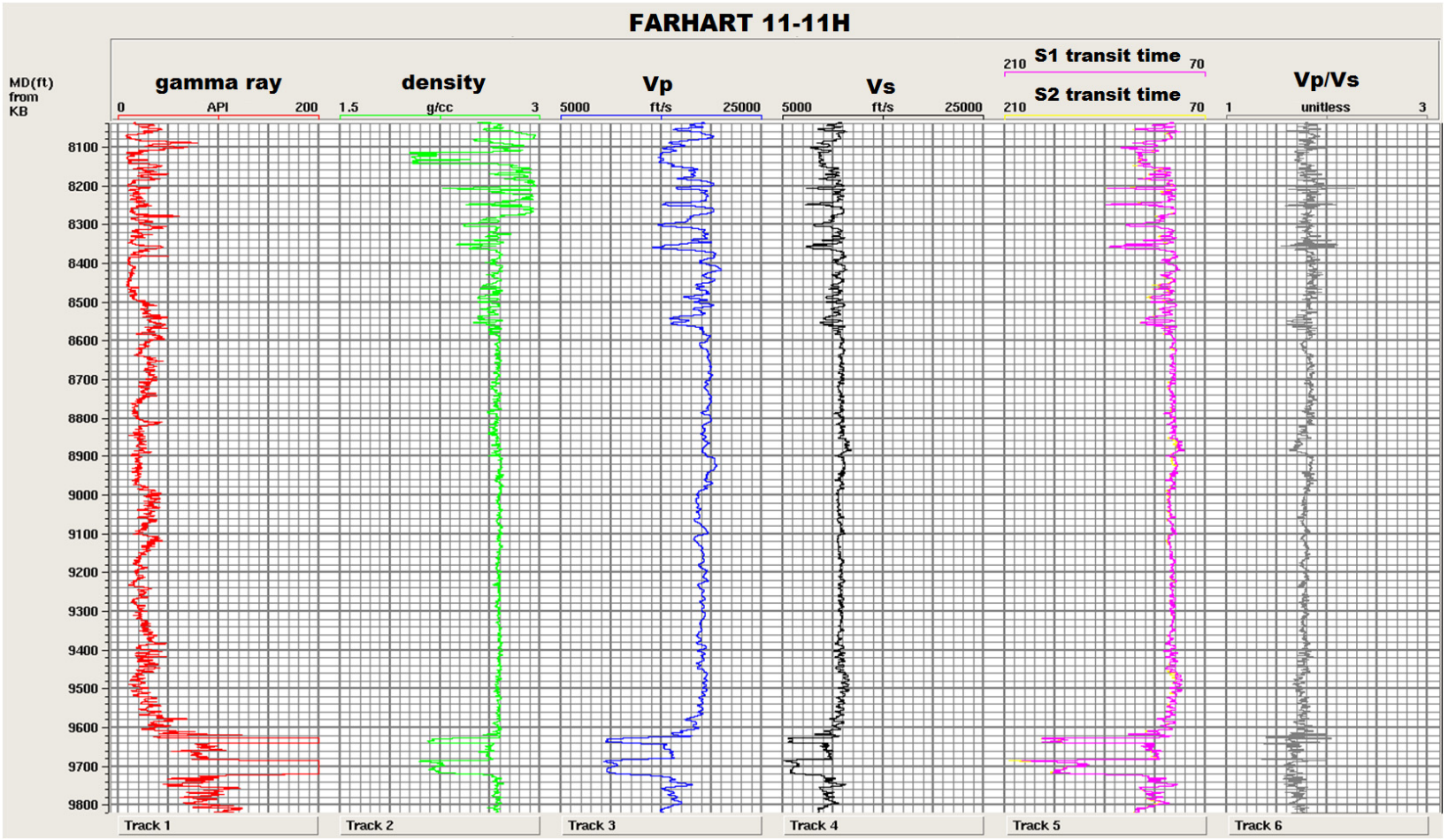

Figure 3.2: Well log data for Farhart 11-11H. Log tracks shown here are gamma ray, density, P wave velocity, S wave velocity, faster shear (S1) and slow shear (S2) transit time, and Vp/Vs ratio.

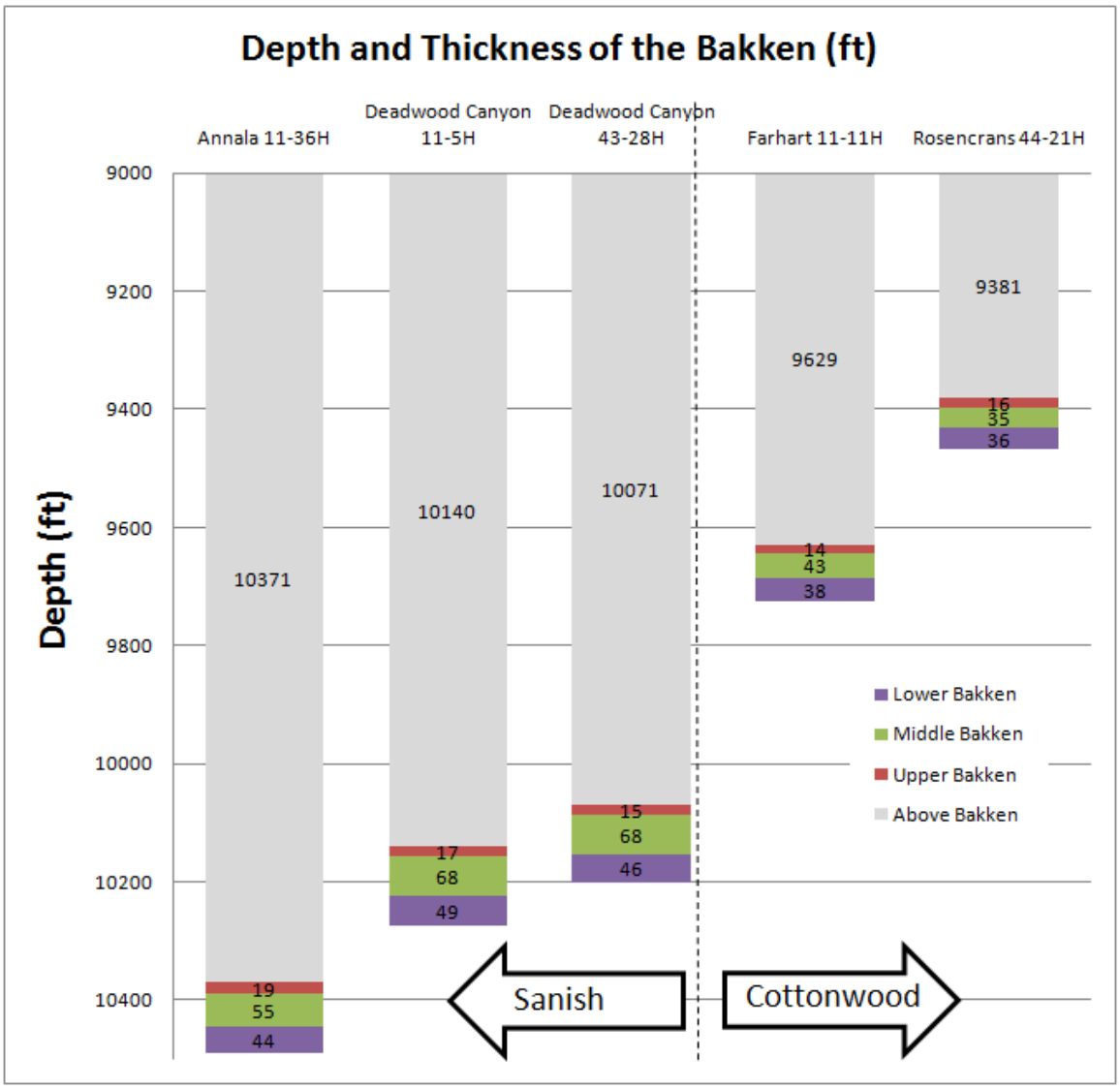

Figure 3.3: Depth and thickness of the Bakken. Depth and thickness values are in ft.

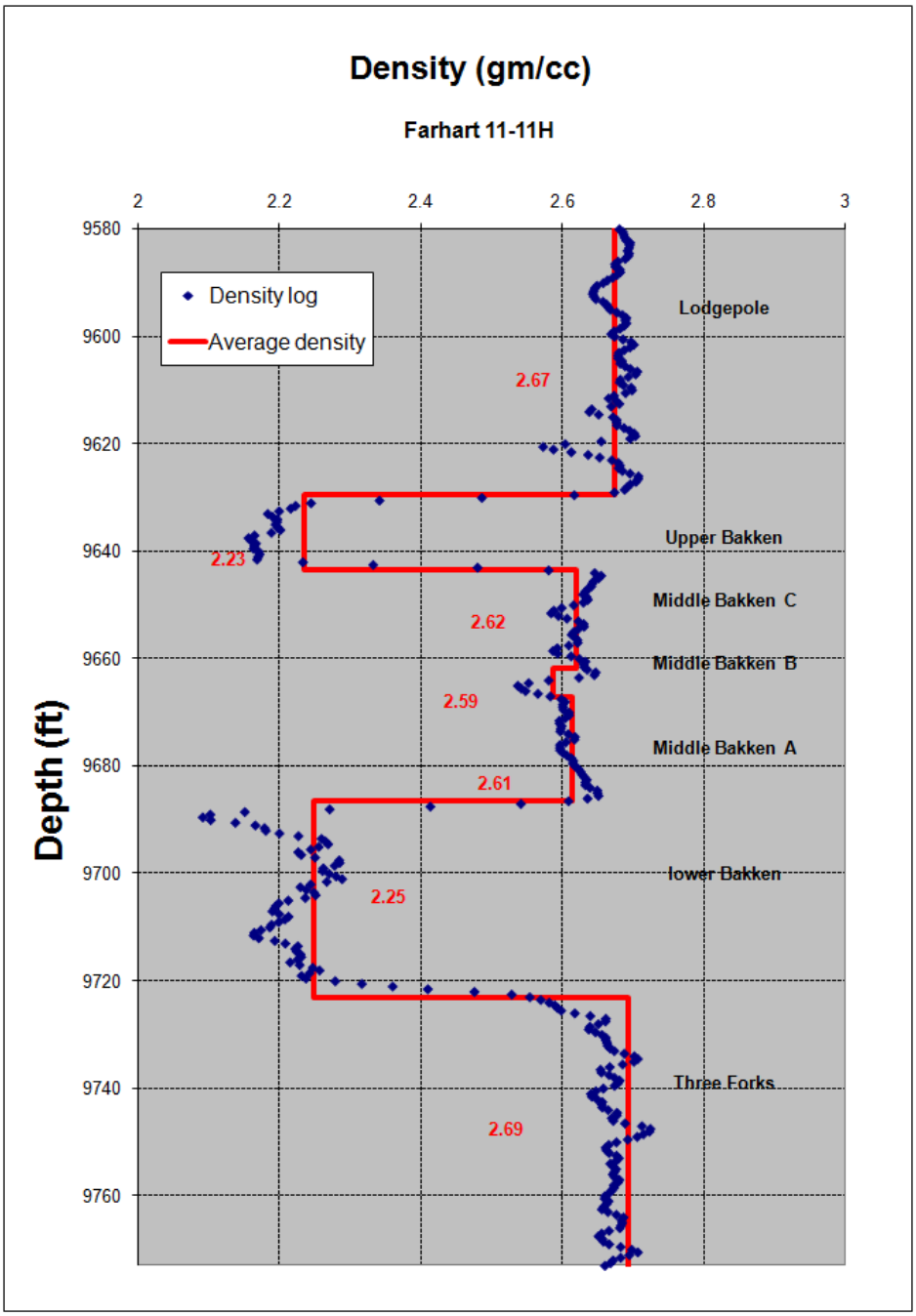

Figure 3.4: Density. Dots are density log data. Solid lines are average density of each interval.

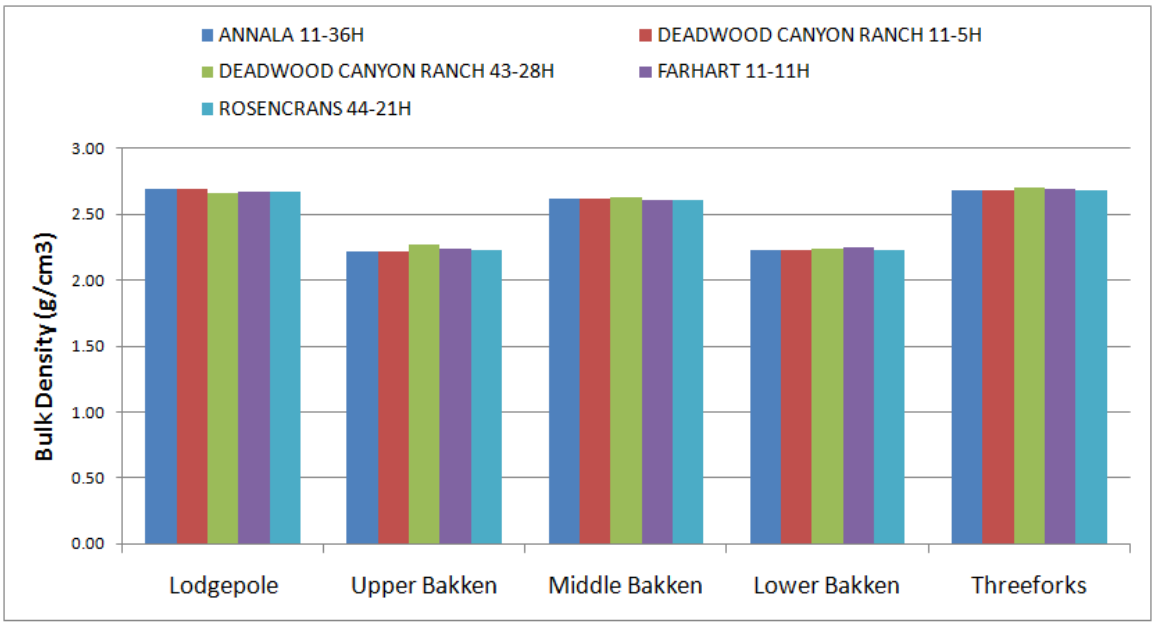

Figure 3.5: Average density.

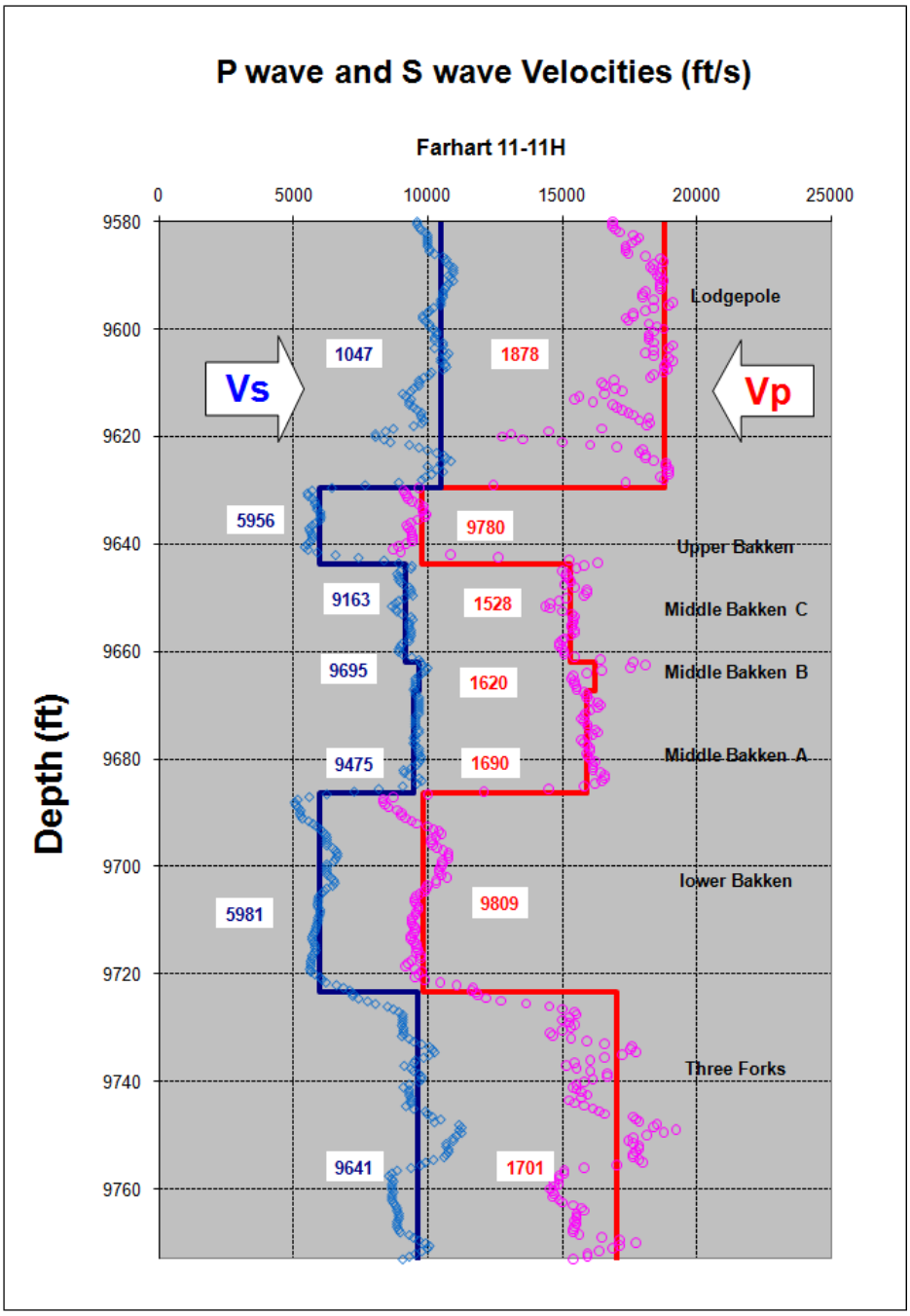

Figure 3.6: P wave and S wave velocities. Dots are log data. Solid lines are average velocities of each interval.

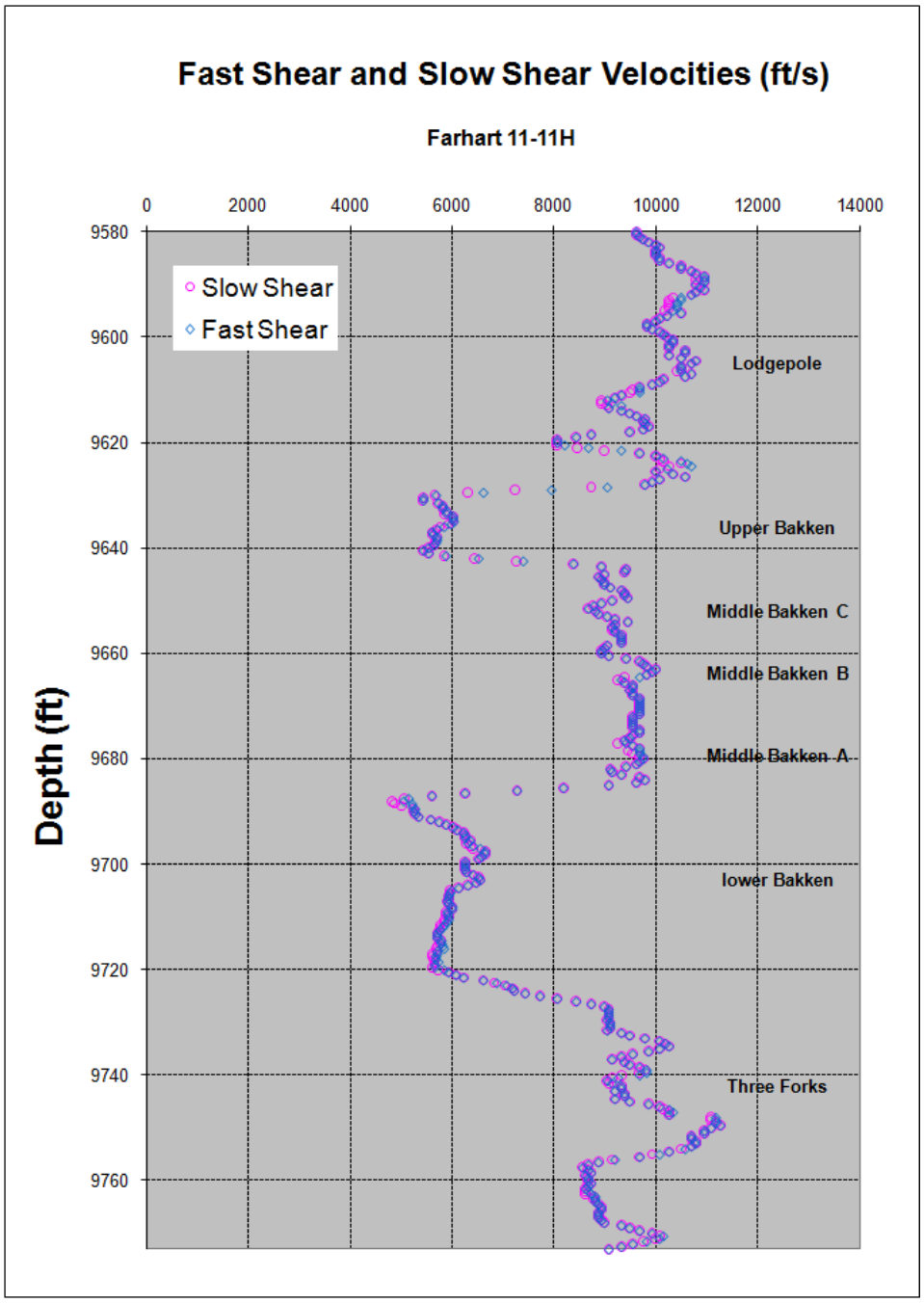

Figure3.7: Fast shear (S1) and slow shear (S2) wave velocities.

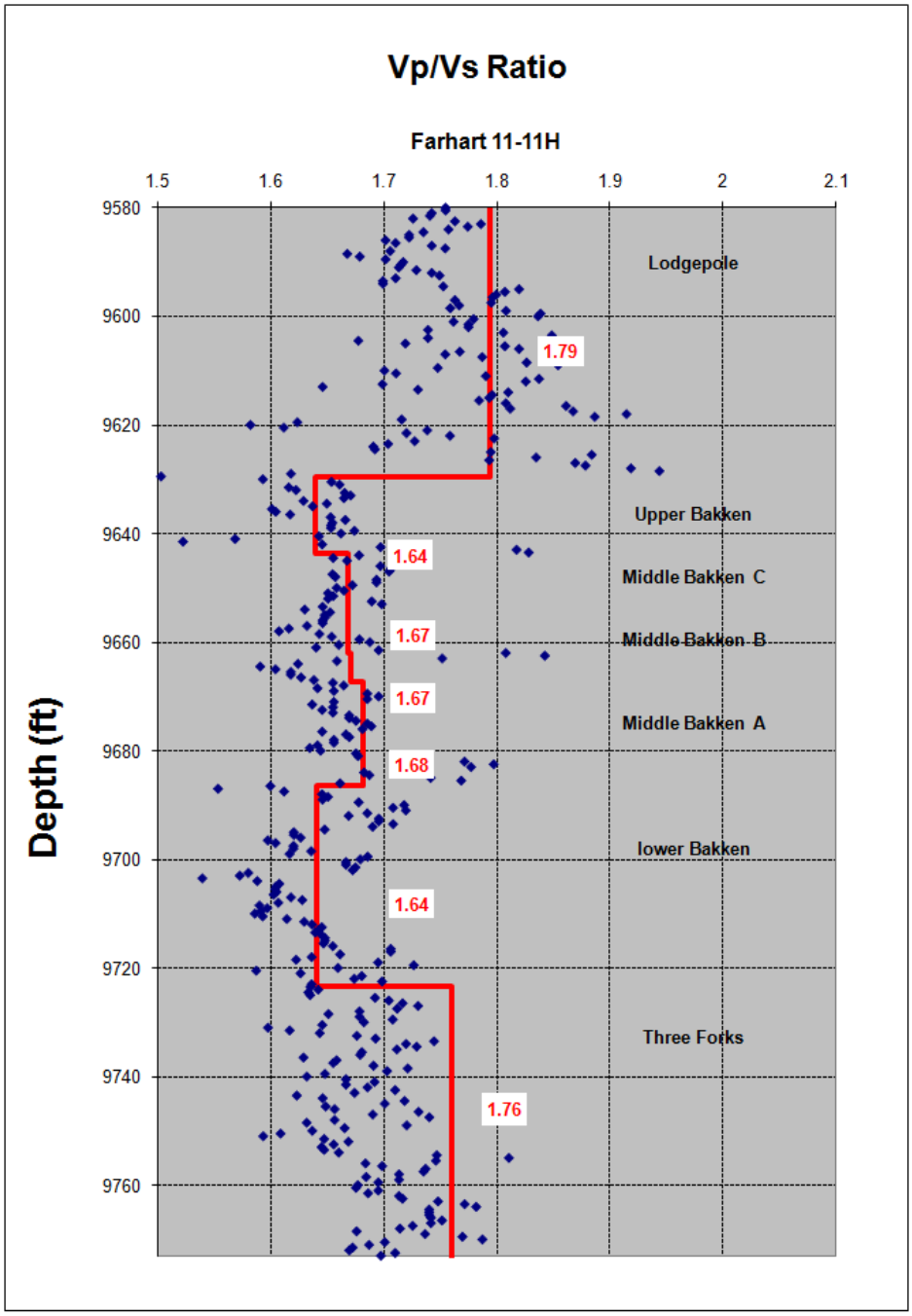

Figure 3.8: Vp/Vs ratio. Dots are from log data. Solid lines are average Vp/Vs ratios of each interval.

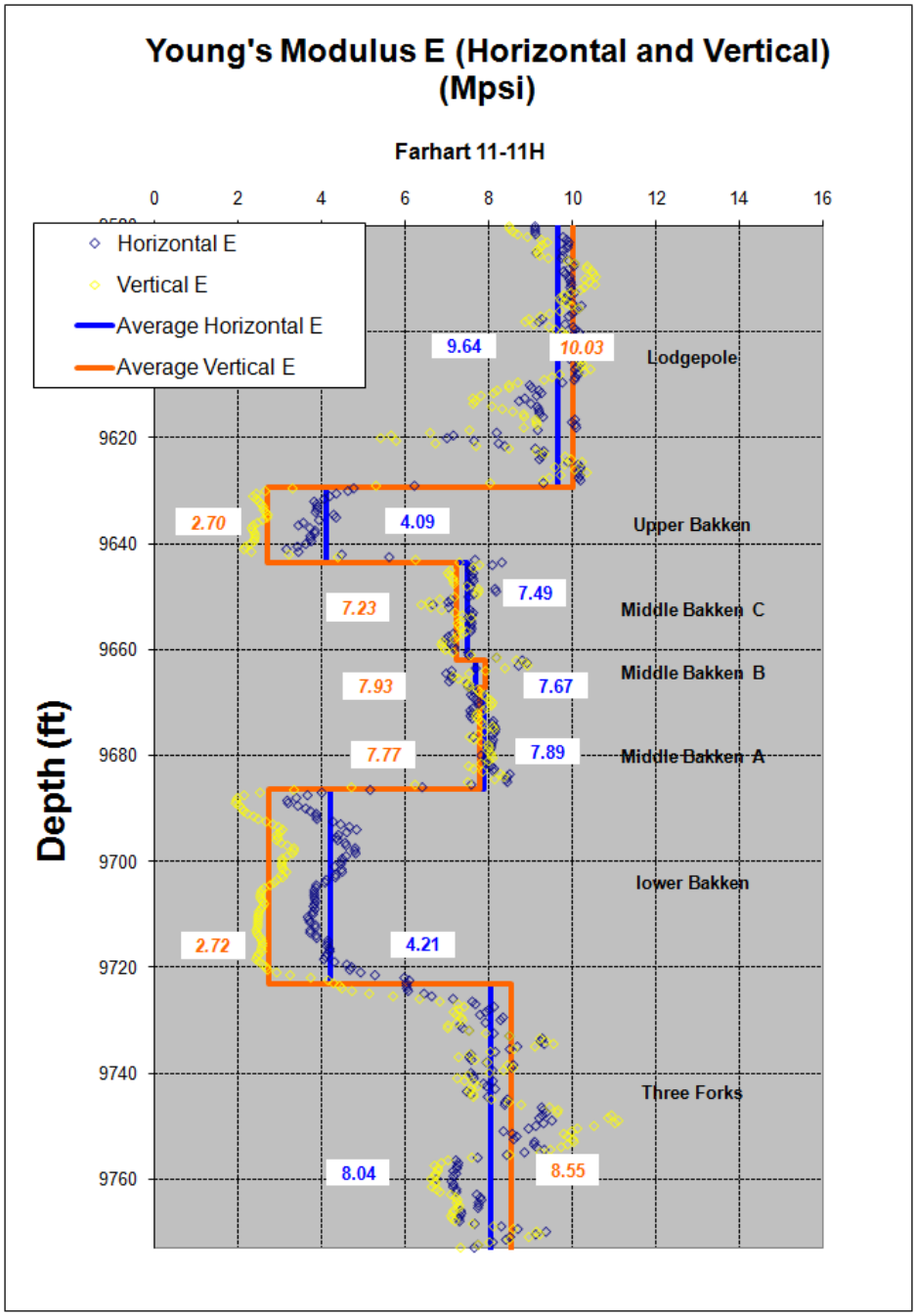

Figure 3.9: Young's modulus. Dots are horizontal and vertical Young's modulus data. Solid lines are average horizontal and vertical values of each interval.

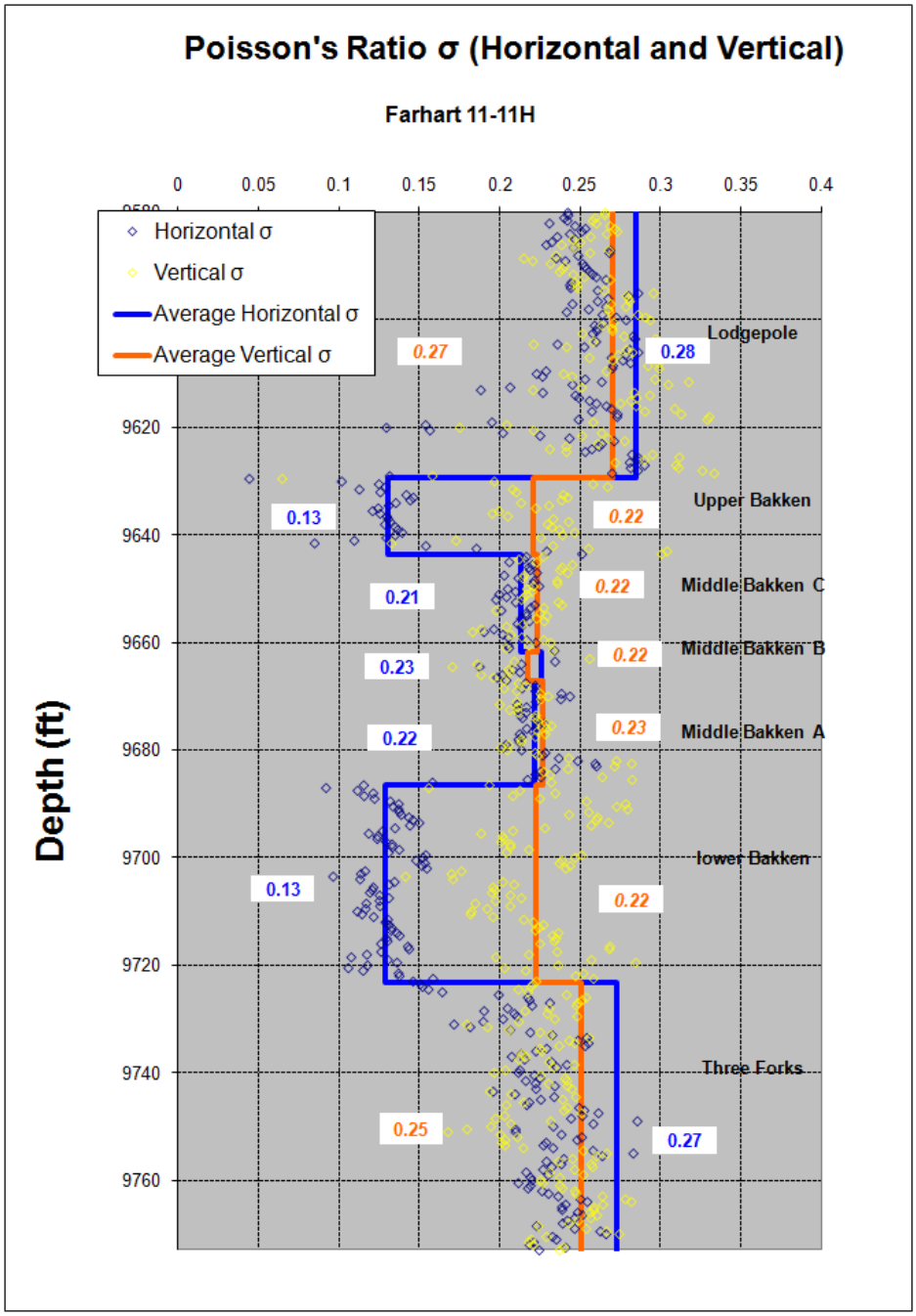

Figure 3.10: Poisson's ratio. Dots are horizontal and vertical Poisson's ratio data. Solid lines are average horizontal and vertical values of each interval.

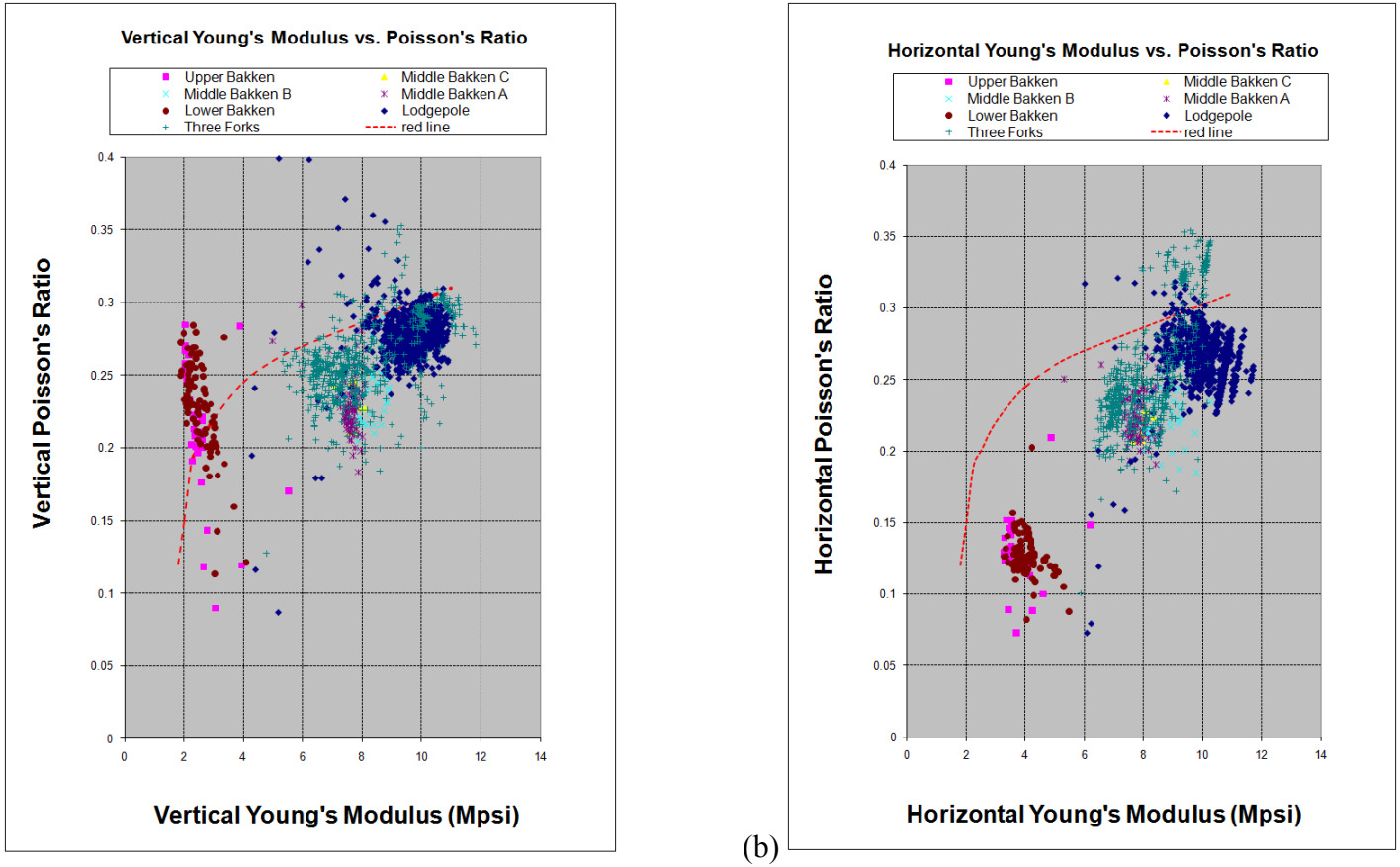

Figure 3.11: Young's modulus versus Poisson's ratio. (a) Vertical Young's modulus versus vertical Poisson's ratio. (b) Horizontal Young's modulus versus horizontal Poisson's ratio. Red line (taken from DFI, 2005) separates the more brittle region on the upper left corner from the more ductile region on the lower right corner.

Chapter 4 Seismic Modeling

4.1 INTRODUCTION

In Chapter 3, I analyzed the well log data for wells from both the Cottonwood and the Sanish fields. Average values of density and wave velocities were calculated for all the intervals from the Lodgepole to the Three Forks. In this chapter, I use these information to construct numerical models to predict the seismic responses of the Bakken. I construct various types of models for both the Cottonwood Field and the Sanish Field, including isotropic models, VTI and HTI models for parts of the Bakken, and the combination of VTI and HTI model. Each model consists of five homogenous, continuous layers. To analyze the effect of bed thickness, I use the actual layer thickness of the Bakken Formation and to minimize interference among reflections, a much greater thickness for comparison. Table 4.1 lists all the models shown in this chapter.

Full offset elastic synthetic seismograms are then generated utilizing a reflectivity algorithm (Sil and Sen, 2008). The code provides analytic solutions to seismic reflectivity for a one-dimensional model, but does accommodate variations in source-receiver offset and azimuth with respect to HTI anisotropy. The software does accommodate attenuation. Note that our modeling algorithm includes all converted waves and multiple reflections.

4.2 ISOTROPIC MODEL

For the modeling experiments conducted in this chapter, I assume that there are 5 layers. Everything above the Bakken Formation is considered as one single layer. The second layer is the Upper Bakken Shale, the third is the Middle Bakken, and the fourth

layer is the Lower Bakken Shale. The fifth layer (half space) is everything below the Bakken Formation. I first assume that all five layers are isotropic (Figure 4.1).

P wave velocity, S wave velocity and density data are from the well log analysis discussed in Chapter 3. Model 1 uses the actual Bakken thickness of the Cottonwood field. A much thicker Bakken model (Model 2) is built as a reference, in which each layer thickness of the Upper, Middle and Lower Bakken is 100 m. Model parameters for Model 1 and Model 2 are listed in Table 4.2 and Table 4.3, respectively.

Full offset elastic synthetic seismograms are then generated using the isotropic models. The seismic responses show the simplest case in which there is no anisotropy.

4.2.1 Explosive source and vertical point source

I apply two different types of sources in the modeling experiments to generate synthetic seismic data. Figure 4.2 and Figure 4.3 show the two-component synthetic seismograms (shot record) for Model 1. Figure 4.2 uses explosive source in the upper layer and Figure 4.3 uses vertical point source. In both Figure 4.2 and Figure 4.3, the vertical component is on the left, and the radial component is on the right. Offset varies from 0 to 6 km.

Note that different scalars are used for plotting the results of the explosive and vertical point source seismograms for better display. However, in this thesis, a constant scalar is applied to all data using vertical point source. Therefore, wiggle plots for all models using vertical point source are comparable (e.g., vertical and radial components, Sanish Field and Cottonwood Field responses).

The explosive source, like dynamite, will result in two primary events. Figure 4.2 shows P wave reflection on top and mode converted P-SV reflection at bottom, which consists of downgoing P wave and upgoing mode-converted SV wave.

The vertical point source is used to simulate the Vibroseis, but with an vertical impulse on the surface. In Figure 4.3, three main events can be easily identified. The first event is P wave reflection. The second event is mode converted P-SV reflection. The third event is pure SV wave, which does not exist when near-surface explosive source is used. Such direct SV waves are commonly observed in large-offset VSP surveys with a Vibroseis source.

Different choice of source results in different seismic responses. Since we have a Vibroseis seismic survey in the Cottonwood Field, I will focus on the vertical point source synthetic seismograms in this work. All synthetic seismograms in the following sections are created by using vertical point source.

4.2.2 Thickness effect

Figure 4.4 shows the synthetic seismograms for a thick (300 m Bakken) model (Model 2). The difference between Model 1 and Model 2 is only layer thicknesses for the Upper, Middle and Lower Bakken. Model 2 uses 100 m for each Bakken layer, while Model 1 uses the actual thickness of the Bakken Formation.

In Figure 4.4, all layers in the model can be identified. However, when the layer thickness reduced from 100 m to the actual Bakken thickness, which is 4.42 m for the Upper Bakken, 12.95 m for the Middle Bakken and 11.28 m for the Lower Bakken, it is no longer possible to resolve each layer individually. There is interference among the reflections from the Upper, Middle and Lower Bakken. In Figure 4.3, each event is not a single reflector response, but rather a combination of the reflections from all three thin layers.

4.3 VTI MODEL

Shales are known to be anisotropic (Johnston and Christensen, 1995). Ultrasonic velocity and anisotropy of the Bakken Shales were measured and studied by laboratory measurements of the Bakken cores (Vernik and Nur, 1992; Vernik and Liu, 1997) to confirm that the Bakken Shales are transversely isotropic. In Chapter 3, I showed that from well log data, both the Upper Bakken and the Lower Bakken can be considered as VTI media.

In Model 3, I assume that the anisotropy of the Upper Bakken Shale and the Lower Bakken Shales have VTI symmetries; all other layers are isotropic. The values of P wave velocity, S wave velocity, density, and layer thickness are the same as isotropic models described in section 4.2.

Anisotropy parameters of the Bakken Shales are based on the data reported by Vernik and Liu (1997). By comparing the depth values of these samples with the Bakken depth of this study, I choose the anisotropy parameters of an sample at 9831 ft and apply that to both the Upper and the Lower Bakken Shales in my models.

Model parameters are shown in Table 4.4.

4.3.1 VTI information in the surface seismic response

The difference between seismic response generated by the VTI model (Model 3) and isotropic model (Model 1) is caused by two VTI layers, the Upper Bakken Shale and the Lower Bakken Shale. Therefore, this difference contains VTI information. I subtract the isotropic response from the anisotropic seismic response to observe sensitivity to the VTI information for the actual Bakken thickness model (Model 3, Figure 4.6) and thick model (Model 4, Figure 4.7). Once these sensitivities are understood, we will need to evolve interpretative strategies to apply the results in the field.

Figure 4.6 shows the difference between the VTI anisotropic seismic response and the isotropic seismic response. For all difference plots, the data were not scaled (gained). Brighter color suggests more difference between the VTI and isotropic seismic responses while black indicates no difference. P-P, P-SV and SV-SV respond differently to VTI anisotropy. The vertical component and the radial component also have different character.

For P wave, sensitivity to the anisotropy is more pronounced at mid to far offset. The vertical component is more anisotropic than the radial component, which is consistent with the fact that the vertical component is originally stronger than the radial component. SV-SV wave is more sensitive to anisotropy at mid offset. The radial component is more sensitive to anisotropy probably because most of the SV-SV energy goes horizontally. For P-SV wave, the near offset radial component and the mid to far offset vertical component are more sensitive to anisotropy.

4.3.2 Thickness effect

Figure 4.7 shows the difference between the VTI and the isotropic seismic responses using the thick model (Model 4). Note that color scheme for the thick model plot is different from that of actual thickness model plot for better display. From the thick model (Figure 4.7) to the actual Bakken thickness model (Figure 4.6), it can be seen that with decreasing layer thickness in the model, the VTI anisotropy information is getting less obvious.

Figure 4.7 shows that for the thick model, the radial component of SV-SV is most sensitive to anisotropy variation, which is not observed in the actual Bakken thickness model case. On the contrary, the actual Bakken example (Figure 4.6) shows that the P-SV response is more sensitive than P-P and SV-SV. This suggests that layer thickness interferes with the sensitivity of anisotropy.

For the actual thickness model, the seismic responses are composite reflections. Therefore, the VTI anisotropies of the Upper and Lower Bakken shales are buried in the interference effects of the seismic responses of the whole Bakken package. Layer thickness affects the total seismic responses. As a result, it also interferes with the anisotropy character.

4.4 HTI MODEL

In HTI models (Figure 4.8), focus on the Middle Bakken. This unit is where natural fractures may occur and contribute to the permeability. It is also the unit that is hydraulically fractured during well completion.

Sturm and Comez (2009) suggested that there are natural fractures dipping from 70-90° in the Middle Bakken. Therefore, I assume that there may be vertical fractures in the Middle Bakken member, so the Middle Bakken has HTI symmetry. The remaining four layers are isotropic. The values of P wave velocity, S wave velocity, density, and layer thickness are the same as isotropic models described in section 4.2.

Let us first consider the case in which the Middle Bakken has one set of vertical fractures oriented normal to the x-direction with crack density of 8% whereas all the rest four layers are isotropic. HTI parameters are calculated based on the method proposed by Bakulin et al. (2000).

4.4.1 Azimuthal anisotropy

I choose five source-receiver azimuths of 0°, 30°, 45°, 60° and 90°, to generate seismic shot records. Azimuth here is the angle between source-receiver line and the orientation of fractures. Figure 4.9 shows the direction of vertical aligned fractures and five azimuths. It is shown that the vertical fractures are parallel to Y axis, and perpendicular to X axis. Azimuth 0° means source-receiver line is perpendicular to the

orientation of fractures. Azimuth 90° means source-receiver line is parallel to the orientation of fractures.

Figure 4.10 shows a set of synthetic seismograms generated using Model 5 (model parameters are shown in Table 4.6), in which actual Bakken thicknesses are used, for 0°, 30°, 45°, 60° and 90° azimuths. Figure 4.11 shows another set of synthetic seismograms generated using thick model (Model 6, model parameters are shown in Table 4.7) for 0°, 30°, 45°, 60° and 90° azimuth. In both sets, there are differences between either two azimuths (Figure 4.12 for the actual thickness model and Figure 4.13 for the 300 m thick Bakken model). These figures show variations with azimuth caused by the presence of vertical aligned fractures or cracks. As expected, the greatest azimuthal difference is between 0° and 90°. The difference between azimuths of 0° and 90° for the actual Bakken thickness model is more subtle than that is observed for the thick model. Compared with the thick model, azimuthal anisotropy of the actual Bakken thickness model is reduced with decreasing layer thicknesses.

4.4.2 Crack density, g and fluid content

Figure 4.14 shows the normal and tangential weaknesses (as introduced by Hsu and Schoenberg, 1993, see Chapter 2, section 2.4) versus crack density e (as defined by Hudson, 1980; see equation(1.16)) for dry and wet (oil or water saturated) cracks. ΔN is the normal weakness and ΔT is the tangential weakness. I use the Vp/Vs of the Middle Bakken, which is 1.67, therefore the squared Vs/Vp ratio g (see equation(1.22)) is 0.357. It shows that weaknesses are proportional to crack density e. If the cracks are filled with liquid, the normal weakness ΔN will be reduced while the tangential weakness ΔT remains unchanged.

Figure 4.15 shows the normal and tangential weaknesses versus g. Crack density e is 8%. Here g = 0.2 is corresponding to Vp/Vs = 2.24 and g = 0.5 is corresponding to

Vp/Vs = 1.41. For the Middle Bakken, Vp/Vs = 1.67, therefore g = 0.357. It can be seen that with increasing g (decreasing Vp/Vs), tangential weaknesses ΔT for both dry and wet cracks increase slightly. The normal weakness ΔN for dry crack decreases with increasing g (decreasing Vp/Vs). The decrease is faster for lower g (higher Vp/Vs). When g is greater than 0.4, the decrease of ΔN slows down.

Figure 4.16 shows anisotropy parameters versus crack density e for dry and wet cracks. $\varepsilon^{(v)}$, $\delta^{(v)}$ and $\gamma^{(v)}$ are anisotropy parameters for HTI media. Here Vp/Vs is 1.67, therefore g is 0.357. It shows that $\varepsilon^{(v)}$, $\delta^{(v)}$ and $\gamma^{(v)}$ are all proportional to crack density e. $\varepsilon^{(v)}$ is most affected by fluid fill in the cracks among the three HTI anisotropy parameters. $\gamma^{(v)}$ is the same for both dry and wet cracks, which indicates that fluid content has no influence on $\gamma^{(v)}$.Figure 4.17 shows anisotropy parameters versus crack density e for dry and wet cracks. $\varepsilon^{(v)}$, $\delta^{(v)}$ and $\gamma^{(v)}$ are anisotropy parameters for HTI media. Crack density is 8%. It can be seen that $\varepsilon^{(v)}$ is not affected by variation in g. $\gamma^{(v)}$ becomes more negative with increasing g (decreasing Vp/Vs). With increasing g (decreasing Vp/Vs), $\delta^{(v)}$ decreases for wet cracks but increases for dry cracks. The difference of $\delta^{(v)}$ between wet and dry cases is getting smaller with increasing g, and $\delta^{(v)}$ is the same for wet and dry cracks when g is 0.5 (equivalently, Vp/Vs = 1.41).

4.4.3 HTI information

The difference between seismic responses generated by the HTI model and isotropic model is caused by HTI of the Middle Bakken. Therefore, this difference contains HTI information. I subtract the isotropic response from the anisotropic seismic response to get the sensitivity to HTI information. As discussed in 4.4.2, crack density e and fluid content will affect the anisotropy parameters. Therefore, they will also affect the HTI information in synthetic seismograms.

To investigate the effect of crack density and fluid fill in the cracks, I construct four models. In Model 5 and Model 8, crack density e is 8%. In Model 7 and Model 9, crack density is 4%. In Model 5 and Model 7, cracks are dry. In Model 8 and Model 9, cracks are wet (oil or water saturated). Model parameters for Model 5, Model 7, Model 8 and Model 9 are listed in Table 4.6, Table 4.8, Table 4.9 and Table 4.10, respectively. Corresponding HTI information is shown in Figure 4.18, Figure 4.19, Figure 4.20 and Figure 4.21. Note the source-receiver line is perpendicular to crack orientation.

First, let us look at the HTI information for different crack densities in dry crack cases. Figure 4.18 and Figure 4.19 show the difference between HTI anisotropic seismic response and isotropic seismic response using crack density of 8% and 4%, respectively. Similar to VTI anisotropy, P-P, P-SV and SV-SV also respond differently to HTI anisotropy. As discussed in section 4.2, P-SV carries more VTI information than P-SV or SV-SV. However, here SV-SV carries more HTI information than P-SV or P-P. Among the three, P-P is the least affected one by HTI.

Next, I change models from dry crack to wet (oil or water saturated) crack. Figure 4.20 and Figure 4.21 are generated using crack density of 8% and 4%, respectively. It can be seen that changing from dry crack to wet crack, the HTI information in SV-SV is slightly affected while the HTI information in both P-P and P-SV is greatly reduced. This indicates that SV-SV seismic response is least affected by fluid fill in the cracks.

Models with higher crack densities show more influence of the fluid on anisotropy than models with lower crack densities. Anisotropies caused by dry cracks are slightly more sensitive to crack densities than anisotropies caused by wet cracks.

4.5 COMBINATION OF VTI AND HTI MODEL

In the previous sections, I showed VTI and HTI models of the Bakken Formation, in which VTI and HTI are analyzed separately to address the sensitivity of each

parameter. In this section, I build a set of models that combine the VTI and HTI models (Figure 4.22). There are also five layers in each model. The top and bottom layers are isotropic while the middle three layers are anisotropic. The Upper Bakken and the Lower Bakken have VTI symmetries. The Middle Bakken has HTI symmetry. The source-receiver line is perpendicular to crack orientation. I use different crack densities and fluid types to get four models. In Model 10 and Model 12, crack density e is 8%. In Model 11 and Model 13, crack density is 4%. In Model 10 and Model 11, cracks are dry. In Model 12 and Model 13, cracks are wet (oil or water saturated). Model parameters for Model 10, Model 11, Model 12 and Model 13 are listed in Table 4.11, Table 4.12, Table 4.13 and Table 4.14, respectively. Corresponding anisotropy information is shown in Figure 4.23, Figure 4.24, Figure 4.25 and Figure 4.26, respectively.

In the combination of VTI and HTI model, both the VTI Bakken shales and the HTI Middle Bakken contribute to the total seismic responses. As discussed in previous sections, there are interferences among the reflections from the Upper, Middle and Lower Bakken. Therefore, the VTI information of the Upper and Lower Bakken and the HTI information of the Middle Bakken are mixing together in the total anisotropy information. Comparing the combination models with the VTI model (Figure 4.27), it can be noted that the seismic anisotropies in P-P, P-SV and SV-SV are enhanced because of the HTI Middle Bakken. We can make the same observations for both dry and wet crack cases.

Figure 4.23, Figure 4.24, Figure 4.25 and Figure 4.26 show that in the combination models, SV-SV and P-SV carry more anisotropy than P-P. If cracks are wet (oil or water saturated), then anisotropies in both P-P and P-SV are less than the SV-SV response. Thus, SV-SV carries most anisotropy information for the combination models.

4.6 MODEL FOR THE SANISH FIELD

As discussed in Chapter 3, the Bakken Formation is shallower and thinner in the Cottonwood Field and deeper and thicker in the Sanish field. In this section, I build models for the Sanish Field following the same procedures used for the Cottonwood Field.

First, I compare the isotropic model of the Sanish Field (Model 14) with the isotropic model of the Cottonwood Field (Model 1). The model parameters of Model 14 are listed in Table 4.15. Figure 4.28 shows the synthetic seismogram generated for the Sanish Field (Figure 4.28a) and the Cottonwood Field (Figure 4.28b). A notable difference between the two seismic responses is that there is less interference among the reflections from the Upper, Middle and Lower Bakken in the Sanish Field. For example, in vertical P-P, there are three peaks for the Sanish Field model while there are only two peaks for the Cottonwood Field model. This indicates the importance of layer thickness on seismic responses. Since the Bakken Formation is thicker in the Sanish Field than in the Cottonwood Field, it may be possible to get more detailed information about the Bakken intervals from the seismic data. Keep in mind that in general, the Sanish Field has the more productive wells than the Cottonwood Field.

Next, I generate synthetic seismograms using VTI model (Model 15, model parameters are listed in Table 4.16) and get the VTI information plot. Figure 4.29 shows the VTI difference information for the Sanish Field and the Cottonwood Field. They have similar characters. However, slightly more anisotropy information can be observed for the Sanish Field, probably resulting from thicker Bakken.

Same as for the Cottonwood Fields, four HTI models (Model 16, Model 17, Model 18 and Model 19, model parameters are listed in Table 4.17, Table 4.18, Table 4.19 and Table 4.20) are constructed for the Sanish Field with different crack density and

fluid fill in the cracks. Figure 4.30 shows the HTI information (difference in isotropic and HTI) for the four models. The HTI information of the Sanish Field has similar characters as the Cottonwood Field. However, as was the case for VTI, slightly more HTI anisotropy information can be observed for the Sanish Field.

I then considered four combination models (Model 20, Model 21, Model 22 and Model 23). Model parameters are listed in Table 4.21, Table 4.22, Table 4.23 and Table 4.24. Figure 4.31 shows the anisotropy information of the four combination models. What I have observed in the Cottonwood Field also apply to the Sanish Field. Once again, slightly more anisotropy can be seen in the Sanish Field.

4.7 SUMMARY

I constructed different types of models including isotropic models, VTI models, HTI models and models combining VTI and HTI, and generated full offset elastic synthetic seismograms for these models to study the seismic responses of the Bakken Formation. Two sets of layer thicknesses of the Bakken were used to investigate the bed thickness effect. Different crack densities and fluids filled in the cracks allowed me to analyze their effects on seismic responses and anisotropies. I also compared models for the Sanish Field with ones for the Cottonwood Field.

Results show that bed thickness of each member of the Bakken is below seismic resolution, therefore there is interference among the reflections from the Upper, Middle and Lower Bakken.

The difference between the anisotropic seismic responses, both VTI and HTI, and the isotropic seismic responses for the Bakken can be observed in both vertical and radial components. P-P, P-SV and SV-SV respond differently to anisotropies. Further, the types of data and the range of source-receiver offsets that are most sensitive to changes in anisotropy were identified.

VTI anisotropy and HTI anisotropy of the Bakken have different characters. P-SV carries more VTI anisotropy information while SV-SV carries more HTI anisotropy information. Both VTI and HTI are affected by bed thickness variation.

Crack densities and fluid contents affect HTI anisotropies. SV-SV is least influenced by the fluid fill in the cracks. However, anisotropies in P-P and P-SV are greatly reduced if the cracks are wet. The fluid effects are more obvious when crack densities are high.

The presence of vertical aligned fractures/cracks results in azimuthal anisotropy, which can be observed from wide azimuth seismic data. Although the Middle Bakken is sandwiched between the VTI Upper and Lower Bakken shales, the presence of HTI in the Middle Bakken can enhance the total anisotropies.

Bakken thickness variation contributes to the difference in seismic responses between the Sanish and Cottonwood Field.

Bed thickness, anisotropy caused by shales, crack densities and fluid fill in the cracks all have influences on the seismic responses of the Bakken Formation.

Name	Field	Type	Thickness	Crack Type	Crack Density
Model 1	Cottonwood	Isotropic	Actual Bakken Thickness	-	-
Model 2			Thick model	-	-
Model 3		VTI	Actual Bakken Thickness	-	-
Model 4			Thick model	-	-
Model 5		HTI	Actual Bakken Thickness	Dry	0.08
Model 6			Thick model	Dry	0.08
Model 7			Actual Bakken Thickness	Dry	0.04
Model 8			Actual Bakken Thickness	Wet	0.08
Model 9			Actual Bakken Thickness	Wet	0.04
Model 10		VTI+HTI	Actual Bakken Thickness	Dry	0.08
Model 11				Dry	0.04
Model 12				Wet	0.08
Model 13				Wet	0.04
Model 14	Sanish	Isotropic	Actual Bakken Thickness	-	-
Model 15		VTI		-	-
Model 16		HTI		Dry	0.08
Model 17				Dry	0.04
Model 18				Wet	0.08
Model 19				Wet	0.04
Model 20		VTI+HTI		Dry	0.08
Model 21				Dry	0.04
Model 22				Wet	0.08
Model 23				Wet	0.04

Table 4.1: List of all models.

Model 1: Cottonwood Field, isotropic, actual Bakken thickness.

	Type	Thickness (km)	Vp (km/s)	Vs (km/s)	Density (g/cm³)
Layer 1: Above	Isotropic	2.93492	5.725	3.192	2.67
Layer 2: Upper Bakken	Isotropic	0.00442	2.981	1.815	2.23
Layer 3: Middle Bakken	Isotropic	0.01295	4.780	2.856	2.61
Layer 4: Lower Bakken	Isotropic	0.01128	2.990	1.823	2.25
Layer 5: Below	Isotropic	0.10424	5.186	2.939	2.69

Table 4.2: Parameters used for Model 1. Properties displayed are type, thickness, P-wave velocity, S-wave velocity and density derived from acoustic, density and Sonic Scanner logs in verticale boreholes.

Model 2: Cottonwood Field, isotropic, thick model.

	Type	Thickness (km)	Vp (km/s)	Vs (km/s)	Density (g/cm³)
Layer 1: Above	Isotropic	2.93492	5.725	3.192	2.67
Layer 2: Upper Bakken	Isotropic	0.10000	2.981	1.815	2.23
Layer 3: Middle Bakken	Isotropic	0.10000	4.780	2.856	2.61
Layer 4: Lower Bakken	Isotropic	0.10000	2.990	1.823	2.25
Layer 5: Below	Isotropic	0.10424	5.186	2.939	2.69

Table 4.3: Parameters used for Model 2. Properties displayed are type, thickness, P-wave velocity, S-wave velocity and density derived from acoustic, density and Sonic Scanner logs in verticale boreholes.

Model 3: Cottonwood Field, VTI, actual Bakken thickness.

	Type	Thickness (km)	Vp (km/s)	Vs (km/s)	Density (g/cm³)	ε	δ	γ
Layer 1: Above	Isotropic	2.93492	5.725	3.192	2.67	0	0	0
Layer 2: Upper Bakken	VTI	0.00442	2.981	1.815	2.23	0.24	0.12	0.24
Layer 3: Middle Bakken	Isotropic	0.01295	4.780	2.856	2.61	0	0	0
Layer 4: Lower Bakken	VTI	0.01128	2.990	1.823	2.25	0.24	0.12	0.24
Layer 5: Below	Isotropic	0.10424	5.186	2.939	2.69	0	0	0

Table 4.4: Parameters used for Model 3. Properties displayed are type, thickness, P-wave velocity, S-wave velocity, density and Thomsen's parameters ε , δ and γ of equivalent VTI media. Anisotropy parameters are from Vernik and Liu (1997).

Model 4: Cottonwood Field, VTI, thick model.

	Type	Thickness (km)	Vp (km/s)	Vs (km/s)	Density (g/cm³)	ε	δ	γ
Layer 1: Above	Isotropic	2.93492	5.725	3.192	2.67	0	0	0
Layer 2: Upper Bakken	VTI	0.10000	2.981	1.815	2.23	0.24	0.12	0.24
Layer 3: Middle Bakken	Isotropic	0.10000	4.780	2.856	2.61	0	0	0
Layer 4: Lower Bakken	VTI	0.10000	2.990	1.823	2.25	0.24	0.12	0.24
Layer 5: Below	Isotropic	0.10424	5.186	2.939	2.69	0	0	0

Table 4.5: Parameters used for Model 4. Properties displayed are type, thickness, P-wave velocity, S-wave velocity, density and Thomsen's parameters ε , δ and γ of equivalent VTI media. Anisotropy parameters are from Vernik and Liu (1997).

Model 5: Cottonwood Field, HTI, actual Bakken thickness, e = 8%, dry.

	Type	Thickness (km)	Vp (km/s)	Vs (km/s)	Density (g/cm³)	ε or $\varepsilon^{(v)}$	δ or $\delta^{(v)}$	γ or $\gamma^{(v)}$
Layer 1: Above	Isotropic	2.93492	5.725	3.192	2.67	0	0	0
Layer 2: Upper Bakken	Isotropic	0.00442	2.981	1.815	2.23	0	0	0
Layer 3: Middle Bakken	HTI	0.01295	4.780	2.856	2.61	-0.21	-0.23	-0.09
Layer 4: Lower Bakken	Isotropic	0.01128	2.990	1.823	2.25	0	0	0
Layer 5: Below	Isotropic	0.10424	5.186	2.939	2.69	0	0	0

Table 4.6: Parameters used for Model 5. Properties displayed are type, thickness, P-wave velocity, S-wave velocity, density. $\varepsilon^{(v)}$, $\delta^{(v)}$ and $\gamma^{(v)}$ are anisotropy parameters of equivalent HTI media caused by dry crack with crack density of 8%.

Model 6: Cottonwood Field, HTI, thick model, e = 8%, dry.

	Type	Thickness (km)	Vp (km/s)	Vs (km/s)	Density (g/cm³)	ε or $\varepsilon^{(v)}$	δ or $\delta^{(v)}$	γ or $\gamma^{(v)}$
Layer 1: Above	Isotropic	2.93492	5.725	3.192	2.67	0	0	0
Layer 2: Upper Bakken	Isotropic	0.10000	2.981	1.815	2.23	0	0	0
Layer 3: Middle Bakken	HTI	0.10000	4.780	2.856	2.61	-0.21	-0.23	-0.09
Layer 4: Lower Bakken	Isotropic	0.10000	2.990	1.823	2.25	0	0	0
Layer 5: Below	Isotropic	0.10424	5.186	2.939	2.69	0	0	0

Table 4.7: Parameters used for Model 6. Properties displayed are type, thickness, P-wave velocity, S-wave velocity, density. $\varepsilon^{(v)}$, $\delta^{(v)}$ and $\gamma^{(v)}$ are anisotropy parameters of equivalent HTI media caused by dry crack with crack density of 8%.

Model 7: Cottonwood Field, HTI, actual Bakken thickness, e = 4%, dry.

	Type	Thickness (km)	Vp (km/s)	Vs (km/s)	Density (g/cm³)	ε or $\varepsilon^{(v)}$	δ or $\delta^{(v)}$	γ or $\gamma^{(v)}$
Layer 1: Above	Isotropic	2.93492	5.725	3.192	2.67	0	0	0
Layer 2: Upper Bakken	Isotropic	0.00442	2.981	1.815	2.23	0	0	0
Layer 3: Middle Bakken	HTI	0.01295	4.780	2.856	2.61	-0.11	-0.11	-0.05
Layer 4: Lower Bakken	Isotropic	0.01128	2.990	1.823	2.25	0	0	0
Layer 5: Below	Isotropic	0.10424	5.186	2.939	2.69	0	0	0

Table 4.8: Parameters used for Model 7. Properties displayed are type, thickness, P-wave velocity, S-wave velocity, density. $\varepsilon^{(v)}$, $\delta^{(v)}$ and $\gamma^{(v)}$ are anisotropy parameters of equivalent HTI media caused by dry crack with crack density of 4%.

Model 8: Cottonwood Field, HTI, actual Bakken thickness, e = 8%, wet.

	Type	Thickness (km)	Vp (km/s)	Vs (km/s)	Density (g/cm³)	ε or $\varepsilon^{(v)}$	δ or $\delta^{(v)}$	γ or $\gamma^{(v)}$
Layer 1: Above	Isotropic	2.93492	5.725	3.192	2.67	0	0	0
Layer 2: Upper Bakken	Isotropic	0.00442	2.981	1.815	2.23	0	0	0
Layer 3: Middle Bakken	HTI	0.01295	4.780	2.856	2.61	0	-0.13	-0.09
Layer 4: Lower Bakken	Isotropic	0.01128	2.990	1.823	2.25	0	0	0
Layer 5: Below	Isotropic	0.10424	5.186	2.939	2.69	0	0	0

Table 4.9: Parameters used for Model 8. Properties displayed are type, thickness, P-wave velocity, S-wave velocity, density. $\varepsilon^{(v)}$, $\delta^{(v)}$ and $\gamma^{(v)}$ are anisotropy parameters of equivalent HTI media caused by wet crack with crack density of 8%.

Model 9: Cottonwood Field, HTI, actual Bakken thickness, e = 4%, wet.

	Type	Thickness (km)	Vp (km/s)	Vs (km/s)	Density (g/cm³)	ε or $\varepsilon^{(v)}$	δ or $\delta^{(v)}$	γ or $\gamma^{(v)}$
Layer 1: Above	Isotropic	2.93492	5.725	3.192	2.67	0	0	0
Layer 2: Upper Bakken	Isotropic	0.00442	2.981	1.815	2.23	0	0	0
Layer 3: Middle Bakken	HTI	0.01295	4.780	2.856	2.61	0	-0.07	-0.05
Layer 4: Lower Bakken	Isotropic	0.01128	2.990	1.823	2.25	0	0	0
Layer 5: Below	Isotropic	0.10424	5.186	2.939	2.69	0	0	0

Table 4.10: Parameters used for Model 9. Properties displayed are type, thickness, P-wave velocity, S-wave velocity, density. $\varepsilon^{(v)}$, $\delta^{(v)}$ and $\gamma^{(v)}$ are anisotropy parameters of equivalent HTI media caused by wet crack with crack density of 4%.

Model 10: Cottonwood Field, VTI-HTI, actual Bakken thickness, e = 8%, dry.

	Type	Thickness (km)	Vp (km/s)	Vs (km/s)	Density (g/cm³)	ε or $\varepsilon^{(v)}$	δ or $\delta^{(v)}$	γ or $\gamma^{(v)}$
Layer 1: Above	Isotropic	2.93492	5.725	3.192	2.67	0	0	0
Layer 2: Upper Bakken	VTI	0.00442	2.981	1.815	2.23	0.24	0.12	0.24
Layer 3: Middle Bakken	Isotropic	0.01295	4.780	2.856	2.61	-0.21	-0.23	-0.09
Layer 4: Lower Bakken	VTI	0.01128	2.990	1.823	2.25	0.24	0.12	0.24
Layer 5: Below	Isotropic	0.10424	5.186	2.939	2.69	0	0	0

Table 4.11: Parameters used for Model 10. Properties displayed are type, thickness, P-wave velocity, S-wave velocity, density and anisotropy parameters. ε , δ and γ are anisotropy parameters of equivalent VTI media. $\varepsilon^{(v)}$, $\delta^{(v)}$ and $\gamma^{(v)}$ are anisotropy parameters of equivalent HTI media caused by dry crack, in which the crack density is 8%.

Model 11: Cottonwood Field, VTI-HTI, actual Bakken thickness, e = 4%, dry.

	Type	Thickness (km)	Vp (km/s)	Vs (km/s)	Density (g/cm³)	ε or $\varepsilon^{(v)}$	δ or $\delta^{(v)}$	γ or $\gamma^{(v)}$
Layer 1: Above	Isotropic	2.93492	5.725	3.192	2.67	0	0	0
Layer 2: Upper Bakken	VTI	0.00442	2.981	1.815	2.23	0.24	0.12	0.24
Layer 3: Middle Bakken	Isotropic	0.01295	4.780	2.856	2.61	-0.11	-0.11	-0.05
Layer 4: Lower Bakken	VTI	0.01128	2.990	1.823	2.25	0.24	0.12	0.24
Layer 5: Below	Isotropic	0.10424	5.186	2.939	2.69	0	0	0

Table 4.12: Parameters used for Model 11. Properties displayed are type, thickness, P-wave velocity, S-wave velocity, density and anisotropy parameters. ε , δ and γ are anisotropy parameters of equivalent VTI media. $\varepsilon^{(v)}$, $\delta^{(v)}$ and $\gamma^{(v)}$ are anisotropy parameters of equivalent HTI media caused by dry crack, in which the crack density is 4%.

Model 12: Cottonwood Field, VTI-HTI, actual Bakken thickness, e = 8%, wet.

	Type	Thickness (km)	Vp (km/s)	Vs (km/s)	Density (g/cm³)	ε or $\varepsilon^{(v)}$	δ or $\delta^{(v)}$	γ or $\gamma^{(v)}$
Layer 1: Above	Isotropic	2.93492	5.725	3.192	2.67	0	0	0
Layer 2: Upper Bakken	VTI	0.00442	2.981	1.815	2.23	0.24	0.12	0.24
Layer 3: Middle Bakken	Isotropic	0.01295	4.780	2.856	2.61	0	-0.13	-0.09
Layer 4: Lower Bakken	VTI	0.01128	2.990	1.823	2.25	0.24	0.12	0.24
Layer 5: Below	Isotropic	0.10424	5.186	2.939	2.69	0	0	0

Table 4.13: Parameters used for Model 12. Properties displayed are type, thickness, P-wave velocity, S-wave velocity, density and anisotropy parameters. ε , δ and γ are anisotropy parameters of equivalent VTI media. $\varepsilon^{(v)}$, $\delta^{(v)}$ and $\gamma^{(v)}$ are anisotropy parameters of equivalent HTI media caused by wet crack, in which the crack density is 8%.

Model 13: Cottonwood Field, VTI-HTI, actual Bakken thickness, e = 4%, wet.

	Type	Thickness (km)	Vp (km/s)	Vs (km/s)	Density (g/cm³)	ε or $\varepsilon^{(v)}$	δ or $\delta^{(v)}$	γ or $\gamma^{(v)}$
Layer 1: Above	Isotropic	2.93492	5.725	3.192	2.67	0	0	0
Layer 2: Upper Bakken	VTI	0.00442	2.981	1.815	2.23	0.24	0.12	0.24
Layer 3: Middle Bakken	Isotropic	0.01295	4.780	2.856	2.61	0	-0.07	-0.05
Layer 4: Lower Bakken	VTI	0.01128	2.990	1.823	2.25	0.24	0.12	0.24
Layer 5: Below	Isotropic	0.10424	5.186	2.939	2.69	0	0	0

Table 4.14: Parameters used for Model 13. Properties displayed are type, thickness, P-wave velocity, S-wave velocity, density and anisotropy parameters. ε , δ and γ are anisotropy parameters of equivalent VTI media. $\varepsilon^{(v)}$, $\delta^{(v)}$ and $\gamma^{(v)}$ are anisotropy parameters of equivalent HTI media caused by wet crack, in which the crack density is 4%.

Model 14: Sanish Field, isotropic, actual Bakken thickness.

	Type	Thickness (km)	Vp (km/s)	Vs (km/s)	Density (g/cm³)
Layer 1: Above	Isotropic	3.09064	5.590	3.066	2.70
Layer 2: Upper Bakken	Isotropic	0.00521	2.870	1.726	2.25
Layer 3: Middle Bakken	Isotropic	0.02070	4.903	2.876	2.62
Layer 4: Lower Bakken	Isotropic	0.01490	2.886	1.735	2.24
Layer 5: Below	Isotropic	0.00020	5.067	2.833	2.70

Table 4.15: Parameters used for Model 14. Properties displayed are type, thickness, P-wave velocity, S-wave velocity and density.

Model 15: Sanish Field, VTI, actual Bakken thickness.

	Type	Thickness (km)	Vp (km/s)	Vs (km/s)	Density (g/cm³)	ε	δ	γ
Layer 1: Above	Isotropic	3.09064	5.590	3.066	2.70	0	0	0
Layer 2: Upper Bakken	VTI	0.00521	2.870	1.726	2.25	0.24	0.12	0.24
Layer 3: Middle Bakken	Isotropic	0.02070	4.903	2.876	2.62	0	0	0
Layer 4: Lower Bakken	VTI	0.01490	2.886	1.735	2.24	0.24	0.12	0.24
Layer 5: Below	Isotropic	0.00020	5.067	2.833	2.70	0	0	0

Table 4.16: Parameters used for Model 15. Properties displayed are type, thickness, P-wave velocity, S-wave velocity, density and Thomsen's parameters ε , δ and γ of equivalent VTI media.

Model 16: Sanish Field, HTI, actual Bakken thickness, e = 8%, dry.

	Type	Thickness (km)	Vp (km/s)	Vs (km/s)	Density (g/cm³)	ε or $\varepsilon^{(v)}$	δ or $\delta^{(v)}$	γ or $\gamma^{(v)}$
Layer 1: Above	Isotropic	3.09064	5.590	3.066	2.70	0	0	0
Layer 2: Upper Bakken	VTI	0.00521	2.870	1.726	2.25	0	0	0
Layer 3: Middle Bakken	Isotropic	0.02070	4.903	2.876	2.62	-0.21	-0.23	-0.09
Layer 4: Lower Bakken	VTI	0.01490	2.886	1.735	2.24	0	0	0
Layer 5: Below	Isotropic	0.00020	5.067	2.833	2.70	0	0	0

Table 4.17: Parameters used for Model 16. Properties displayed are type, thickness, P-wave velocity, S-wave velocity, density and anisotropy parameters. ε , δ and γ are anisotropy parameters of equivalent VTI media. $\varepsilon^{(v)}$, $\delta^{(v)}$ and $\gamma^{(v)}$ are anisotropy parameters of equivalent HTI media caused by dry crack, in which the crack density is 8%.

Model 17: Sanish Field, HTI, actual Bakken thickness, e = 4%, dry.

	Type	Thickness (km)	Vp (km/s)	Vs (km/s)	Density (g/cm³)	ε or $\varepsilon^{(v)}$	δ or $\delta^{(v)}$	γ or $\gamma^{(v)}$
Layer 1: Above	Isotropic	3.09064	5.590	3.066	2.70	0	0	0
Layer 2: Upper Bakken	VTI	0.00521	2.870	1.726	2.25	0	0	0
Layer 3: Middle Bakken	Isotropic	0.02070	4.903	2.876	2.62	-0.11	-0.11	-0.05
Layer 4: Lower Bakken	VTI	0.01490	2.886	1.735	2.24	0	0	0
Layer 5: Below	Isotropic	0.00020	5.067	2.833	2.70	0	0	0

Table 4.18: Parameters used for Model 17. Properties displayed are type, thickness, P-wave velocity, S-wave velocity, density and anisotropy parameters. ε , δ and γ are anisotropy parameters of equivalent VTI media. $\varepsilon^{(v)}$, $\delta^{(v)}$ and $\gamma^{(v)}$ are anisotropy parameters of equivalent HTI media caused by dry crack, in which the crack density is 4%.

Model 18: Sanish Field, HTI, actual Bakken thickness, e = 8%, wet.

	Type	Thickness (km)	Vp (km/s)	Vs (km/s)	Density (g/cm³)	ε or $\varepsilon^{(v)}$	δ or $\delta^{(v)}$	γ or $\gamma^{(v)}$
Layer 1: Above	Isotropic	3.09064	5.590	3.066	2.70	0	0	0
Layer 2: Upper Bakken	VTI	0.00521	2.870	1.726	2.25	0	0	0
Layer 3: Middle Bakken	Isotropic	0.02070	4.903	2.876	2.62	0.00	-0.13	-0.09
Layer 4: Lower Bakken	VTI	0.01490	2.886	1.735	2.24	0	0	0
Layer 5: Below	Isotropic	0.00020	5.067	2.833	2.70	0	0	0

Table 4.19: Parameters used for Model 18. Properties displayed are type, thickness, P-wave velocity, S-wave velocity, density and anisotropy parameters. ε , δ and γ are anisotropy parameters of equivalent VTI media. $\varepsilon^{(v)}$, $\delta^{(v)}$ and $\gamma^{(v)}$ are anisotropy parameters of equivalent HTI media caused by wet crack, in which the crack density is 8%.

Model 19: Sanish Field, HTI, actual Bakken thickness, e = 4%, wet.

	Type	Thickness (km)	Vp (km/s)	Vs (km/s)	Density (g/cm³)	ε or $\varepsilon^{(v)}$	δ or $\delta^{(v)}$	γ or $\gamma^{(v)}$
Layer 1: Above	Isotropic	3.09064	5.590	3.066	2.70	0	0	0
Layer 2: Upper Bakken	VTI	0.00521	2.870	1.726	2.25	0	0	0
Layer 3: Middle Bakken	Isotropic	0.02070	4.903	2.876	2.62	0.00	-0.06	-0.05
Layer 4: Lower Bakken	VTI	0.01490	2.886	1.735	2.24	0	0	0
Layer 5: Below	Isotropic	0.00020	5.067	2.833	2.70	0	0	0

Table 4.20: Parameters used for Model 19. Properties displayed are type, thickness, P-wave velocity, S-wave velocity, density and anisotropy parameters. ε , δ and γ are anisotropy parameters of equivalent VTI media. $\varepsilon^{(v)}$, $\delta^{(v)}$ and $\gamma^{(v)}$ are anisotropy parameters of equivalent HTI media caused by wet crack, in which the crack density is 4%.

Model 20: Sanish Field, VTIHTI, actual Bakken thickness, e = 8%, dry.

	Type	Thickness (km)	Vp (km/s)	Vs (km/s)	Density (g/cm³)	ε or $\varepsilon^{(v)}$	δ or $\delta^{(v)}$	γ or $\gamma^{(v)}$
Layer 1: Above	Isotropic	3.09064	5.590	3.066	2.70	0	0	0
Layer 2: Upper Bakken	VTI	0.00521	2.870	1.726	2.25	0.24	0.12	0.24
Layer 3: Middle Bakken	Isotropic	0.02070	4.903	2.876	2.62	-0.21	-0.23	-0.09
Layer 4: Lower Bakken	VTI	0.01490	2.886	1.735	2.24	0.24	0.12	0.24
Layer 5: Below	Isotropic	0.00020	5.067	2.833	2.70	0	0	0

Table 4.21: Parameters used for Model 20. Properties displayed are type, thickness, P-wave velocity, S-wave velocity, density and anisotropy parameters. ε , δ and γ are anisotropy parameters of equivalent VTI media. $\varepsilon^{(v)}$, $\delta^{(v)}$ and $\gamma^{(v)}$ are anisotropy parameters of equivalent HTI media caused by dry crack, in which the crack density is 8%.

Model 21: Sanish Field, VTIHTI, actual Bakken thickness, e = 4%, dry.

	Type	Thickness (km)	Vp (km/s)	Vs (km/s)	Density (g/cm³)	ε or $\varepsilon^{(v)}$	δ or $\delta^{(v)}$	γ or $\gamma^{(v)}$
Layer 1: Above	Isotropic	3.09064	5.590	3.066	2.70	0	0	0
Layer 2: Upper Bakken	VTI	0.00521	2.870	1.726	2.25	0.24	0.12	0.24
Layer 3: Middle Bakken	Isotropic	0.02070	4.903	2.876	2.62	-0.11	-0.11	-0.05
Layer 4: Lower Bakken	VTI	0.01490	2.886	1.735	2.24	0.24	0.12	0.24
Layer 5: Below	Isotropic	0.00020	5.067	2.833	2.70	0	0	0

Table 4.22: Parameters used for Model 21. Properties displayed are type, thickness, P-wave velocity, S-wave velocity, density and anisotropy parameters. ε , δ and γ are anisotropy parameters of equivalent VTI media. $\varepsilon^{(v)}$, $\delta^{(v)}$ and $\gamma^{(v)}$ are anisotropy parameters of equivalent HTI media caused by dry crack, in which the crack density is 4%.

Model 22: Sanish Field, VTIHTI, actual Bakken thickness, e = 8%, wet.

	Type	Thickness (km)	Vp (km/s)	Vs (km/s)	Density (g/cm³)	ε or $\varepsilon^{(v)}$	δ or $\delta^{(v)}$	γ or $\gamma^{(v)}$
Layer 1: Above	Isotropic	3.09064	5.590	3.066	2.70	0	0	0
Layer 2: Upper Bakken	VTI	0.00521	2.870	1.726	2.25	0.24	0.12	0.24
Layer 3: Middle Bakken	Isotropic	0.02070	4.903	2.876	2.62	0.00	-0.13	-0.09
Layer 4: Lower Bakken	VTI	0.01490	2.886	1.735	2.24	0.24	0.12	0.24
Layer 5: Below	Isotropic	0.00020	5.067	2.833	2.70	0	0	0

Table 4.23: Parameters used for Model 22. Properties displayed are type, thickness, P-wave velocity, S-wave velocity, density and anisotropy parameters. ε , δ and γ are anisotropy parameters of equivalent VTI media. $\varepsilon^{(v)}$, $\delta^{(v)}$ and $\gamma^{(v)}$ are anisotropy parameters of equivalent HTI media caused by wet crack, in which the crack density is 8%.

Model 23: Sanish Field, VTIHTI, actual Bakken thickness, e = 4%, wet.

	Type	Thickness (km)	Vp (km/s)	Vs (km/s)	Density (g/cm³)	ε or $\varepsilon^{(v)}$	δ or $\delta^{(v)}$	γ or $\gamma^{(v)}$
Layer 1: Above	Isotropic	3.09064	5.590	3.066	2.70	0	0	0
Layer 2: Upper Bakken	VTI	0.00521	2.870	1.726	2.25	0.24	0.12	0.24
Layer 3: Middle Bakken	Isotropic	0.02070	4.903	2.876	2.62	0.00	-0.06	-0.05
Layer 4: Lower Bakken	VTI	0.01490	2.886	1.735	2.24	0.24	0.12	0.24
Layer 5: Below	Isotropic	0.00020	5.067	2.833	2.70	0	0	0

Table 4.24: Parameters used for Model 23. Properties displayed are type, thickness, P-wave velocity, S-wave velocity, density and anisotropy parameters. ε , δ and γ are anisotropy parameters of equivalent VTI media. $\varepsilon^{(v)}$, $\delta^{(v)}$ and $\gamma^{(v)}$ are anisotropy parameters of equivalent HTI media caused by wet crack, in which the crack density is 4%.

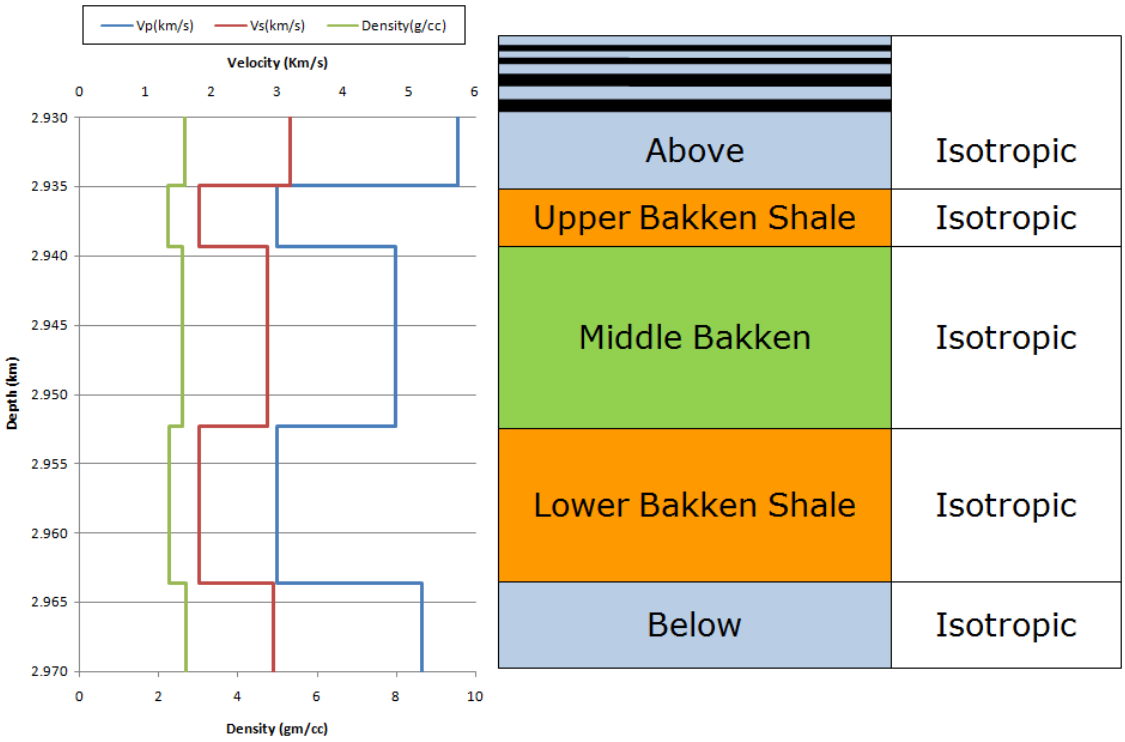

Figure 4.1. Model used to generate synthetic seismograms. All five layers are isotropic for the Cottonwood Field.

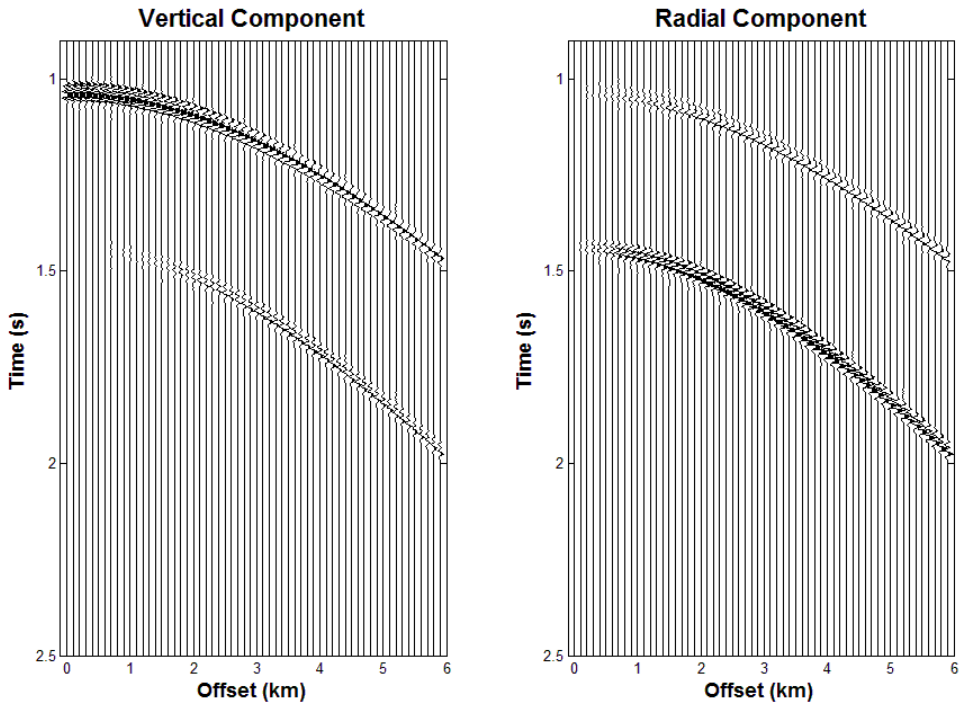

Figure 4.2: Synthetic seismograms generated using an explosive source for Model 1. Note both P-P and P-SV reflections. Note a constant scalar is applied to all data using vertical point source in this thesis.

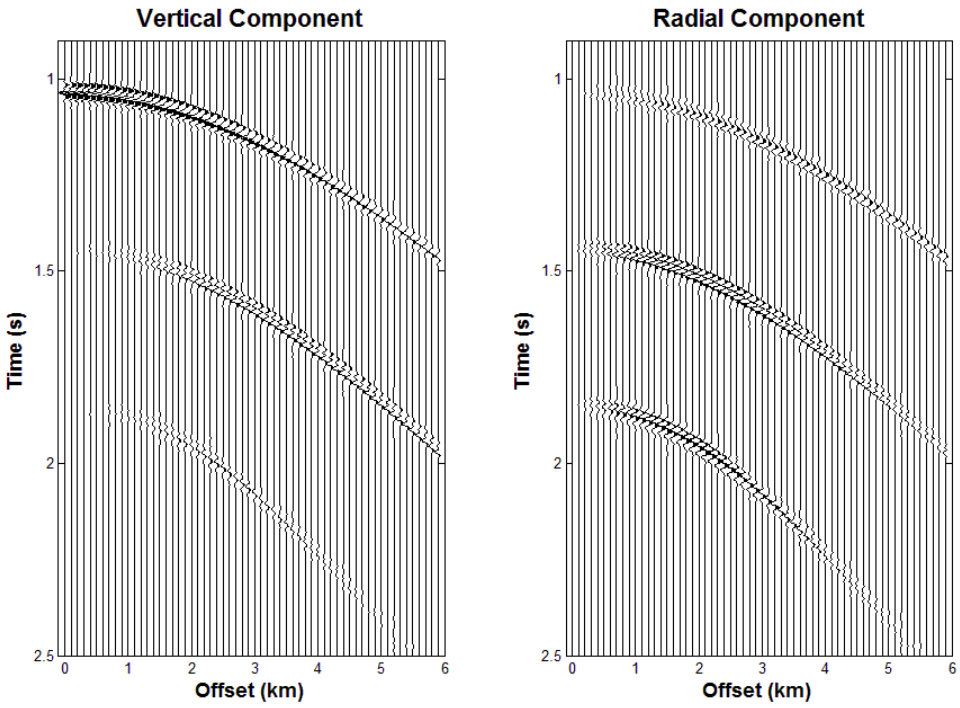

Figure 4.3: Synthetic seismograms generated using a vertical point source (analogous to Vibroseis) for isotropic model 1. Note the direct shear (SV-SV) reflection at large offsets.

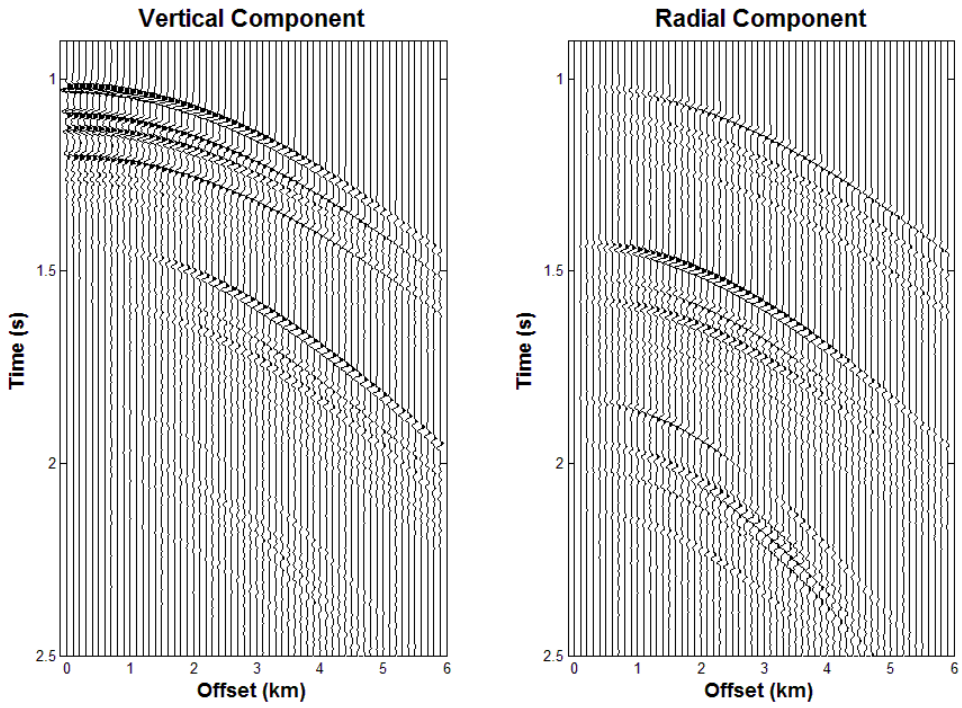

Figure 4.4: Synthetic seismograms generated using vertical point source for isotropic, thick model (Model 2). Note individual reflections for the four interfaces associated with the Bakken.

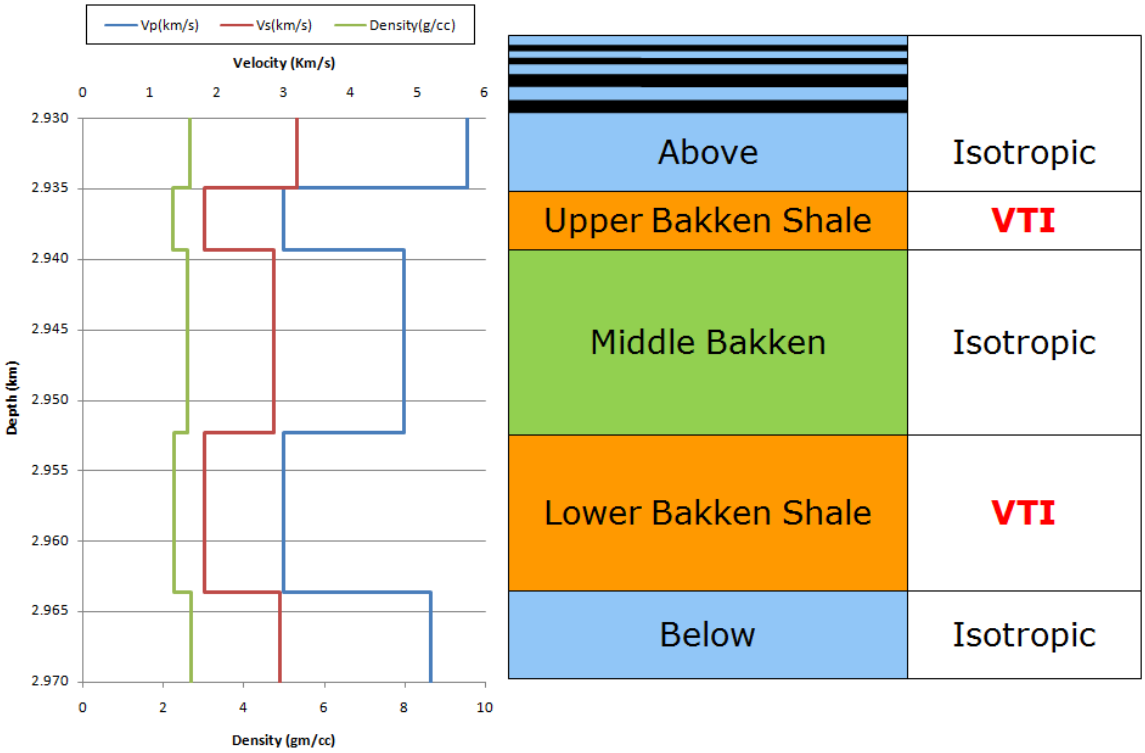

Figure 4.5: VTI Model used to generate synthetic seismograms for the Cottonwood Field.

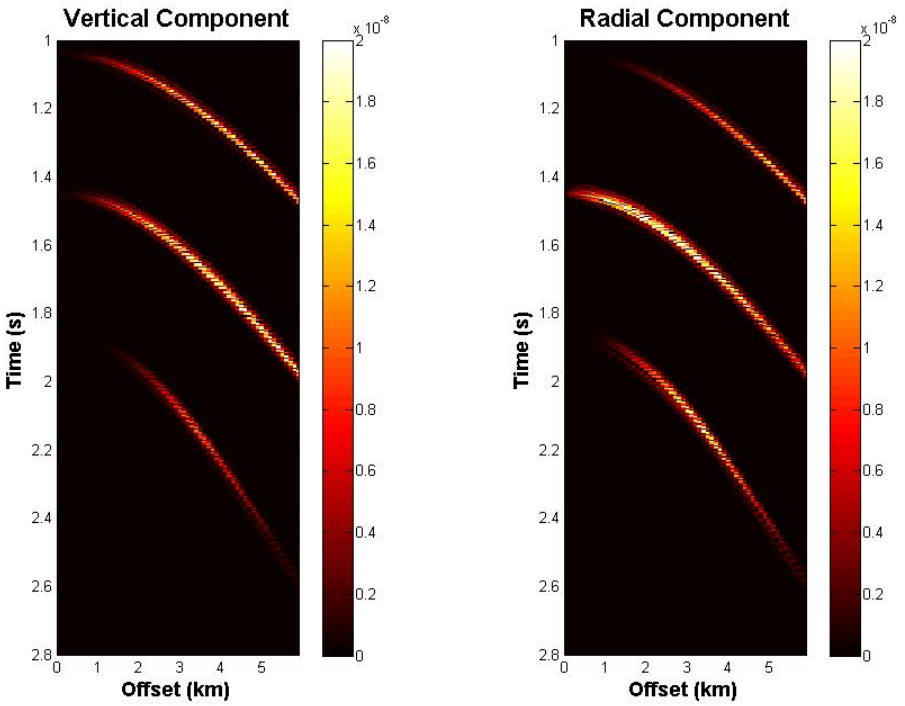

Figure 4.6: Difference between VTI and isotropic seismic responses. These differences are a combination of total amplitude difference and travel time shifts in the original response.

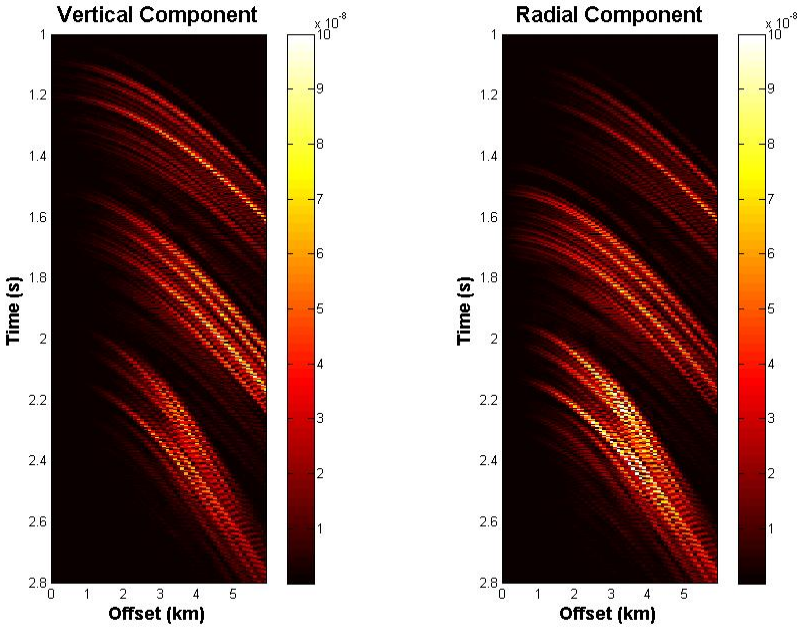

Figure 4.7: Difference between VTI and isotropic seismic responses using thick models with isolated reflections. These differences are a combination of total amplitude difference and travel time shifts in the original response. The color scheme for the thick model plot is different from that of actual thickness model plot for better display. Note the strong effect of time differences in this thick-section model.

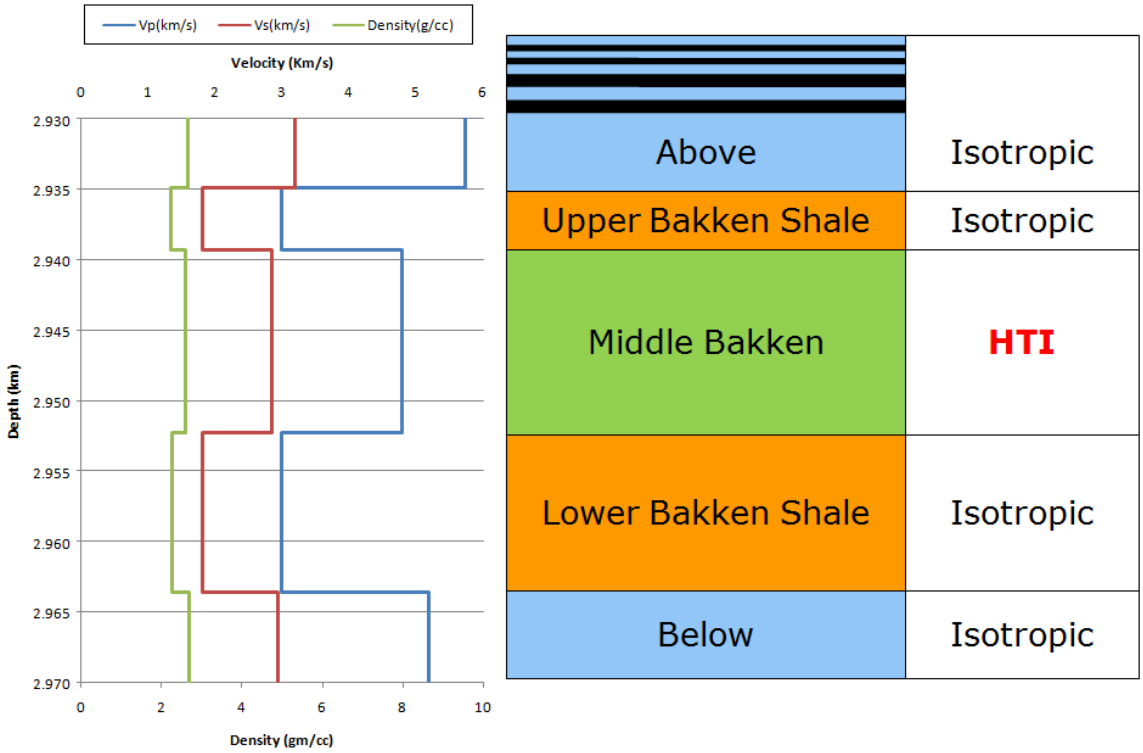

Figure 4.8: HTI model used to generate synthetic seismograms for the Cottonwood Field.

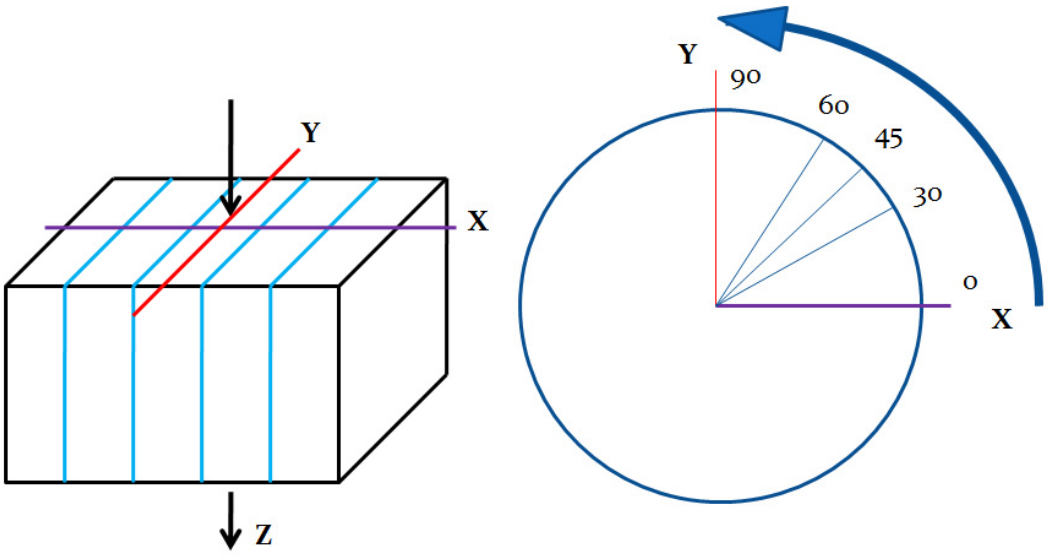

Figure 4.9: Fractures and azimuths. Fractures are parallel to y-direction. Five azimuths of 0°, 30°, 45°, 60° and 90° are used to generate seismograms.

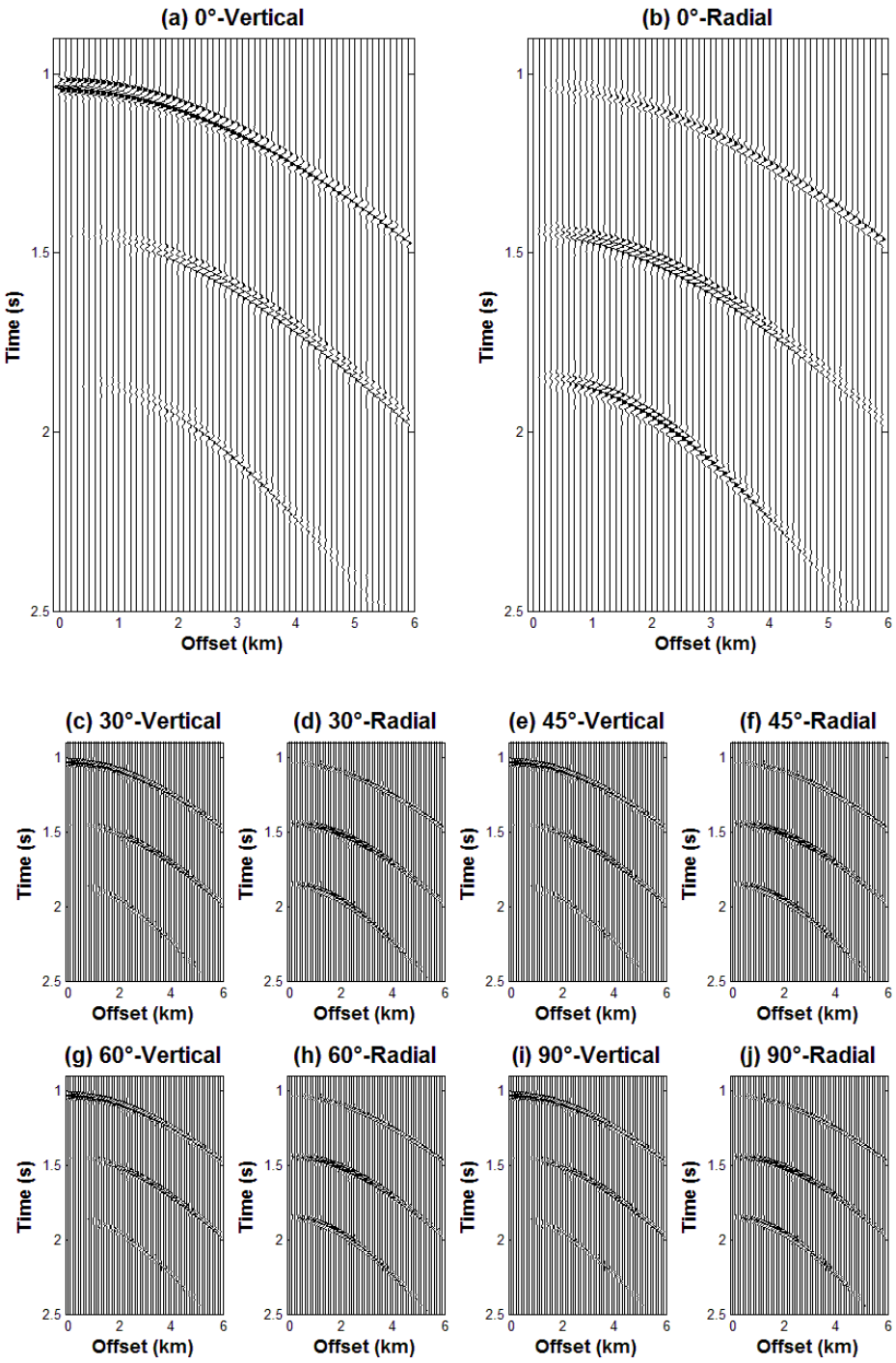

Figure 4.10: Synthetic seismograms of 0°(a, b), 30°(c, d), 45°(e, f), 60°(g, h) and 90°(i, j) azimuth using HTI models with actual Bakken thicknesses.

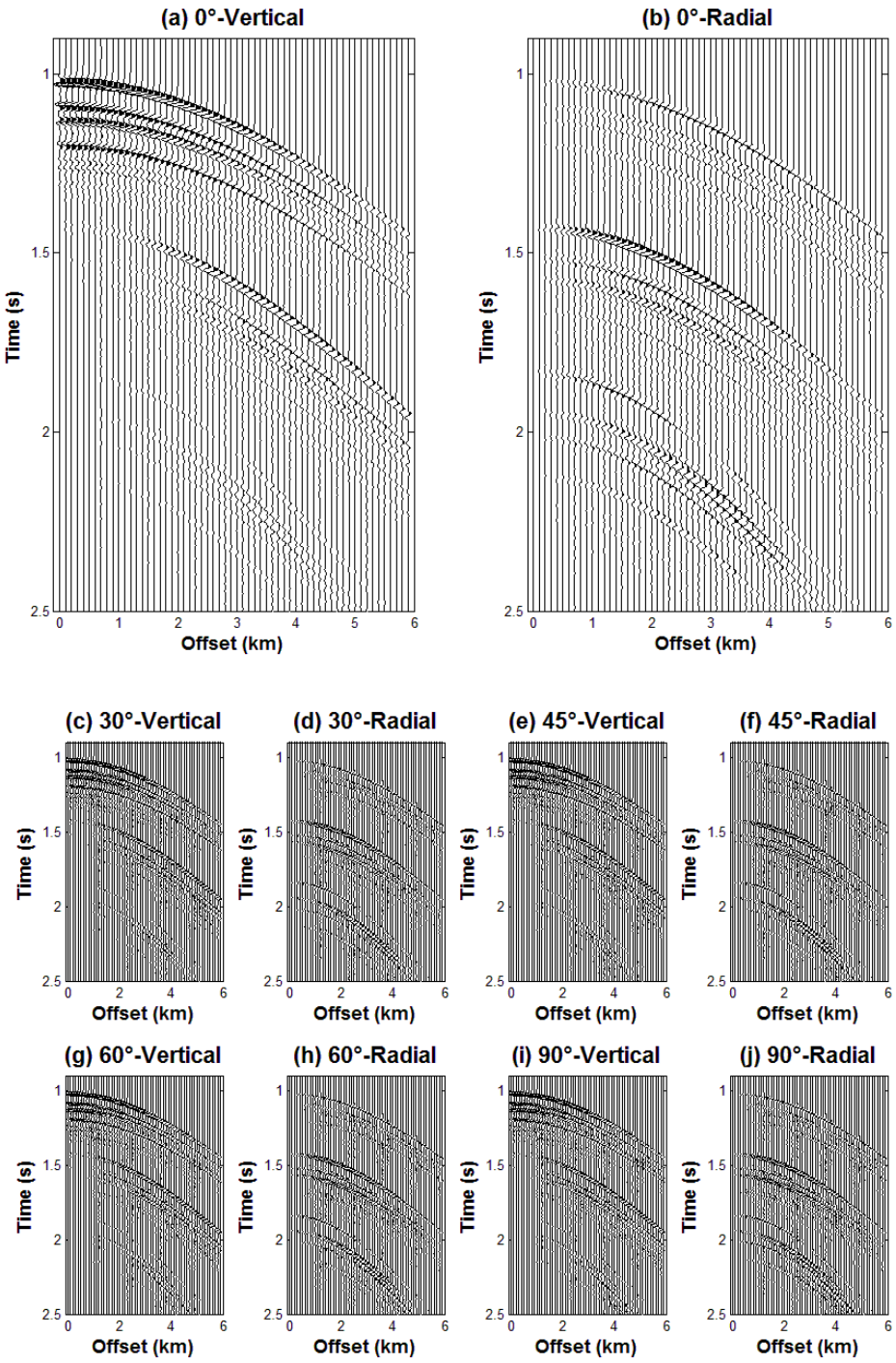

Figure 4.11: Synthetic seismograms of 0°(a, b), 30°(c, d), 45°(e, f), 60°(g, h) and 90°(i, j) azimuth using thick HTI models.

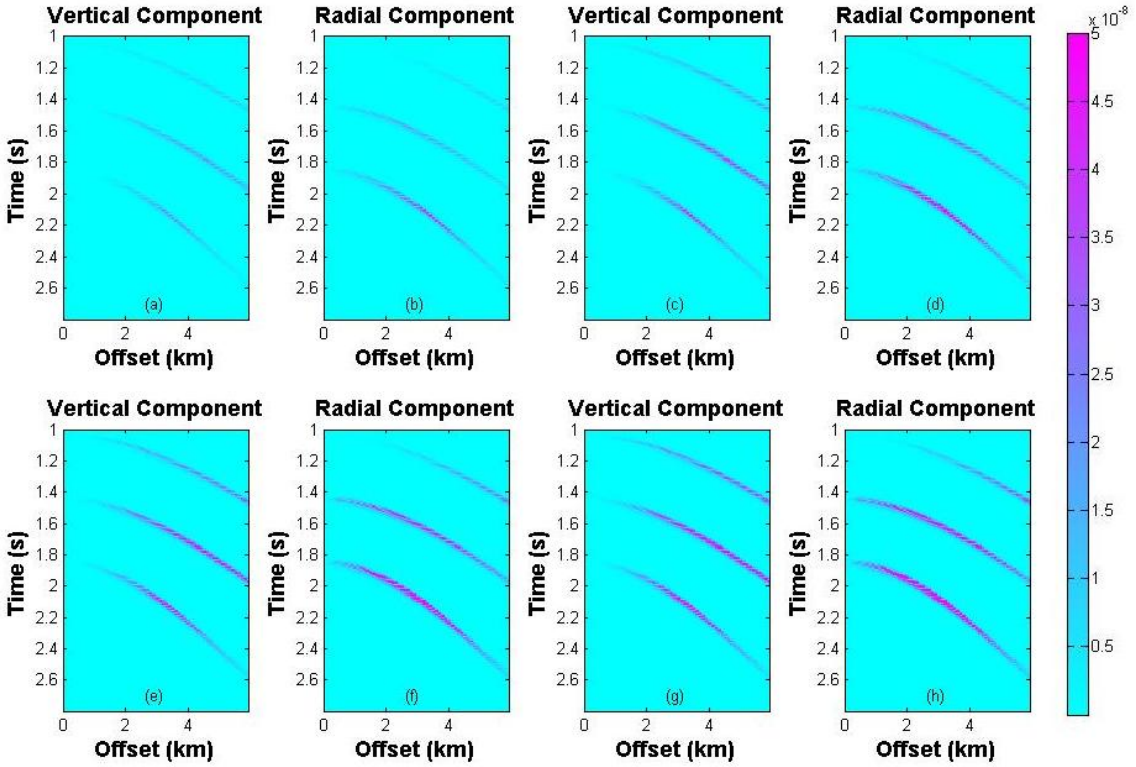

Figure 4.12: Azimuthal variation of HTI model using actual Bakken thickness. Shown here are the difference between 60° and 90° azimuth (a, b), 40° and 90° azimuth (c, d), 30° and 90° azimuth (e, f), and 0° and 90° azimuth (g, h). These differences are a combination of total amplitude difference and travel time shifts in the original response.

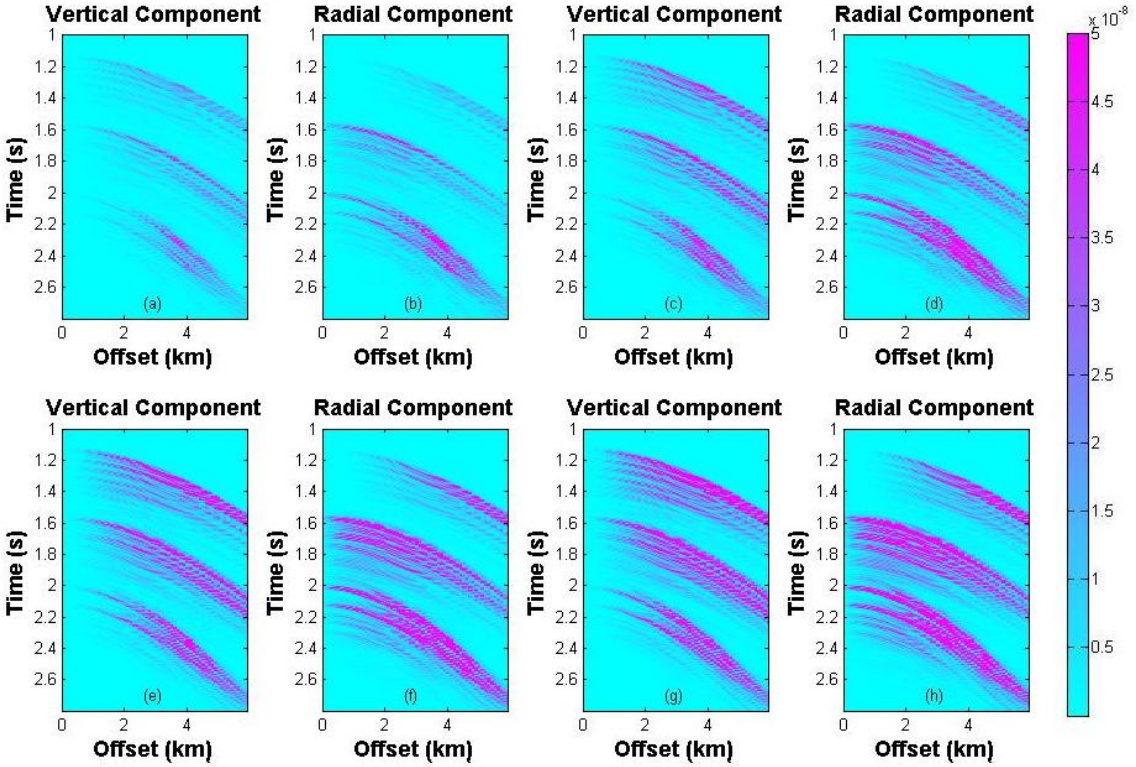

Figure 4.13: Azimuthal variation of thick HTI models. Shown here are the difference between 60° and 90° azimuth (a, b), 40° and 90° azimuth (c, d), 30° and 90° azimuth (e, f), and 0° and 90° azimuth (g, h). These differences are a combination of total amplitude difference and travel time shifts in the original response.

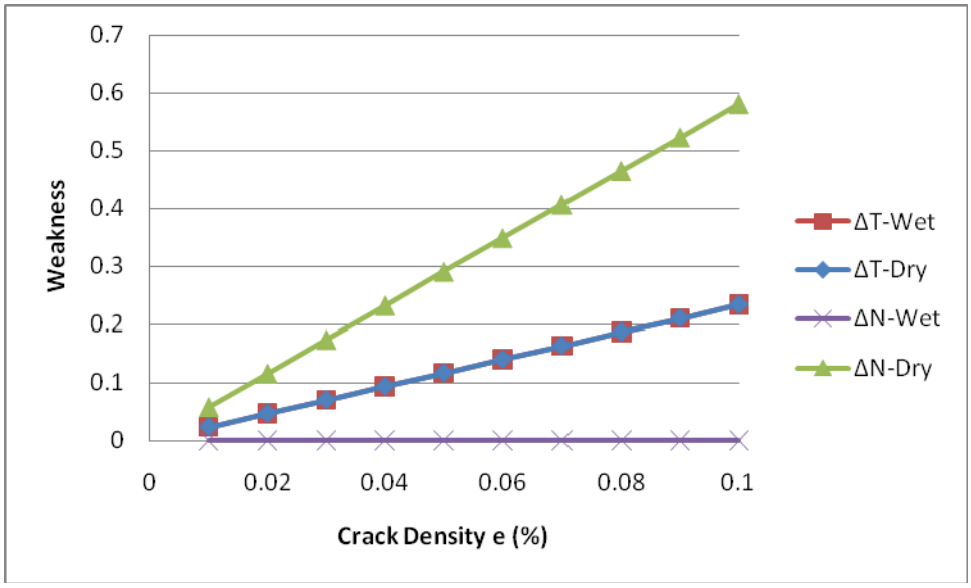

Figure 4.14: Normal and tangential weaknesses versus crack density e for dry and wet cracks. ΔN is the normal weakness and ΔT is the tangential weakness. Here Vp/Vs is 1.67, therefore g is 0.357.

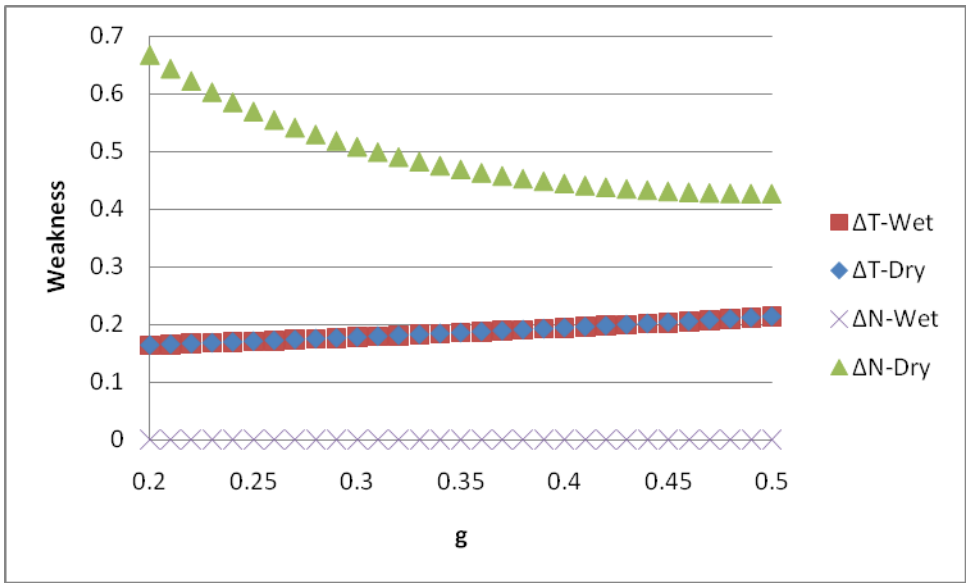

Figure 4.15: Normal and tangential weaknesses versus g for dry and wet cracks. ΔN is the normal weakness and ΔT is the tangential weakness. Crack density is 8%.

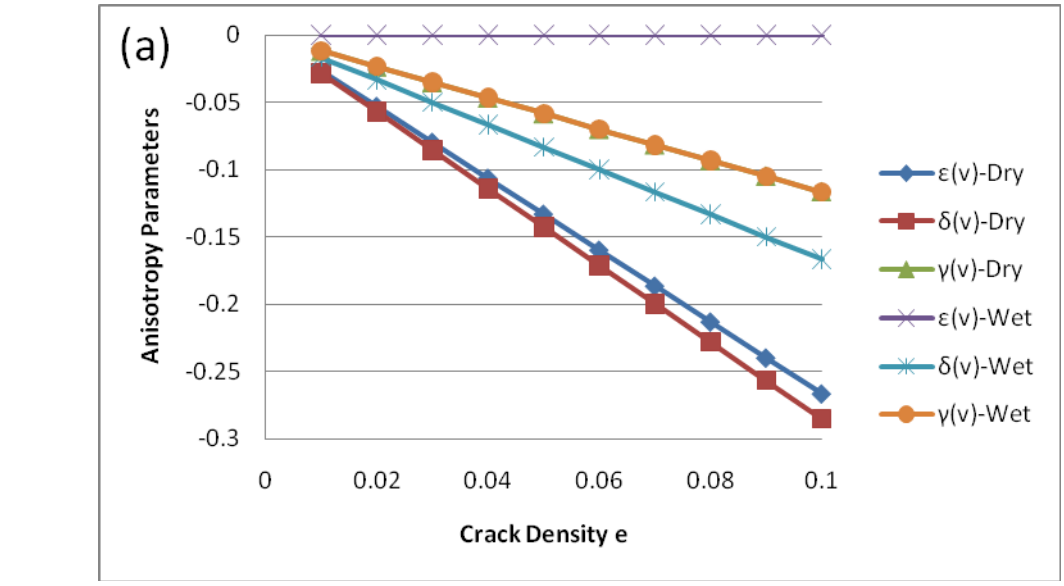

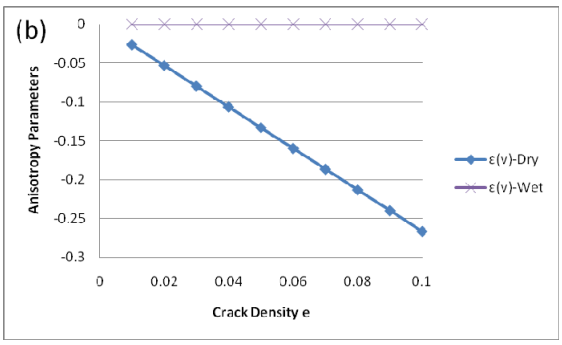

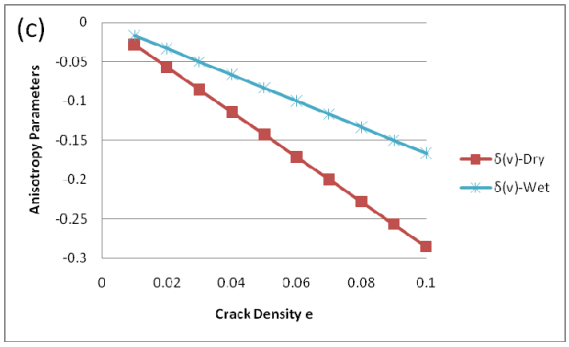

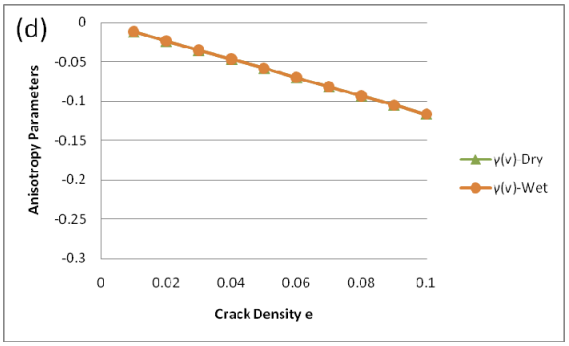

Figure 4.16: Anisotropy parameters versus crack density e for dry and wet cracks. $\varepsilon^{(v)}$ (b), $\delta^{(v)}$ (c), and $\gamma^{(v)}$ (d) are anisotropy parameters for HTI media. Here Vp/Vs is 1.67, therefore g is 0.357.

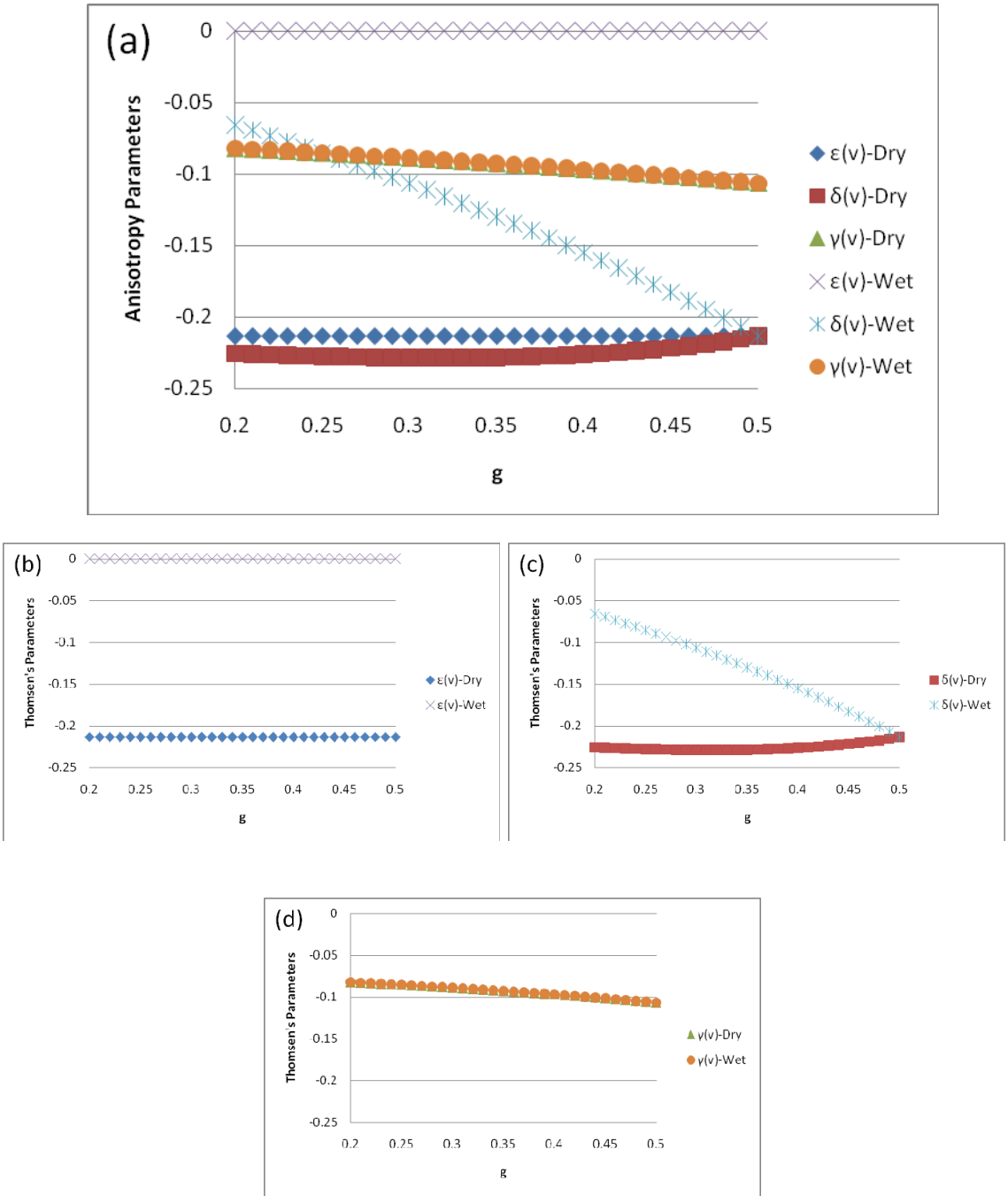

Figure 4.17: Anisotropy parameters versus crack density e for dry and wet cracks. $\varepsilon^{(v)}$ (b), $\delta^{(v)}$ (c), and $\gamma^{(v)}$ (d) are anisotropy parameters for HTI media. Crack density is 8%.

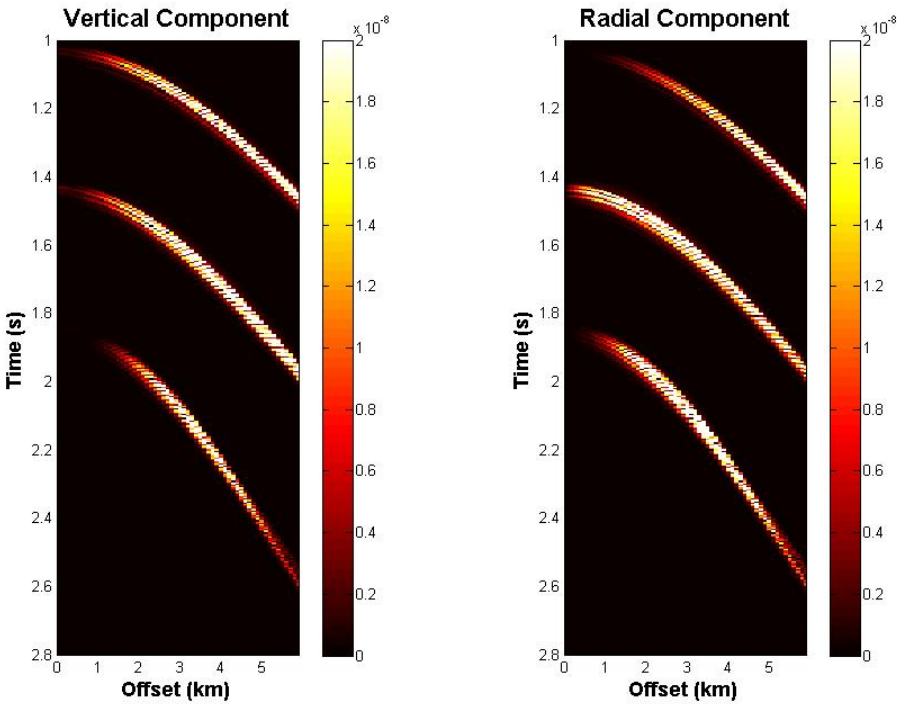

Figure 4.18 Difference between HTI and isotropic seismic responses. Crack density is 8%. Dry. The source-receiver line is perpendicular to crack orientation.

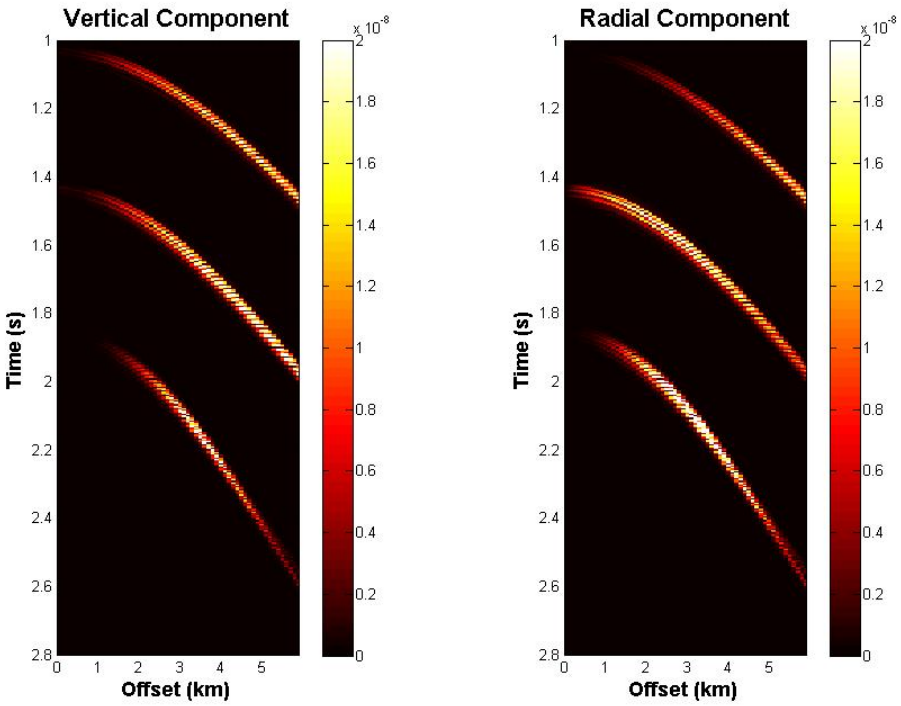

Figure 4.19: Difference between HTI and isotropic seismic responses. Crack density is 4%. Dry. The source-receiver line is perpendicular to crack orientation.

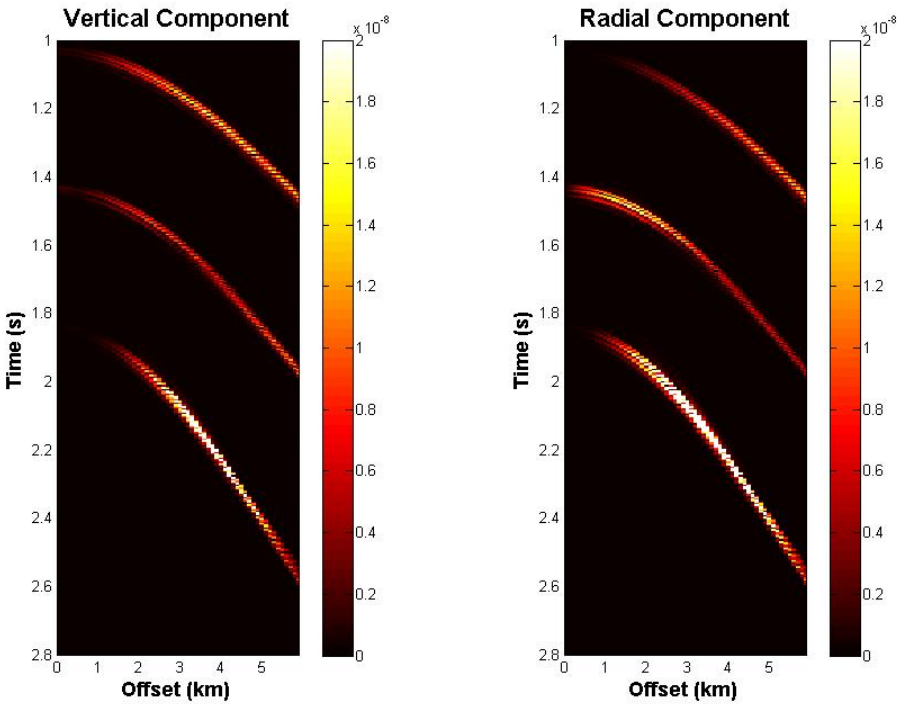

Figure 4.20: Difference between HTI and isotropic seismic responses. Crack density is 8%. Wet (oil or water saturated). The source-receiver line is perpendicular to crack orientation.

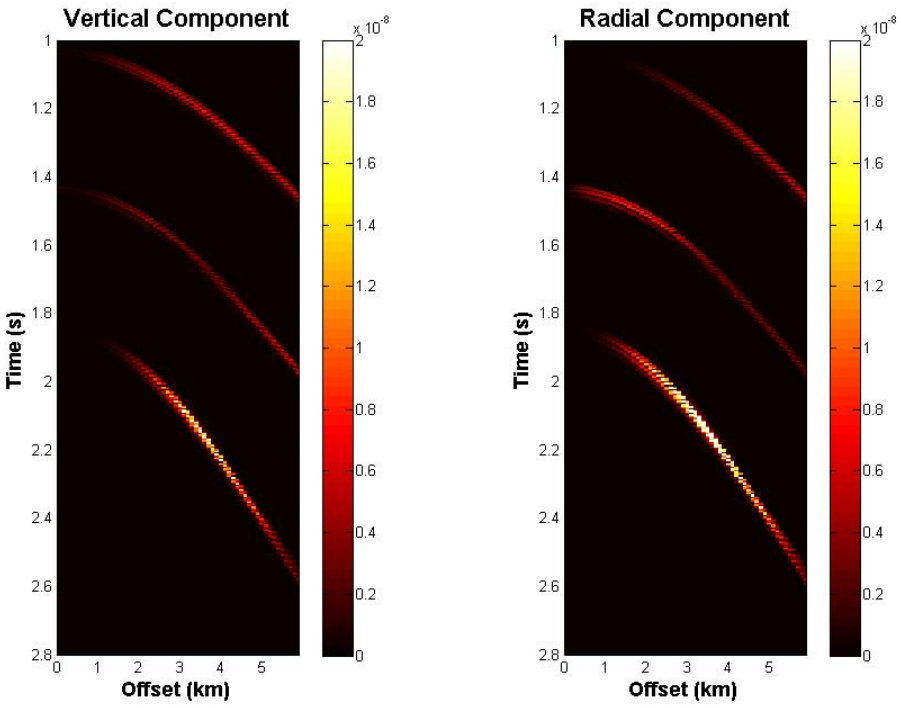

Figure 4.21: Difference between HTI and isotropic seismic responses. Crack density is 4%. Wet (oil or water saturated). The source-receiver line is perpendicular to crack orientation.

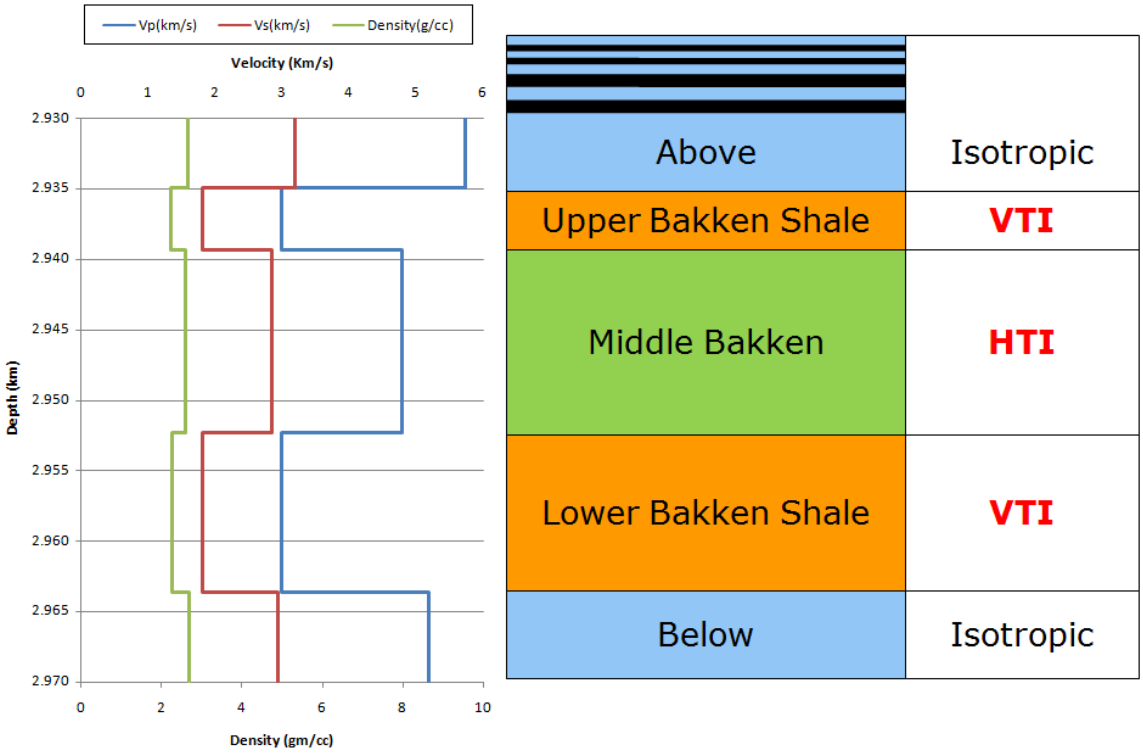

Figure 4.22: Combination of VTI and HTI Model used to generate synthetic seismograms for the Cottonwood Field.

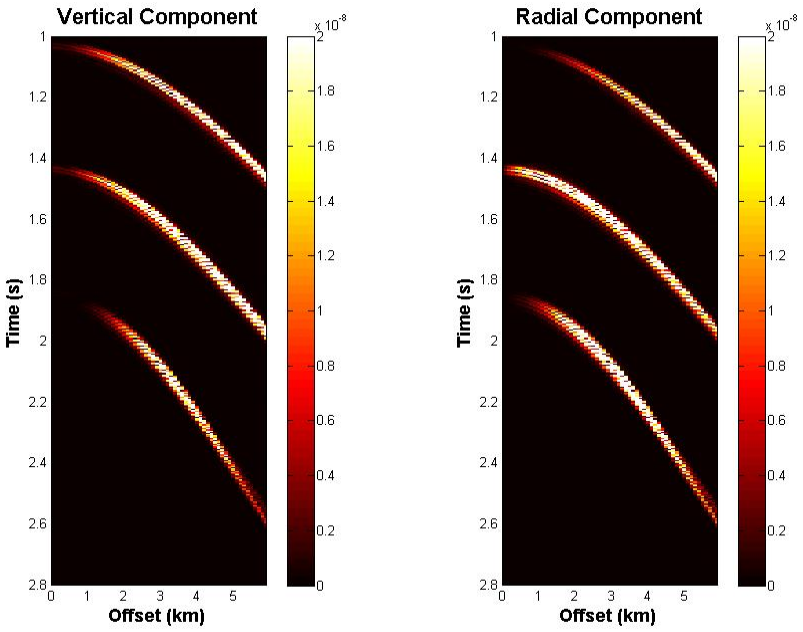

Figure 4.23: Difference between anisotropic and isotropic seismic responses. Crack density is 8%. Dry. The source-receiver line is perpendicular to crack orientation.

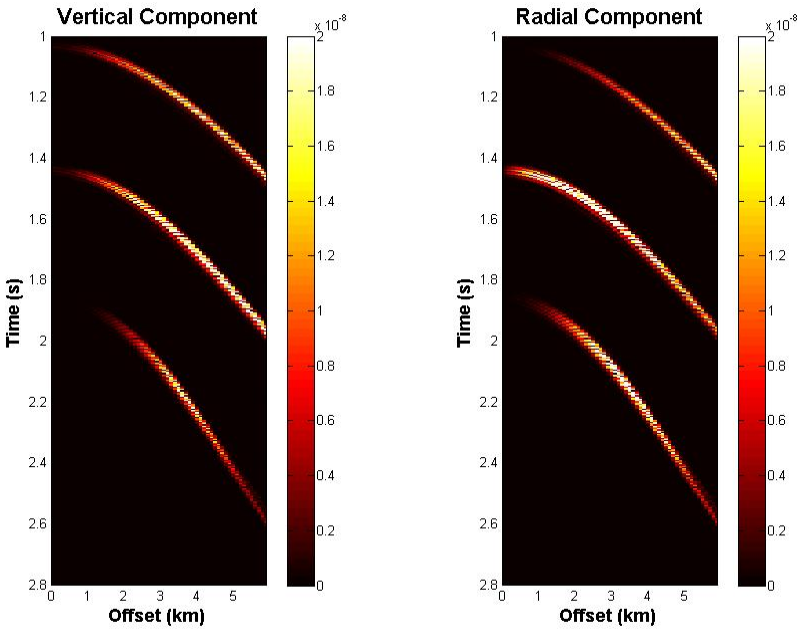

Figure 4.24: Difference between anisotropic and isotropic seismic responses. Crack density is 4%. Dry. The source-receiver line is perpendicular to crack orientation.

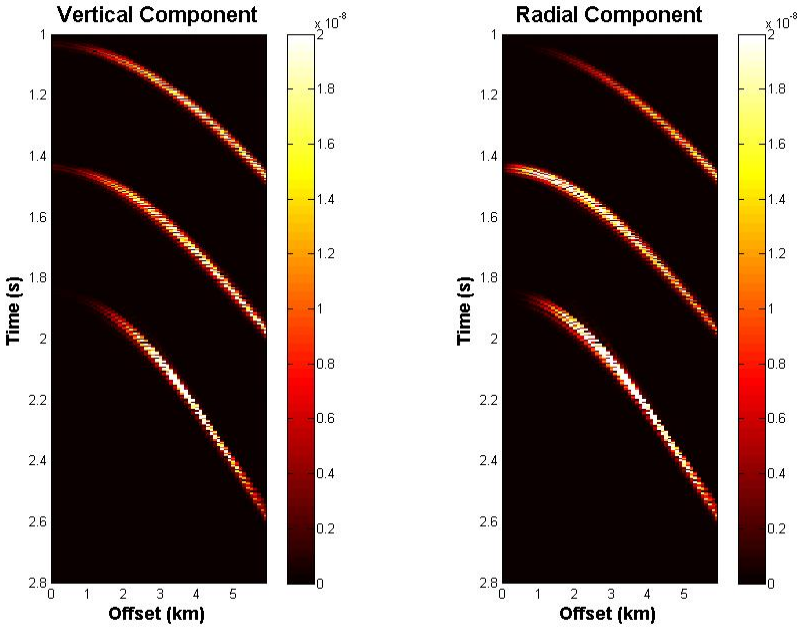

Figure 4.25: Difference between anisotropic and isotropic seismic responses. Crack density is 8%.Wet (oil or water saturated). The source-receiver line is perpendicular to crack orientation.

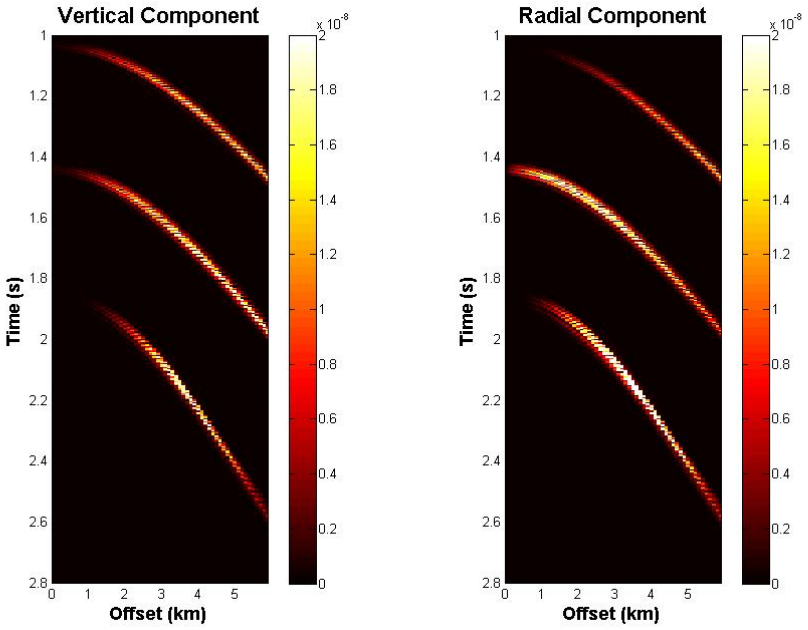

Figure 4.26: Difference between anisotropic and isotropic seismic responses. Crack density is 4%. Wet (oil or water saturated). The source-receiver line is perpendicular to crack orientation.

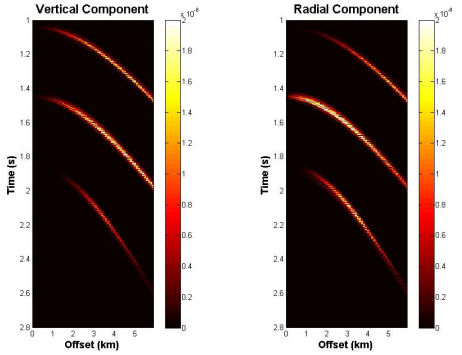

(a) VTI

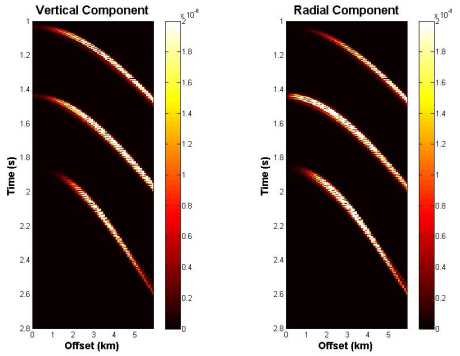

(b) Dry crack, e=8%

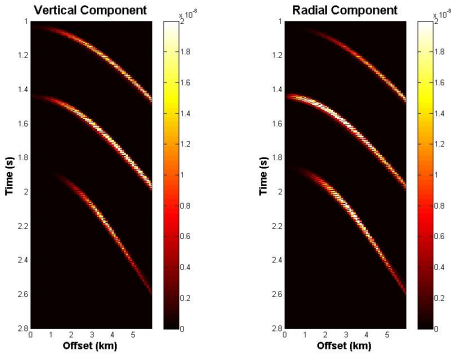

(c) Dry crack, e=4%

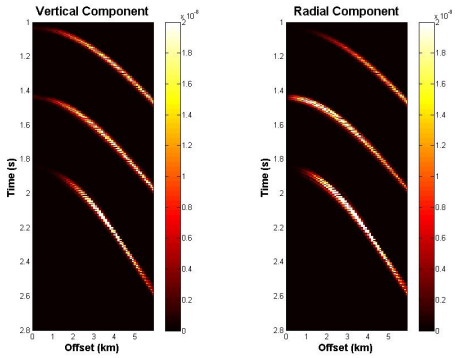

(d) Wet crack, e=8%

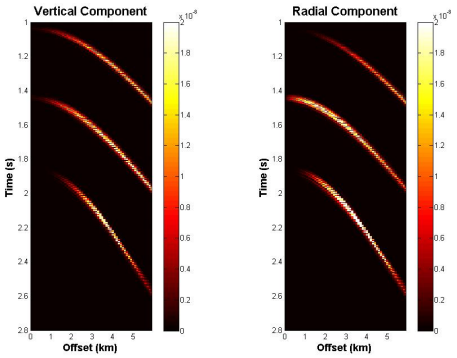

(e) Wet crack, e=4%

Figure 4.27: Comparison between VTI information and anisotropy information for combination models. (a) VTI information; (b), (c), (d) and (e) are anisotropic information for combination models. The source-receiver line is perpendicular to crack orientation.

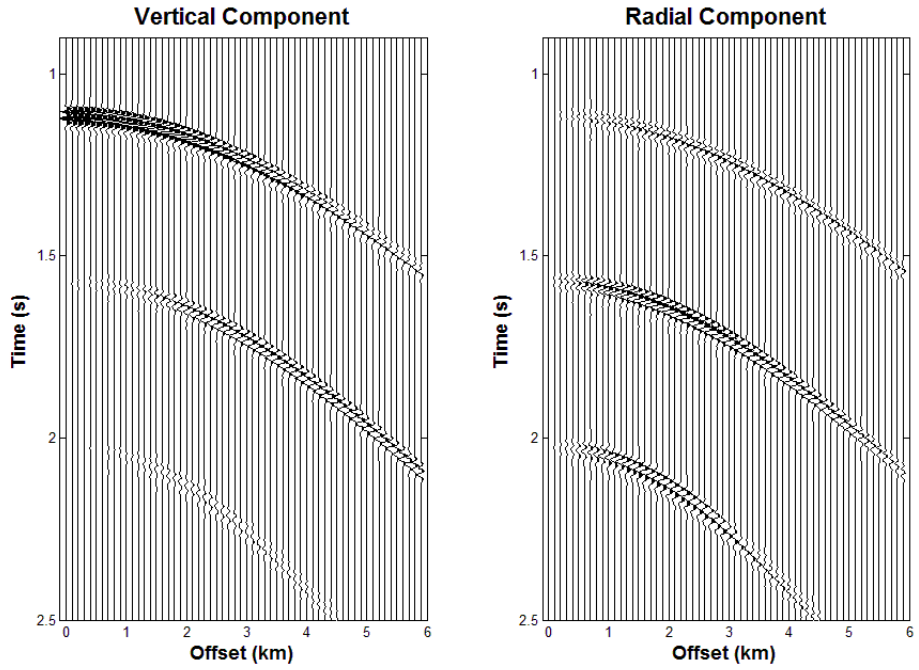

(a)

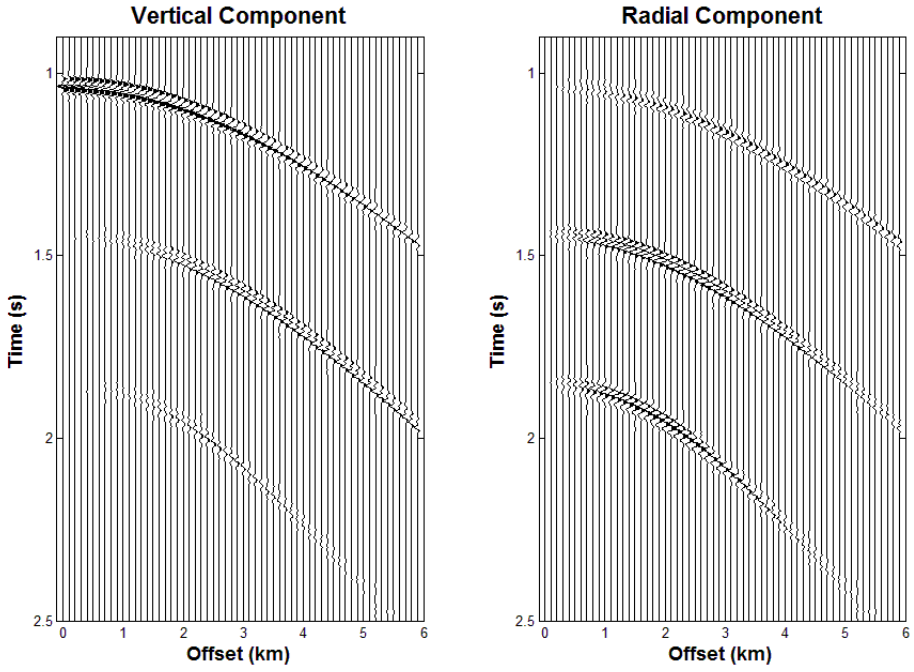

(b)

Figure 4.28: Isotropic seismic responses. a) Sanish Field; b) Cottonwood Field.

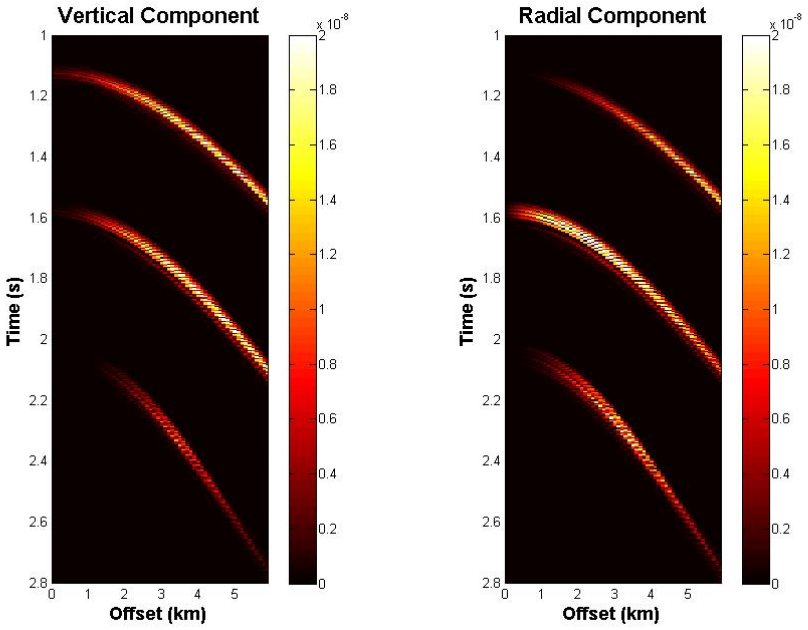

(a)

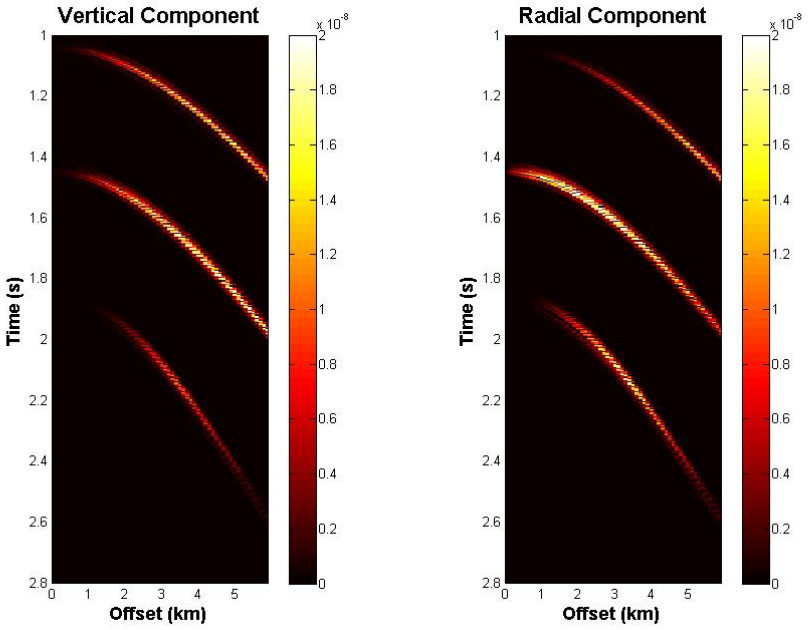

(b)

Figure 4.29: Difference between VTI and isotropic seismic responses. (a) Sanish Field; (b) Cottonwood Field.

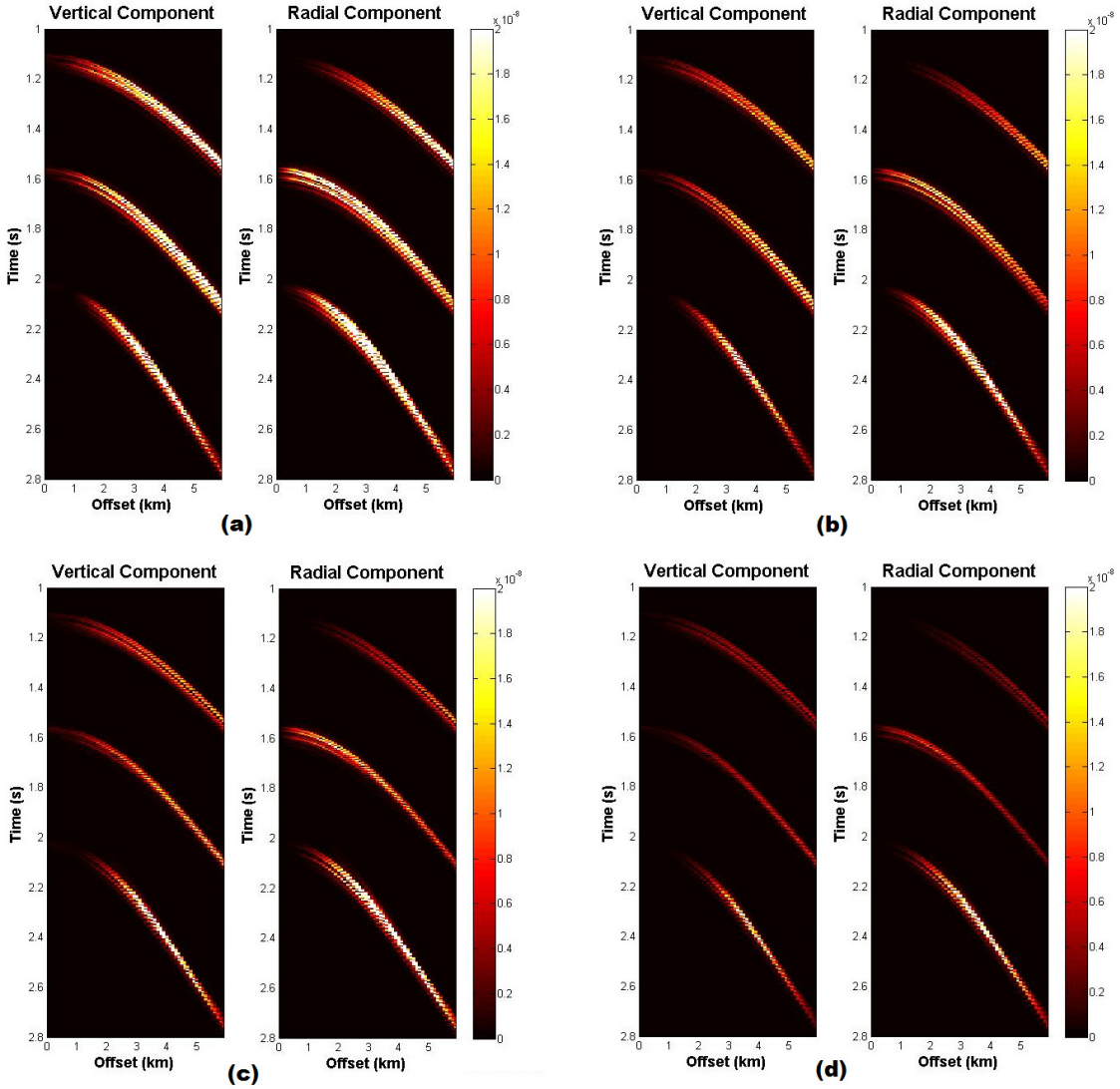

Figure 4.30: Difference between HTI and isotropic seismic responses for the Sanish Field. The Middle Bakkan has HTI symmetry caused by (a) Dry crack, e=8%; (b) Dry crack, e=4%; (c) Wet crack, e=8%; (d) Wet crack, e=4%. The source-receiver line is perpendicular to crack orientation.

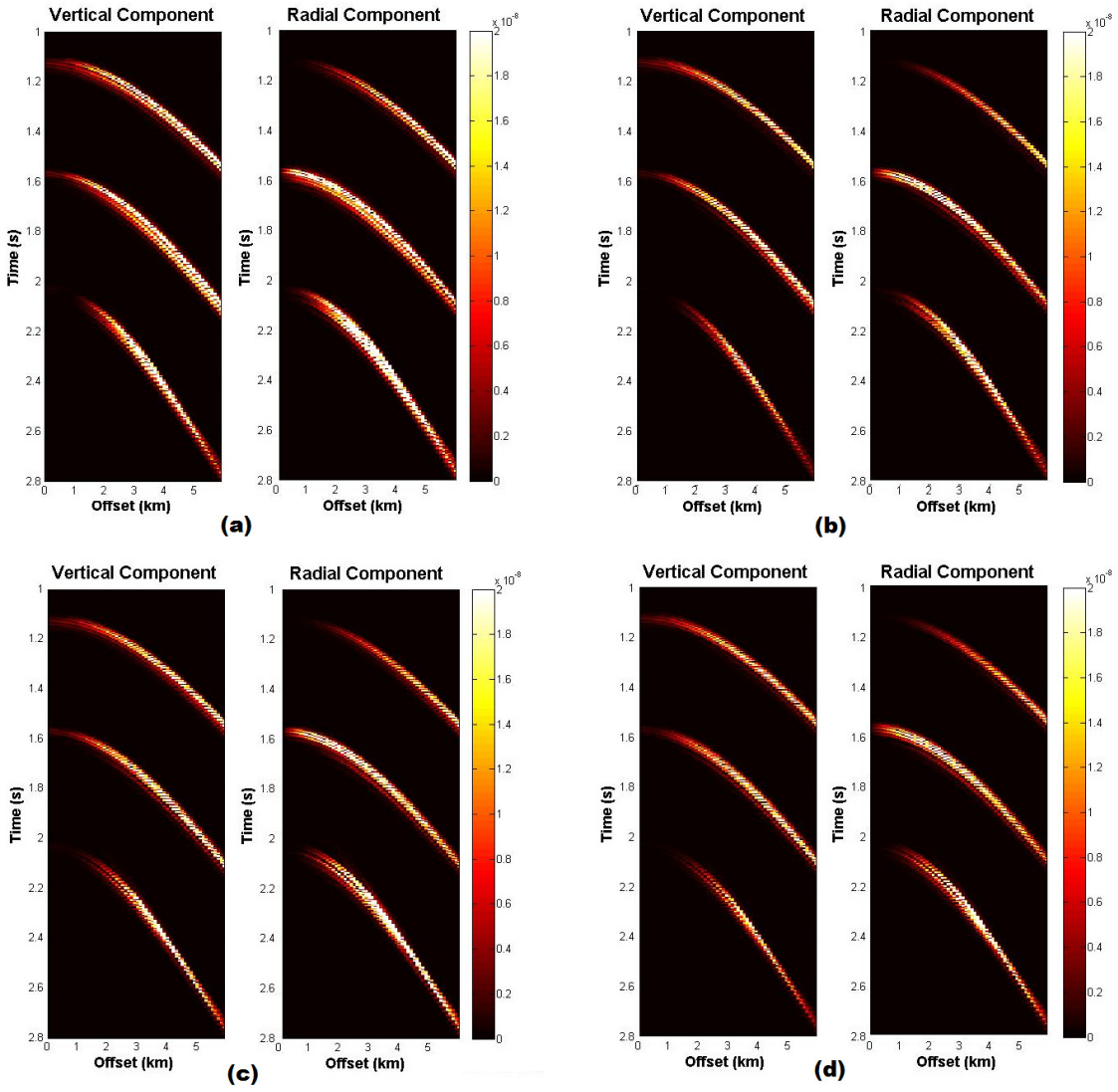

Figure 4.31: Difference between anisotropic and isotropic seismic responses for the Sanish Field. The Upper and Lower Bakken have VTI symmetry. The Middle Bakkan has HTI symmetry caused by (a) Dry crack, e=8%; (b) Dry crack, e=4%; (c) Wet crack, e=8%; (d) Wet crack, e=4%. The source-receiver line is perpendicular to crack orientation.

Chapter 5 Summary, Conclusions and Future Work

5.1 SUMMARY

The Bakken Formation in the Williston Basin is a closed, low-permeability petroleum system (Pitman et al., 2001) that produces both oil and gas. There is production variation in the study area, which is located in the east Williston Basin, North Dakota. The objective of this work is to identify differences in the character of the Bakken interval between locations with high and poor production rates, and to predict the seismic responses of the Bakken Formation to discriminate the difference in character between better and poorer producing areas or wells.

Chapter 1, developed the motivation of this work and provided introduction of the Bakken Formation and its geological background. Production in the Bakken has been established over a relatively long period for resource plays, and provides an ideal setting to test geophysical concerns.

Chapter 2, reviewed the classification and origin of anisotropy, particularly transverse isotropy, and showed anisotropy parameters for both VTI and HTI media. I reviewed anisotropy origins that are important to this work, fractures and cracks (HTI) and shales (VTI), and showed the relationship between anisotropy parameters and fracture/crack properties. We may speculate that HTI represents vertical fractures or aligned pores in the more "brittle" Middle Bakken, and VTI may be related to alignment of clay minerals, and perhaps total organic content, in the source-rich and sealing Upper and Lower Bakken units.

In Chapter 3, I characterized the Bakken Formation in five wellbores by analyzing well log data acquired by the Sonic Scanner tool for both the Cottonwood Field and the Sanish Field. Density, velocity, Vp/Vs ratio, Young's modus and Poisson's ratio are

analyzed for all the wells, and are averaged for five intervals, the Lodgepole, Upper Bakken, Middle Bakken, Lower Bakken and Three Forks.

The Bakken formation is a total of about 100 ft thick at a depth of about 10000 ft. The Bakken Formation is deeper and slightly thicker in the Sanish Field and is shallower and thinner in the Cottonwood Field. The Upper and Lower Bakken shales are similar in both areas and can be characterized by low density, low P and S wave velocities and low Vp/Vs ratios. Vp/Vs ratio of the shales are only slightly lower than that of the Middle Bakken, therefore may not be used as an effective lithology indicator to differentiate between the Bakken shales and Middle Bakken. For both the Upper and Lower Bakken shales, the vertical Young's modulus is much less than the horizontal Young's modulus while the vertical Poisson's ratio is much greater than the horizontal Poisson's ratio. Based on log data analysis, the Upper and Lower Bakken shales can be treated as VTI media and the Middle Bakken may be considered as isotropic.

As shown in Chapter 1, the Sanish Field is more productive than the Cottonwood Field. However, although there is some variation of the properties among wells, the main differences between the Sanish Field and the Cottonwood Field are depths and thicknesses. Thicker Bakken in the Sanish Field may contribute to better the production. Considering the significant impact of drilling and completion techniques on the Bakken production, there is possibility that the length of horizontal wells, success of completion, and number of hydrofracing stages are all associated with the production difference between the Sanish and Cottonwood Fields. In other words, even if the Bakken is the same in the two fields, the difference in drilling and completion may cause production difference. Thus, the paucity of data for poor-production limited the success of discrimination between good and poorly producing areas.

In Chapter 4, I built different types of models including isotropic models, VTI models, HTI models and models combining VTI and HTI. I generated full offset elastic synthetic seismograms to study the seismic responses of the Bakken Formation. I varied layer thickness of the Bakken, crack density and fluids filled in the cracks to investigate their influences on seismic responses and anisotropies. I also compared models for the Sanish Field with ones for the Cottonwood Field.

The bed thickness of each member of the Bakken is below seismic resolution, therefore there is interference among the reflections from the Upper, Middle and Lower Bakken. Thickness variation of the Bakken Formation between the Sanish Field and the Cottonwood Field do contribute to differences in seismic responses.

The difference between the anisotropic seismic responses, both VTI and HTI, and the isotropic seismic responses for the Bakken can be observed in both vertical and horizontal (radial) components. P-P, P-SV and SV-SV respond differently to anisotropies.VTI anisotropy and HTI anisotropy of the Bakken have different characters. P-SV carries more VTI anisotropy information while SV-SV carries more HTI anisotropy information. Both VTI and HTI are affected by bed thickness variation.

Crack densities (as defined by Hudson, 1980) and fluid contents (dry or water/oil saturated) affect the HTI anisotropies. SV-SV anisotropy is least influenced by the fluid fill in the cracks while P-P and P-SV anisotropies are greatly reduced if the cracks are wet. The fluid effects are more obvious when crack densities are high.

The presence of vertical aligned fractures/cracks results in azimuthal anisotropy, which can be observed from wide azimuth seismic data. Although the Middle Bakken is sandwiched between the VTI Upper and Lower Bakken shales, the presence of HTI in the Middle Bakken can enhance the total observed anisotropies.

Bed thickness, anisotropies of the Bakken shales that are related to kerogen content and maturation level, fractures/cracks and fluid fill in the cracks all have influences on the seismic responses of the Bakken Formation.

Ultimate production of the Bakken Formation may be associated with variation in reservoir thickness, source rock maturity, presence of nature fracture and success of hydraulic fracturing and completion techniques. All these factors are related to anisotropy. Therefore, study the anisotropy of the Bakken Formation may be critical to understand the variation in production.

5.2 FUTURE WORK

It will be interesting to analyze the field seismic data and compare the synthetic modeling results with real data. The field data should come from both the Cottonwood Field and the Sanish Field to make comparison between two fields possible. As shown in this work, P-P, P-SV, SV-SV respond differently to anisotropy, P-P may be less effective to analyze the anisotropy than P-SV and SV-SV. For this reason, it is preferred to use multi-component data.

I performed some preliminary azimuthal analysis of a small set of test P wave seismic data of the Cottonwood Field. I observed the azimuthal variation of both traveltime and amplitude for Bakken reflections. In this preliminary analysis, the fast and slow directions and the higher amplitude direction are consistent with the azimuth distribution of the data, which may suggest an acquisition footprint. This showed that the seismic data should be processed and prepared for azimuthal analysis.

Further, techniques to fully evaluate sensitivities to VTI and HTI need to be developed. This sensitivity study does show pronounced differences in the seismic reflection response between isotropic and anisotropic models. Techniques to differentiate

between spatial variations in anisotropy or estimation of anisotropy parameters are expected to follow these demonstrations of sensitivity to anisotropy.

Bibliography

Bakulin, A., V., Grechka, and I. Tsvankin, 2000, Estimation of fracture parameters from reflection seismic data-Part I: HTI model due to a single fracture set: Geophysics, **65**, 1788-1802.

Banik, N. C., 1984, Velocity anisotropy of shales and depth estimation in the North Sea Basin: Geophysics, **49**, 1411-1419.

Beckham, W. E., 1996, Seismic anisotropy and natural fractures from VSP and borehole sonic tools-A field study: Geophysics, **61**, 456-466.

Brocher, T. M., and N. I. Christensen, 1990, Seismic anisotropy due to preferred mineral orientation observed in shallow crustal rocks in southern Alaska: Geology, **18**, 737-740.

Carrion, P., J. Costa, J. E. F. Pinheiro, and M. Schoenberg, 1992, Cross-borehole tomography in anisotropy media: Geophysics, **57**, 1194-1198.

Cheadle, S. P., J. Brown, and D. C. Lawton, 1991, Orthorhombic anisotropy: A physical seismic modeling study: Geophysics, **56**, 1603-1613.

Domenico, S. N., 1984, Rock lithology and porosity determination from shear and compressional wave velocity: Geophysics, **49**, 1188-1195.

Digital Formation, Inc., 2005, Petrophysical Analysis of the Bakken Interval, Nance Petroleum, Larson 11-26 Well, Richland County, Montana, PowerPoint presentation, http://pttc.mines.edu/casestudies/Bakken/BakkenPetro.pdf, accessed 20 July 2008.

Durham, L. S., 2009, Experience paid off at Parshall: AAPG Explorer, http://www.aapg.org/explorer/2009/06jun/johnson0609.cfm, accessed 20 December 2009.

Grover, P. W., 1996, Stratigraphy and diagenesis of the Mississippian Bakken Shale-Lodgepole Limestone sequence, Williston Basin, North Dakota: Ph.D. thesis, Texas A&M University.

Hayes, M. D., 1984, Conodonts of the Bakken Formation (Devonian and Mississippian), Williston Basin, North Dakota: M.S. thesis, University of North Dakota.

Hornby, B. E., 1998, Experimental laboratory determination of the dynamic elastic properties of wet, drained shales: Journal of Geophysical Research, **103**, No. B12, 29945-29964.

Hsu, C. J., and M. Schoenberg, 1993, Elastic waves through a simulated fractured medium: Geophysics, **58**, 964-977.

Hudson, J. A., 1980, Overall properties of a cracked solid: Mathematical Proceedings of the Cambridge Philosophical Society, **88**, 371-384.

Hudson, J. A., 1981, Wave speeds and attenuation of elastic waves in material containing cracks: Geophysical Journal of the Royal Astronomical Society, **64**, 133-150.

Hudson, J. A., 1991, Overall properties of heterogeneous material: Geophysical Journal International, **107**, 505-511.

Johnston, J. E., and N. I. Christensen, 1995, Seismic anisotropy of shales: Journal of Geophysical Research, **100**, No. B4, 5991-6003.

Jones, L. E. A., and H. F. Wang, 1981, Ultrasonic velocities in cretaceous shales from the Williston Basin: Geophysics, **46**, 288-297.

Karasinski D. R., 2006, Sedimentology and hydrocarbon potential of the Devonian Three Forks and Mississippian Bakken Formations, Sinclair Area, southeast Saskatchewan-southweat Manitoba: M.S. thesis, University of Manitoba (Canada).

LeFever, J. A., C. D. Martiniuk, E. F. R. Dancsok, and P. A. Mahnic, 1991, Petroleum potential of the middle member, Bakken Formation, Williston Basin, in J. E. Christopher and F. Haidl, eds., Proceedings of the 6th International Williston Basin Symposium: Saskatchewan Geological Society Special Publication 11, 74-94.

LeFever, J. A., 2008, Isopach of the Bakken Formation: North Dakota Geological Survey Geologic Investigations 59, Bakken Formation map series, scale 1:1,000,000.

Levin, F. K., 1979, Seismic velocities in transversely isotropic media: Geophysics, **44**, 918-936.

Lewis, C., T. L. Davis, and C. Vuillermoz, 1992, Three-dimensional multicomponent imaging of reservoir heterogeneity, Silo Field, Wyoming, in Sheriff, R. E., ed., Reservoir geophysics: Society of Exploration Geophysicists, 337-372.

Li, X. Y., and M. C. Mueller, 1997, Case studies of multicomponent seismic data for fracture characterization: Austin Chalk examples, in Marfurt, K. J., ed., Carbonate seismology: Society of Exploration Geophysicists, 337-372.

Lynn, H. B. and L. Thomsen, 1990, Reflection shear-wave data collected near the principal axes of azimuthal anisotropy, Geophysics, **55**, 147-156.

Meissner, F. F., 1976, Abnormal electric resistivity and fluid pressure in Bakken Formation, Williston basin, and its relation to petroleum generation, migration, and accumulation (abs.): AAPG Bulletin, **60**, 1403-1404.

Meissner, F. F., 1978, Petroleum geology of the Bakken Formation Williston Basin, North Dakota and Montana, in D. Rehrig, ed., 1978 Williston Basin symposium: Montana Geological Society, 207-227.

Meissner, F. F., J. Woodward, and J. L. Clayton, 1984, Stratigraphic relationships and distribution of source rocks in the greater Rocky Mountain region, in J. Woodward, F. F. Meissner, and J. L. Clayton, eds., Hydrocarbon source rocks of the greater Rocky Mountain region: Rocky Mountain Association of Geologists Guidebook, 1-34.

MacBeth C., and H. B. Lynn, 2000, Applied seismic anisotropy: Theory, background, and field studies: Society of Exploration Geophysicists.

McDonal, F. J., F. A. Angona, R. L. Mills, R. L. Sengbush, R. G. van Nostrand, J. E. White, 1958, Attenuation of shear and compressional waves in Pierre Shale: Geophysics, **23**, 421-439.

Mavko, G., T. Mukerji, and J. Dvorkin, 2003, The rock physics handbook: Tools for seisic analysis in porous media: Cambridge University Press.

Molotkov, L. A., and A. V. Bakulin, 1997, An effective model of a fractured medium wit h fractures modeled by the surfaces of discontinuity of displacements: Journal of Mathematical Sciences, **86**, 2735-2746.

Mueller, M. C., 1992, Using shear waves to predict lateral variability in vertical fracture intensity: The Leading Edge, **11**, No. 2, 29-35.

Mukerji, T., and M. Prasad, 2004, Analysis of microstructural textures and wave propagation characteristics in shales, http://www.osti.gov/bridge/servlets/purl/89053-yafcdC/890503.pdf, accessed 9 February 2010.

Mukerji, T., and M. Prasad, 2007, Image processing of acoustic microscopy data to estimate textural scales and anisotropy in shales: Acoustical Imaging, **28**, 21-29.

Nordeng, S. H., 2008, Time-temperature index of the Bakken Formation in North Dakota: North Dakota Geological Survey Geologic Investigation 61, https://www.dmr.nd.gov/ndgs/Publication_List/pdf/geoinv/GI_61.pdf, accessed 5 March 2009.

Nordeng, S. H., and J. A. LeFever, 2008, The Bakken: A question of maturity: 16th Annual Williston Basin Petroleum Conference, North Dakota Geological Survey, PowerPoint presentation.

Nordeng, S., 2010, A brief history of oil production from the Bakken formation in the Williston Basin: NDGS Newsletter, **37**, 5-9.

Prasad, M., and T. Mukerji, 2003, Analysis of Microstructural textures and wave propagation characteristics in shales: 73th Annual International Meeting, SEG, Expanded Abstracts, 1648-1651.

Peterson J. A., 1995, Williston Basin Province (031): U.S. Geological Survey Digital Data Series DDS-30, http://certmapper.cr.usgs.gov/data/noga95/prov31/text/prov31.pdf, accessed 20 November 2009.

Pickett, G. R., 1963, Acoustic character logs and their application in formation evaluation: Journal of Petroleum Technology, **15**, 659-667.

Pitman, J. K., L. C. Price, and J. A. LeFever, 2001, Diagenesis and fracture development in the Bakken Formation, Williston Basin: Implications for reservoir quality in the Middle Member: U.S. Geological Survey Professional Paper 1653.

Pollastro, R. M., T.M. Cook, L.N.R. Robert, C. J. Schenk, M.J. Lewan, L.O. Anna, S. B. Gaswirth, P. G. Lillis, T. R. Klett, and R. R. Charpentier, 2008, Assessment of undiscovered oil resources in the Devonian-Mississippian Bakken Formation, Williston Basin Province, Montana and North Dakota, 2008: U.S. Geological Survey Fact Sheet 2008-3021, http://pubs.usgs.gov/fs/2008/3021/, accessed 12 July 2008.

Pollastro, R.M., L.N.R. Roberts, T.A. Cook, and M.D. Lewan, 2008, Assessment of undiscovered technically recoverable oil and gas resources of the Bakken Formation, Williston Basin, Montana and North Dakota, 2008: U.S. Geological Survey Open-File Report 2008–1353.

Price, L. C., and J. A. LeFever, 1994, Dysfunctionalism in the Williston Basin: The mid-Madison/Bakken petroleum system: Bulletin of Canadian Petroleum Geology, **42**, 187-218.

Ruger, A., 1997, P-wave reflection coefficients for transversely isotropic models with vertical and horizontal axis of symmetry: Geophysics, **62**, 713-722.

Schoenberg M., 1980, Elastic wave behavior across linear slip interfaces: Journal of the Acoustical Society of America, **68**, 1516-1521.

Schoenberg M., 1983, Reflection of elastic waves from periodically stratified media with interfacial slip: Geophysical Prospecting, **31**, 265-292.

Schoenberg M., and J. Douma, 1988, Elastic wave propagation in media with parallel fractures and aligned cracks: Geophysical Prospecting, **36**, 571-590.

Schoenberg M., and F. Muir, 1989, A calculus for finely layered anisotropic media: Geophysics, **54**, 581-589.

Schoenberg M., and C. Sayers, 1995, Seismic anisotropy of fractured rock: Geophysics, **60**, 204-211.

Sheriff, R. E., 2002, Encyclopedic dictionary of applied geophysics: Society of Exploration Geophysicists.

Sil, S., and M. K. Sen, 2008, Azimuthal tau-p analysis in anisotropic media: Geophysical Journal International, **175**, 587-597.

Sil, S., 2009, Two-way traveltime analysis for seismic reservoir characterization: Ph.D. thesis, University of Texas at Austin.

Smith, M. G., and R. M. Bustin, 1995, Sedimentology of the Late Devonian and Early Mississippian Bakken Formation, Williston Basin, in Vern Hunter, L. D., and R. A. Schalla, eds., Seventh International Williston Basin Symposium 1995 Guidebook: Montana Geological Society, North Dakota Geological Society, and Saskatchewan Geological Society, 103-114.

Smith, M. G., 1996, The Bakken Formation (Late Devonian-Early Mississippian): A black shale source rock in the Williston Basin: Ph.D. thesis, University of British Columbia.

Sonnenberg, S. A., and A. Pramudito, 2009, Petroleum geology of the giant Elm Coulee field, Williston Basin: AAPG Bulletin, **93**, 1127-1153.

Sturm, S. D., and E. Gomez, 2009, Role of natural fracturing in production from the Bakken Formation, Williston Basin, North Dakota, http://www.searchanddiscovery.net/documents/2009/50199sturm/index.htm, accessed 11 November 2009.

Tatham R. H., 1982, Vp/Vs and lithology: Geophysics, **47**, 336-344.

Tatham, R. H., and M. D. McCormack, 1991, Multicomponent Seismology in Petroleum Exploration: Society of Exploration Geophysicists.

Tatham, R. H., M. D. Matthews, K. K. Sekharan, C. J. Wade, and L. M. Liro, 1992, A physical model study of shear-wave splitting and fracture intensity: Geophysics, **57**, 647-652.

Thomsen L., 1986, Weak elastic anisotropy: Geophysics, **51**, 1954-1966.

Tsvankin, I., 1997, Reflection moveout and parameter estimation for horizontal transverse isotropy: Geophysics, **62**, 614-629.

Vernik, L., and C. Landis, 1996, Elastic anisotropy of source rocks: Implications for hydrocarbon generation and primary migration: AAPG Bulletin, **80**, 531-544.

Vernik, L., and X. Liu, 1997, Velocity anisotropy in shales: A petrophysical study: Geophysics, **62**, 521-532.

Vernik, L., and A. Nur, 1992, Ultrasonic velocity and anisotropy of hydrocarbon source rocks: Geophysics, **57**, 727-735.

Vernik, L., and A. Nur, 1990, Ultrasonic velocity and anisotropy of petroleum source rocks: The Bakken formation, 60th Annual International Meeting, SEG, Expanded Abstracts, 845-848.

Webster, R. L., 1982, Analysis of petroleum source rocks of the Bakken Formation (Devonian and Mississippian) in North Dakota: M.S. thesis, University of North Dakota.

Webster, R. L., 1984, Petroleum source rocks and stratigraphy of the Bakken Formation in North Dakota, in Woodward, J., F. F. Meissner, and J. L. Clayton, eds., Hydrocarbon source rocks of the Greater Rocky Mountain Region: Rocky Mountain Association of Geologists, 57-81.

White, J. E., L. Martineau-Nicoletis, and C. Monash, 1983, Measured anisotropy in Pierre shale: Geophysical Prospecting, **31**, 709-725.

Winterstein, D. F., 1986, Anisotropy effects in P-wave and SH-wave stacking velocities contain information on lithology: Geophysics, **51**, 661-672.

Vita

Fang Ye received her B.E. and M.E. degrees from the Ocean University of China. She joined the M.S. program at the University of Texas at Austin in January, 2008. During the summer of 2008 and 2009, she interned with Kerogen Resources Inc. and BP America Inc., respectively. Upon graduation, she will join BP America as a Geophysicist, in Houston, Texas. She is a member of SEG and AAPG.

Permanent email: fionaye@gmail.com

This thesis was typed by Fang Ye.